AD-A181 550 STUDIES OF GAS TURBINE HEAT TRANSFER AIRFOIL SURFACE AND END-WALL..(U) MINNESOTA UNIV MINNEAPOLIS DEPT OF MECHANICAL ENGINEERING E R ECKERT ET AL. APR 87 1/1

UNCLASSIFIED AFOSR-TR-87-0701 F49620-85-C-0049 F/G 21/5 NL

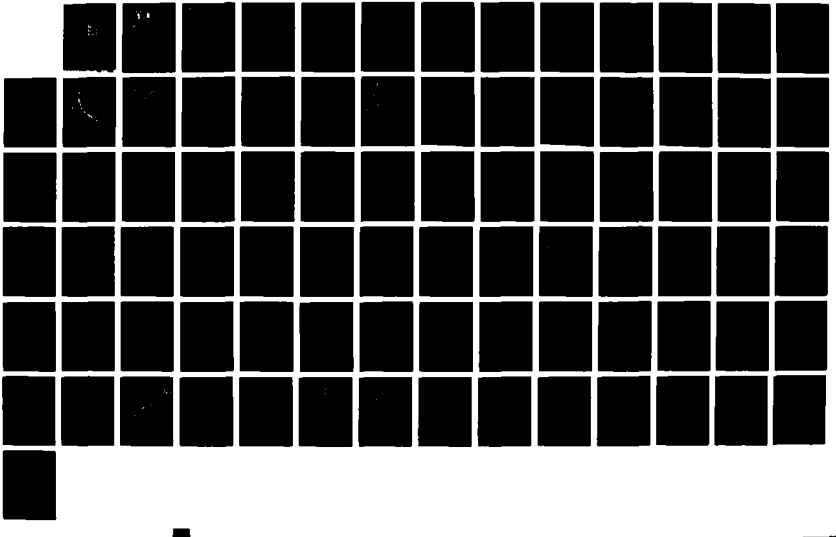

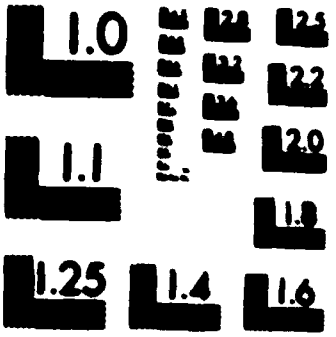

UNCLASSIFIED DTIC FILE COPY (2)

SECURITY CLASSIFICATION OF THIS PAGE

REPORT DOCUMENTATION

AD-A181 558

1a. REPORT SECURITY CLASSIFICATION: UNCLASSIFIED	1b. RESTRICTIVE MARKINGS
2a. SECURITY CLASSIFICATION AUTHORITY	3. DISTRIBUTION/AVAILABILITY OF REPORT: Approved for public release; distribution unlimited
2b. DECLASSIFICATION/DOWNGRADING SCHEDULE	
4. PERFORMING ORGANIZATION REPORT NUMBER(S)	5. MONITORING ORGANIZATION REPORT NUMBER(S): AFOSR-TR- 87-0701
6a. NAME OF PERFORMING ORGANIZATION: Mechanical Engrg. Dept. Univ. of Minnesota	6b. OFFICE SYMBOL (If applicable)
6c. ADDRESS (City, State and ZIP Code): 111 Church St. S.E. Minneapolis, MN 55455	7a. NAME OF MONITORING ORGANIZATION: Air Force Office of Scientific Research
8a. NAME OF FUNDING/SPONSORING ORGANIZATION: Bolling AFB, DC 20332	8b. OFFICE SYMBOL (If applicable): NA
8c. ADDRESS (City, State and ZIP Code): AFOSR/NA Bolling AFB, DC 20332	7b. ADDRESS (City, State and ZIP Code): Bolling Air Force Base Washington, D.C. 20332
	9. PROCUREMENT INSTRUMENT IDENTIFICATION NUMBER: F49620-85-C-0049
	10. SOURCE OF FUNDING NOS.

PROGRAM ELEMENT NO.	PROJECT NO.	TASK NO	WORK UNIT NO
61102F	2307	A4	

11. TITLE (Include Security Classification): Studies of Gas Turbine Heat Transfer Airfoil Surface and End-Wall

12. PERSONAL AUTHOR(S): Eckert, Ernst; Goldstein, Richard J; Simon, Terrence W.

13a. TYPE OF REPORT	13b. TIME COVERED	14. DATE OF REPORT (Yr., Mo., Day)	15. PAGE COUNT
Annual Progress	FROM 2/28/86 TO 4/1/87	April 1987	73

16. SUPPLEMENTARY NOTATION

17. COSATI CODES		
FIELD	GROUP	SUB GR

18. SUBJECT TERMS (Continue on reverse if necessary and identify by block number): Gas Turbines, Heat Transfer, Cascades, End-Wall Curvature

19. ABSTRACT (Continue on reverse if necessary and identify by block number)

The annual progress report documents work at the University of Minnesota Heat Transfer Laboratory, under AFOSR sponsorship, on the topic of heat transfer from gas turbine airfoil, end-wall and internal passage surfaces. The research is divided into the following subtopics: curvature effects, including transition and film cooling and airfoil heat transfer, including portions near the endwall.

20. DISTRIBUTION/AVAILABILITY OF ABSTRACT	21. ABSTRACT SECURITY CLASSIFICATION
UNCLASSIFIED/UNLIMITED ☐ SAME AS RPT ☒ DTIC USERS ☐	UNCLASSIFIED

22a. NAME OF RESPONSIBLE INDIVIDUAL	22b. TELEPHONE NUMBER (Include Area Code)	22c. OFFICE SYMBOL
J. D. Wilson, Program Manager	[202] 767-4935	AFOSR/NA

DD FORM 1473, 83 APR EDITION OF 1 JAN 73 IS OBSOLETE. UNCLASSIFIED

SECURITY CLASSIFICATION OF THIS PAGE

UNIVERSITY OF MINNESOTA
TWIN CITIES

Department of Mechanical Engineering
125 Mechanical Engineering
111 Church Street S.E.
Minneapolis, Minnesota 55455

April 10, 1987

Dr. James D. Wilson
Program Manager
AFOSR
Bolling Air Force Base
Washington, D.C. 20332

Re: Grant No. F49620-85-C-0049

Attached are five copies of our annual report which documents progress on our studies of gas turbine heat transfer. The report covers the period 4/15/86 to 3/15/87. We would be most happy to discuss this material with you by letter, phone or visitation.

Sincerely,

Terry Simon,
Associate Professor

TWS:dh
Encls. (5)

Accesion For	
NTIS CRA&I	☑
DTIC TAB	☐
Unannounced	☐
Justification	
By	
Distribution /	
Availability Codes	
Dist | Avail and / or Special	
A-1	

Annual Progress Report
(15 April 1986 - 15 March 1987)

STUDIES OF GAS TURBINE HEAT TRANSFER AIRFOIL SURFACE AND END-WALL

AFOSR GRANT #F49620-85-C-0049
(1 March 1983 - 30 April 1987)

E.R.G. Eckert, R. J. Goldstein, T. W. Simon
Co-Principal Investigators

April 1987

INTRODUCTION

The following annual progress report documents work at the University of Minnesota Heat Transfer Laboratory, under AFOSR sponsorship, on the topic of heat transfer from gas turbine airfoil, end-wall and internal passage surfaces. The research is divided into the following subtopics: curvature effects, including transition and film cooling and airfoil heat transfer, including portions near the endwall. Progress on each is discussed separately.

A. The Effect of Convex Curvature on Heat Transfer and Hydrodynamics of Turbulent Boundary Layers -- Including the Process of Recovery from Curvature

Three experiments were conducted to investigate the effect of streamwise curvature over the range from $\delta/R = 0.01$ to 0.04 and to study the effect of free-stream turbulence on fully turbulent curved boundary layers. An attached fully turbulent boundary layer, grown on a flat plate is introduced to a convex wall of constant radius of curvature followed by flat recovery wall.

1. Objectives

The effect of varying the radius of curvature on curved, two-dimensional boundary layers, including the recovery process, was investigated to further understand the transport mechanism and to extend the data base for prediction model development. Two different free-stream turbulence intensity cases were employed to study the effect of the free-stream turbulence intensity on the curved boundary layer. Significant additions to the previous data base are:

a. The recovery process, with heat transfer, was investigated for cases of milder curvature than in previous studies.
b. The radius of curvature was varied from case to case in the same study.
c. Curvature effects for cases of δ/R between those of mild and strong curvature were investigated in the same facility.
d. Free-stream turbulence intensity effects on the curved boundary layer were investigated for the first time.

2. Progress and Accomplishments

The important observations from the three experiments were published in You, Simon and Kim (1986a), You, Simon and Kim (1986b) and Kim and Simon (1987). Some details of the turbulent heat flux measurements, not given in a previous progress report, follow:

The effects of streamwise convex curvature, recovery, and free-stream turublence intensity on the turbulent transport of heat and momentum has been investigated. A special three-wire hot-wire probe based on the work of Blair and Bennett (1984) has been developed for this purpose. Two cases with free-stream turbulence levels of 0.68% and 2.0%, taken in the facility described earlier with $\delta/R = 0.03$ (a moderate strength of curvature) were compared. A summary of the results follows.

1. Profiles of $\overline{u'v'}$, t', $\overline{u't'}$ and $\overline{v't'}$ are reduced by curvature. An asymptotic profile was achieved very early. Recovery in the weak

portion of the profile occurs quickly, with the profiles often overshooting the flat plate (upstream of the curve) values.
2. A reversal of sign in the shear stress is seen for the high TI case (TI=2.0%) for $y/\delta > 0.5$. This behavior was observed by other researchers in strongly curved flow with lower turbulence intensity.
3. Because the measured turbulent Prandtl number profiles show considerable scatter, one can only conclude that the effect of curvature is no more than about 20%. But the data appear to show a decrease by the end of recovery from curvature. This does not refute Pr_t values deduced in earlier studies from mean velocity and temperature profiles, but does not provide support for the 20% increase noted by You, et al. (1986a). Negative turbulent Prandtl numbers were seen in the wake for the high TI case, indicating a breakdown in Reynolds analogy.
4. Curvature effects dominate turbulence intensity effects for the cases studied.

The reader is referred to Kim and Simon (1987) for more details.

B. The Concave Wall Study

1. Objectives

A major weakness in the design of gas turbines lies in the ability to predict the location of transition from laminar to turbulent flow on the blades. Graham (1979) stated that a 35% error in the prediction of heat transfer coefficient results in a wall temperature error of 56°C, and an order of magnitude decrement in blade life. Since as much as 50-80% of the blade can be covered by flow undergoing transition, and since the skin friction and convective heat transfer increase significantly during the transition process, the ability to predict the momentum and heat transport in this region is crucial.

Some of the parameters known to influence boundary layer transition are free-stream turbulence, acoustic disturbances, surface vibration, surface roughness, streamwise acceleration, blowing and suction, boundary layer separation, compressibility, body forces, and streamwise curvature. The effect of streamline curvature, pressure gradient, and free-stream turbulence are investigated in the present study. The effect of the other variables and various other uncontrollable parameters are minimized by using a unique flexible test wall, e.g, Wang (1984) enabling all experiments to be run on a single rig.

The study is to begin with a baseline case on a straight wall with no streamwise acceleration and low turbulence intensity. All subsequent runs will be compared to this case so that the effects of the above three parameters on transition can be isolated. The proposed experimental runs are summarized below:

Case	TI	R(cm)	Acc.	Description
1	0.68	∞	No	Baseline Case--Plane surf., Low TI
2	0.68	-180	No	45 deg-bend, Low TI, No. acc.
3	0.68	-90	No	45 deg-bend, Low TI, No. acc.
4	2.0	∞	No	Plane surface, High TI, No acc.
5	2.0	-180	No	45 deg-bend, High TI, No acc.
6	2.0	-90	No	90 deg-bend, High TI, No acc.
7	0.68	∞	Yes	Plane surf., streamwise acc., Low TI
8	0.68	-180	Yes	45 deg-bend, Streamwise acc., Low TI
9	2.0	∞	Yes	Plane surf., streamwise acc., High TI

The above ac./dec. runs will be with constant β values (self-similar). Special cases may be added where the acc./dec. values simulate the blade pressure side and the turbulence intensity is elevated above 2%, simulating blade conditions.

The experimental program consists of measuring, as a minimum, the following quantities.

1. Mean and fluctuating components of streamwise velocity. This is measured using a pitot tube in the heated flow, and by a horizontal hot-wire in isothermal flows.
2. Mean temperature profiles. The thermocoupls probe described by Wang (1984) will be used.
3. Local Stanton number. One hundred thirty thermocouples embedded in the test wall are for this purpose.
4. Shear stress profiles and profiles of the fluctuating component of cross-stream velocity in isothermal flows where the boundary layer is sufficiently thick. A cross-wire probe will be used.
5. Transverse velocity correlation coefficient in the free-stream as well as profiles of the autocorrelation of streamwise veoocity. Two horizontal hot-wire probes will be used.

If the boundary layers are thick enough, measurements of the three components of velocity along with their cross-correlations will be made with a triple wire where the flow displays considerable three-dimensionality. Streamwise

vorticity measurements using a probe similar to that described by Wallace (1984) are also being considered.

A probe to measure the apparent turbulent heat flux $\overline{u't'}$ and $\overline{v't'}$ in two-dimensional boundary layers similar to that described by Blair and Bennet (1984) has been developed. The reader is referred to Kim and Simon (1987) for details. The utility of this probe on the concave wall will depend on the two-dimensionality of the boundary layer.

If there is a formation of counter-rotating longitudinal vortices on the concave wall prior to transition, the flow will be strongly three-dimensional. It is therefore necessary to know where, in relation to the vortices, the measurements are taken. Flow visualization is thus necessary.

The main method of visualization is by using a sheet of cholesteric liquid crystal bonded to the surface of the concave wall. The crystals change color with temperature, enabling the temperature field to be mapped. Also, with a constant heat flux boundary condition, lines of constant color correspond to lines of constant heat transfer coefficient. By heating the wall slightly, the variation in wall temperature caused by the longitudinal vortices may be seen. Lower temperature lines correspond to downwash between the vorticies, while higher temperature lines correspond to the upwash. This method of visualization enables one to monitor the formation and growth of the vortices as well as determine their spacing.

Two other methods of visualization are being considered. Infrared scanning of the concave wall would also enable mapping of the surface temperature field. An IR scanner is currently available. The other method of visualization being considered is the smoke-wire method. A thin wire covered with oil is stretched across the test section, and resistance heating of the wire vaporizes the oil, producing "smoke". Visualization of the vortices is made possible due to lumping of the smoke at the upwash. The electronic circuit which drives a smoke-wire system has been built. A helium bubble generator is also available for visualization, as are high speed movie cameras.

2. Status

The test wall to be used in this study has been built. A schematic of it is given in Fig. 1. The design is similar to that described by Wang (1984), with the exception of using a lexan/liquid crystal composite instead of the stainless steel and the 3M P-19 film. The lexan was necessary for many reasons. The smoothness of the lexan eliminates the possibility of early transition due to waviness. It also permits the machining of a leading edge onto the wall. A measurement program in which the emissivity of the liquid crystal was measured eliminated the need for the P-19 reflective film that had been used for radiation control. The thermal conductivity of the lexan/liquid crystal was also measured.

Installation of the test wall has been completed. Qualification of the test wall with regards to transition location was performed by heating the wall and visualizing transition using the liquid crystal. Transition was assumed to occur at the location where the liquid crystal first changes color. This corresponds to the hottest wall temperature or, since the wall heat flux is uniform, the location of lowest heat transfer coefficient. Various parameters, such as the leading edge suction flow rate, the distance from the nozzle exit, etc. were optimized such that transition occurred as far downstream as possible for a given free-stream velocity and turbulence intensity. The outer flexible wall was adjusted such that there was no

pressure gradient along the wall. The Reynolds number based on displacement and momentum thickness at the beginning of transition were measured to be 1920 and 737, respectively. The free-stream turbulence intensity was 0.43%. A plot of Re_δ, vs. free-stream turbulence intensity for the present study is shown on Fig. 2, and is seen to be in excellent agreement with the data of previous researchers.

Further qualification of the test wall will be performed using momentum and energy balances. Programs to do this are currently being written.

C. Modeling of Curved Turbulent and Transitional Flows

Previously, experiments on boundary layer transition had been executed in the Heat Transfer Laboratory (Wang, Simon and Buddhavarapu (1985) and Wang and Simon (1985)). In addition to this, fully-turbulent boundary layer experiments have been made as discussed in the above section (You, Simon and Kim (1986a), You, Simon and Kim (1986b) and Kim and Simon (1987)). These sets, all taken in our lab with the same experimental techniques, give us a unique opportunity to evaluate some of the models typically employed in gas turbine heat load evaluation; in particular, empirical transition modeling and empirical correction for convex curvature effects to the mixing length hypothesis turbulence model. The results of this work are given in Park and Simon (1987), which is attached.

1. Objectives

a. To test present design models against the flat plate transitional data and the convex-wall curve-flow data, separately.
b. To test the combined model, which has a chosen transition model and curvature convection to the turbulence model, against the curved-wall transition data.
c. To test the hypothesis that curvature correction need by applied to the transition start, length and intermittency submodels.

2. Progress and Accomplishments

The work is documented in Park and Simon (1987). A major conclusion is that transition models can be found which "predict" the transition data but prediction from the various models which were chosen for review disagree somewhat from one to another and that a model chosen based on one case does not "predict" another case particularly well. A most useful finding was that, when free-stream turbulence intensity (T.I.) values are around 2% (and it is presumed the same could be said for higher T.I. values), the above hypothesis is true and curvature corrections need not be incorporated into the transition start, length and intermittency submodels. When the T.I. is 0.7% (and it is presumed to be true for values below 1%) the hypothesis fails. This lends some support to present design methods which ignore the curvature effect on transition location.

3. Expected Activities for Next Year

Further mixing length hypothesis modeling will remain "on hold" until the concave transitional data sets have been completed. Modeling with more sophisticated and general turbulence closure models will continue under the direction of Professor S.V. Patankar.

D. Film Cooling of Curved Surfaces

1. Objectives

The purpose of this study is to secure basic understanding of the processes involved in film cooling on curved surfaces. More specifically, the behavior of flow emerging from a row of round jets on the convex and concave walls of a curved duct is being examined with particular attention to how well these jets protect the walls of the duct from the free-stream conditions. Recently, an investigation into the effects of injection rate and curvature has been concluded. A brief summary of the findings is given in the next section. In the following phase of this study, the importance of injection angle will be examined.

2. Progress and Accomplishments

Film cooling through a row of holes over a convex and a concave surface has been studied. The holes were inclined at 35 degrees to the main flow and were spaced three diameters center-to-center. The effects of injection rate and strength of curvature on performance were studied. A foreign gas injection technique, employing the mass transfer analogy to heat transfer, was used.

Large variations in lateral profiles of local effectiveness on the convex surface were found. At all but the highest blowing rates, the local effectiveness was generally high at points in line with an injection hole and low half-way between two holes. Lateral profiles on the concave surface were comparatively flat. This was attributed to concave instabilities which enhanced mixing there.

Stronger convex curvature was found to enhance lateral average effectiveness at low blowing rates, while at high blowing rates, strength of curvature seemed to diminish in importance. Also at high blowing rates, the centrifual force of the jet caused the jet to lift off the surface. Momentum flux ratio was determined to be the parameter which influenced when lift-off would occur. Further increase in blowing rate or momentum flux ratio caused the jets to merge and blockage of the mainflow from the wall resulted. An increase in effectiveness was, therefore, encountered.

For film cooling of concave surfaces, momentum flux ratio had relatively little influence on the performance of film cooling on concave surfaces. This was probably because the normal momentum of the jets worked to degrade performance, while the tangential momentum (centrifugal force) caused an improvement. With the present injection geometry, the effects cancelled each other except just downstream of injection, where high normal momentum promoted lift-off. After twelve diameters from injection, blowing rate, rather than momentum flux ratio, was the dominant parameter.

On the concave wall, lateral average effectiveness behaved very similarly to analytical correlations for slot injection on a flat plate. The magnitude of the performance was consistently lower than the slot-flat plate correlations, but the trends were very much the same. Excessive lateral mixing, promoting blockage of the mainflow from the wall was the reason for this effect.

3. Expected Activities for Next Year

It is known that jet centrifugal force and normal momentum are two important parameters determining the behavior of a jet; increased jet centrifugal force enhances performance on the concave surface but degrades performance on the convex surface. Jet normal momentum, on the other hand, degrades performance on both surfaces. Both injection rate and injection angle significantly influence jet normal and tangential momentum.

From the previous phase, understanding of the effect of injection rate has been obtained. The present thrust is to quantify the effect of injection angle.

E. Mass Transfer on a Turbine Blade

Better understanding of the characteristics of heat transfer on a turbine blade will improve the design of the gas turbine engine. Although past researchers reported numerous results, these data mainly were measured in the two-dimensional flow region. Also, these investigations were not able to show detail due to conduction problems. Because the ratio of span to chord length is not large enough to ignore the effect of the endwall, data at the two-dimensional region are of marginal usefulness. Goldstein and Karni (1984) reported that mass transfer on the front portion of the cylinder in a narrow span next to the endwall is increased 90 to 700 percent over the two-dimensional region. Further investigation of heat transfer on a blade in the three-dimensional region is necessary. Flow in a turbomachine is so complex that no computational calculation can predict it accurately. Direct measurement therefore becomes essential for both development of computational models and improvement of the engine design. In the present study, a naphthalene sublimation technique is used. Sublimation rates on two hundred and fifty locations on both surfaces of a blade are measured. The wind tunnel and a linear cascade of six blades used in the study are shown in Fig. 3.

1. Objectives

First, measurements on a blade in the two-dimensional region are conducted to compare with other studies. Because the Taylor-Gortler vortex structure might occur on the concave surface of the blade, measurements searching for such a vortex system and its effects on heat transfer are made. Finally, measurements will be conducted near the end wall and the effect of the secondary flow system on heat transfer from the blade surface will be carefully investigated.

2. Progress and Accomplishments

Presently, the data acquisition system has been built and some preliminary tests have been made. It is expected that most of the measurements will be taken at the end of this summer.

a) Static pressure coefficients are measured on the blade surfaces and the approaching velocity is measured 12.9 cm upstream of the blade. Values of pressure coefficient on the concave side and convex side are shown in Fig. 4 and Fig. 5, respectively. Values of X are measured from the stagnation point of the blade and S is the chord length. Distribution of pressure coefficient on the concave side is quite uniform. The nonuniformity

of the convex side mainly results from the higher pressure at X/S = 0.43 which might cause the suction side horseshoe vortex to lift away from the wall.

b) Data Acquisition System

The flow chart of the data acquisition system is shown in Fig. 6. The main part of this data acquisition system, a four-axis table, is shown in Fig. 7. The construction of this table, motor-controller, and interface between all individual parts have been in progress over the past year. The software to control the stepper motors and LVDT for scanning a blade surface has been tested. Some preliminary tests were conducted, i.e. the effect of the vibration on the system and the repeatability of measurements on a solid cylinder.

3. Future Activities

We plan to perform measurements on a blade in the two-dimensional region for different Reynolds number flows. The effect of the Taylor-Gorlter vortex structure on blade heat transfer will be investigated at this time. Measurements of mass transfer in the near-end-wall region will then be conducted.

REFERENCES

Blair, M. F., and Bennett, J. C., 1984, "Hot-Wire Measurements of Velocity and Temperature Fluctuations in a Heated Turbulent Boundary Layer," Twenty-ninth ASME International Gas Turbine Conference, Amsterdam.

Goldstein, R. J., and Karni, J., 1984, "The Effect of a Wall Boundary Layer on Local Mass Transfer From a Cylinder in Crossflow," Journal of Heat Transfer, Vol. 106, pp. 260-267.

Graham, R. W., 1979, "Fundamental Mechanisms that Influence the Estimate of Heat Transfer to Gas Turbine Blades," NASA, TM-79128, 1979, or ASME Paper 79-HT-43.

Kim, J., and Simon T. W., 1987, "Measurements of the Turbulent Transport of Heat and Momentum in Convexly Curved Boundary Layers: Effects of Curvature, Recovery, and Free-Stream Turbulence", to be presented at the Int. Gas Turbine Conf., Anaheim, CA.

Kim, J. and T. W. Simon, 1987, "Measurements of the Turbulent Transport of Heat and Momentum in Convexly Curved Boundary Layers: Effects of Curvature, Recovery and Free-Stream Turbulence," Accepted for the ASME Int. Gas Turbine Conf.

Park, W. and Simon, T. W., 1987, "Prediction of Convex-Curved Transitional Boundary Layer Heat Transfer Behavior Using MLH Models, Proc. of the 1987 ASME-JSME Thermal Engr. Joint Conf.

Wallace, J. M., 1984, "The Measurement of Vorticity in Turbulent Flows," Ph.D. Thesis, U. of Maryland.

Wang, T., Simon, T. W. and Buddhavarapu, J., 1985, "Heat Transfer and Fluid Mechanics Measurements in Transitional Boundary Layer Flows," J. Engr. Gas Turbines and Power, Vol. 107, No. 4, pp. 1007-1015.

Wang, T. and Simon, T. W., 1985, "Heat Transfer and Fluid Mechanics Measurements in a Boundary Layer Undergoing Transition on a Convex-Curved Wall," ASME Paper 85-HT-60.

Wang, T., 1984, "An Experimental Investigation of Curvature and Freestream Turbulence Effects on Heat Transfer and Fluid Mechanics in Transitional Boundary Layers," Ph.D. Thesis, U. of Minnesota.

You, S. M., T. W. Simon, and J. Kim (1986a), "Boundary Layer Heat Transfer and Fluid Mechanics Measurements on a Mildly-Curved Convex Wall," Proceedings of the 8th Int. Heat Trans. Conf., Vol. 3, pp. 1089-1094.

You, S. M., T. W. Simon, and J. Kim (1986b), "Free-Stream Turbulence Effects on Convexly Curved Turbulent Boundary Layers," ASME, 86-WA/HT-46.

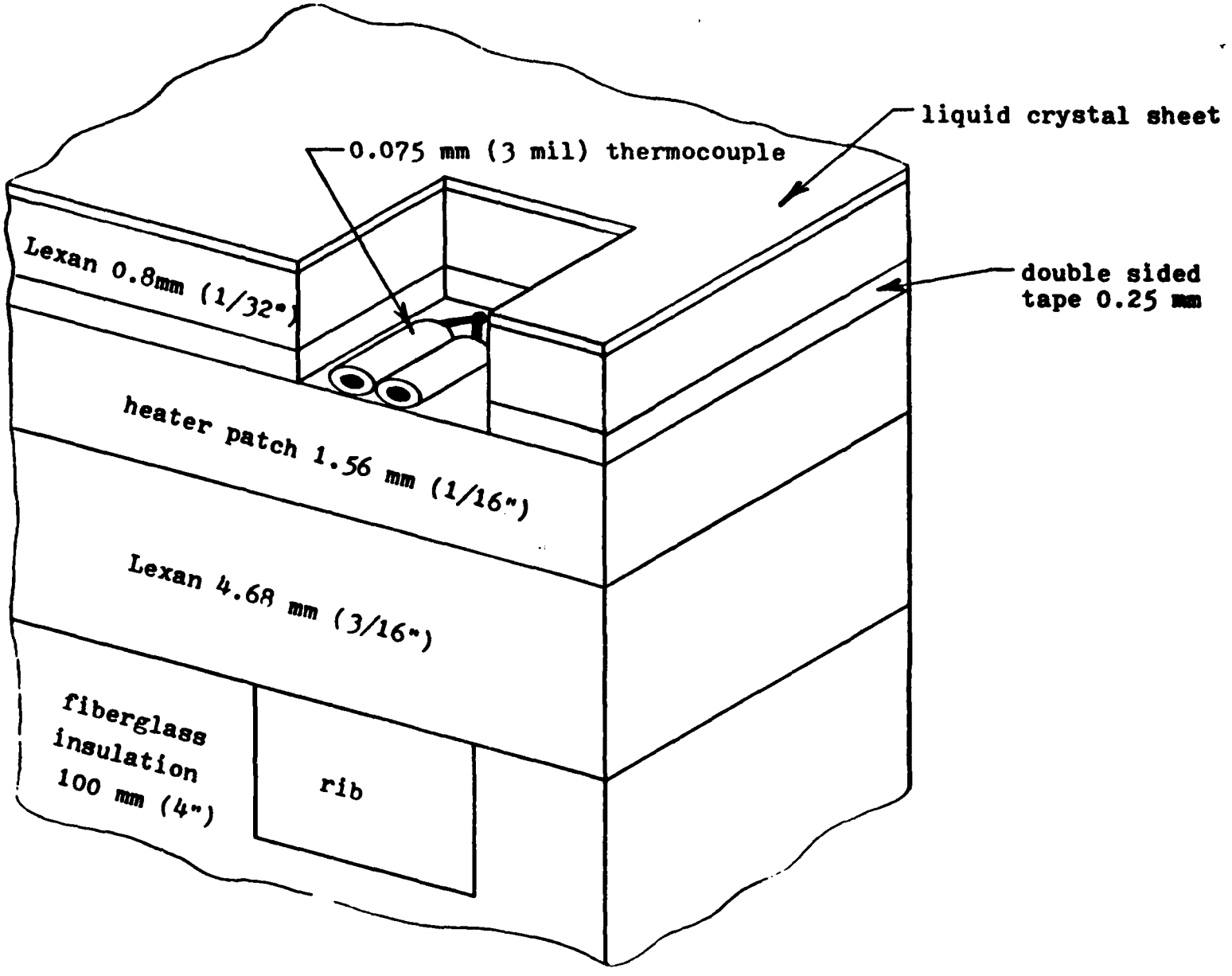

Fig. 1 -- Cross-section of Heated Wall (not to scale)

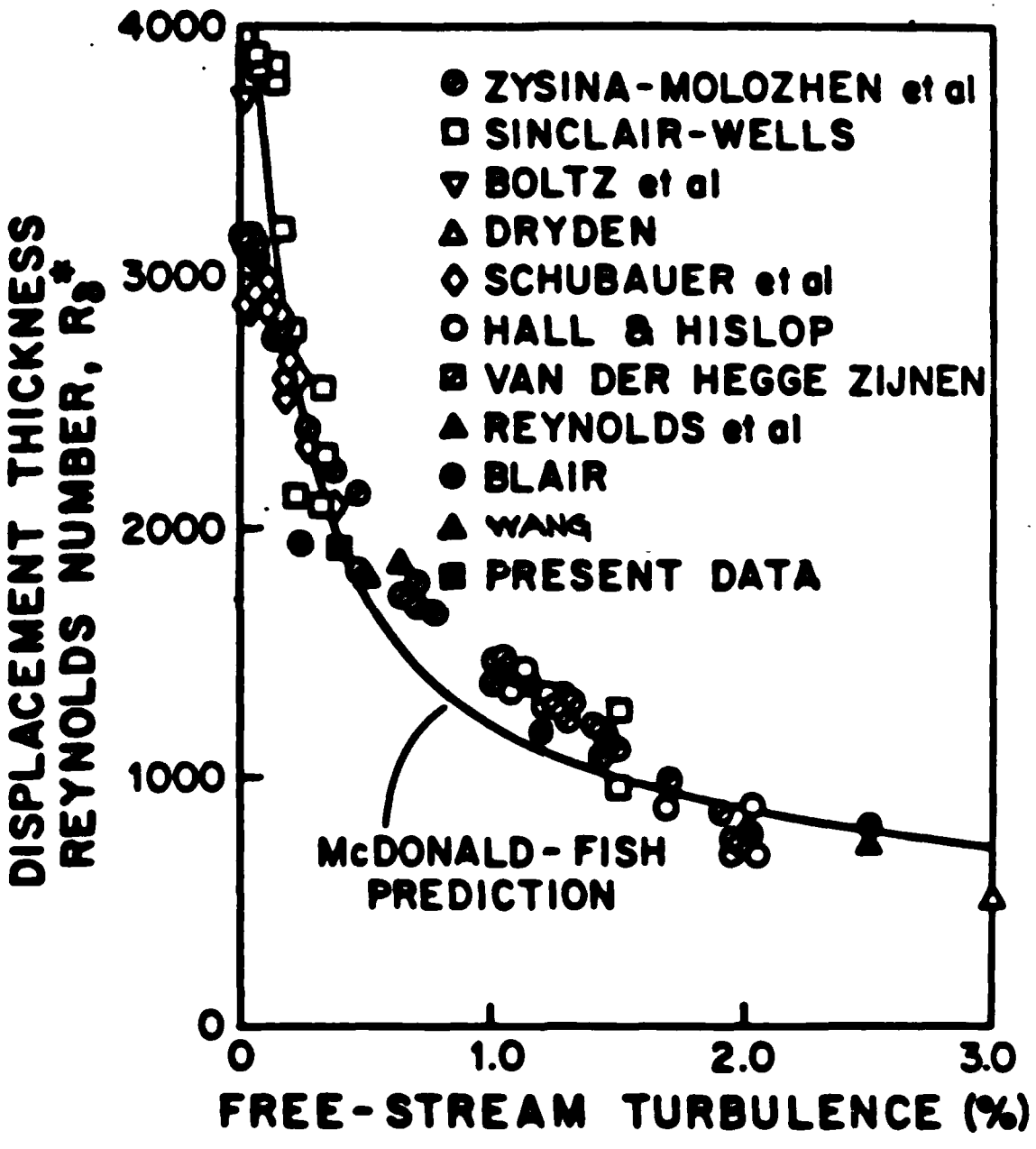

Fig. 2 -- Comparison of present transition location with that of other researchers.

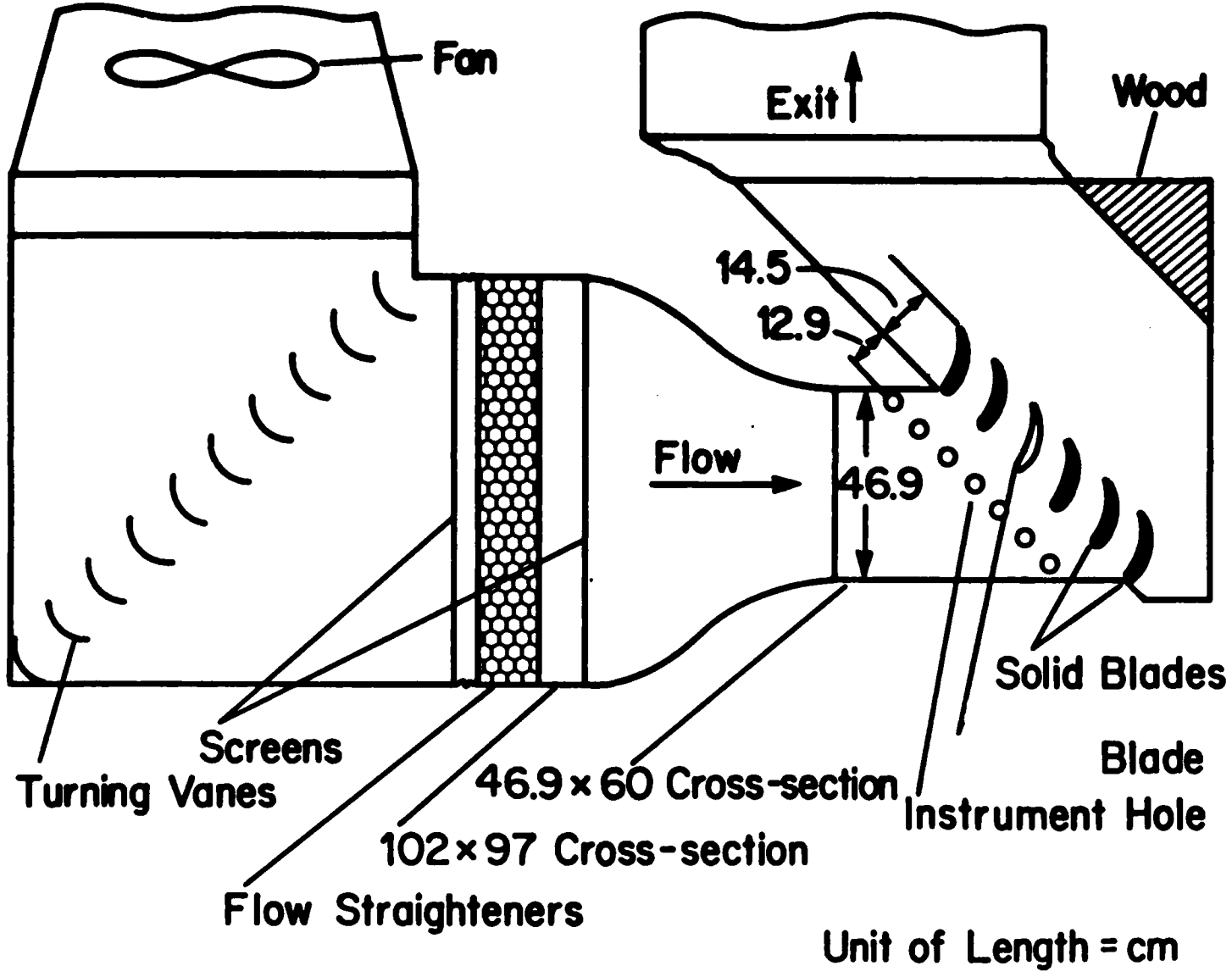

Fig. 3 Wind tunnel and test blades

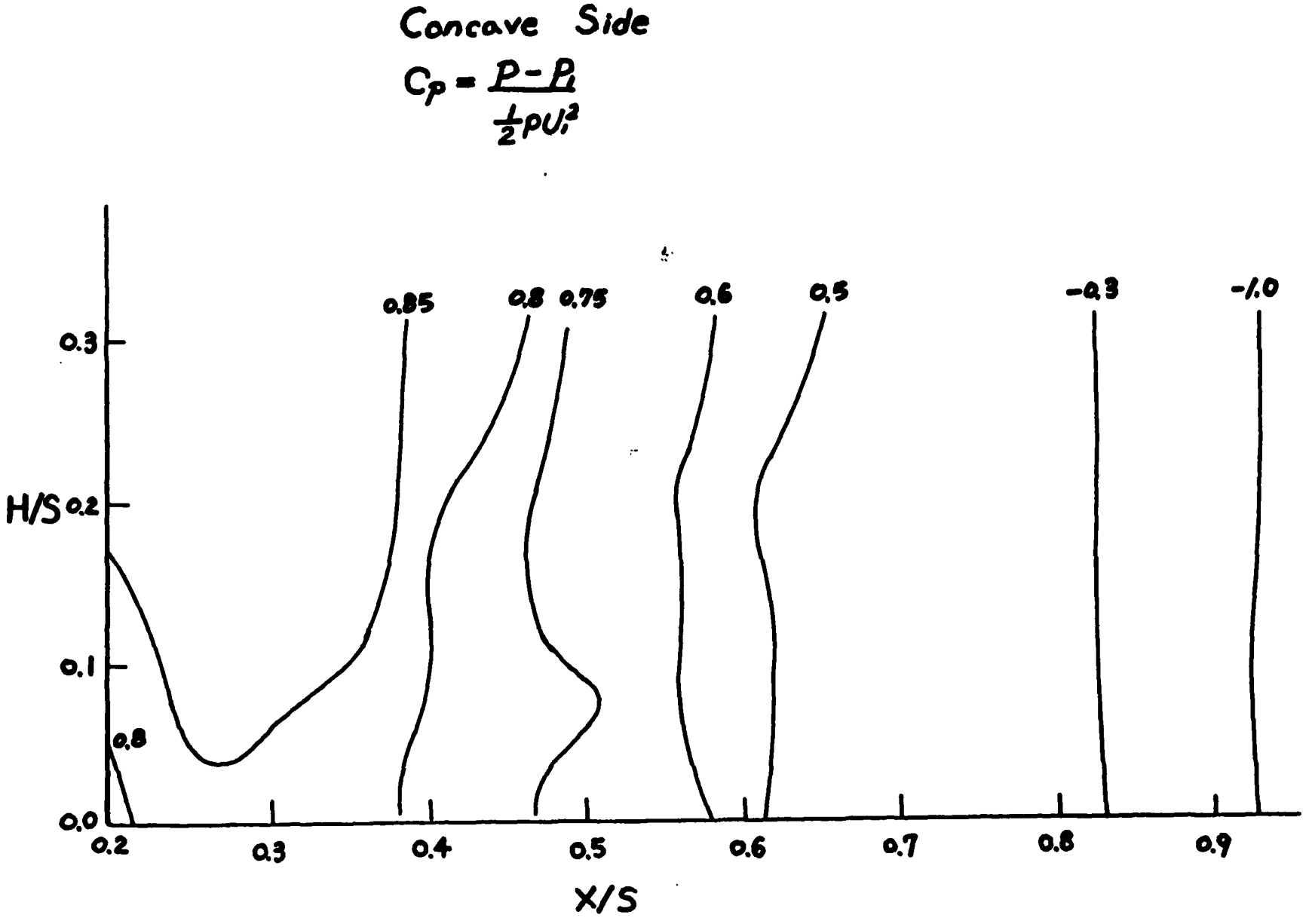

Fig. 4 Distribution of static pressure coefficient on the concave side of a blade

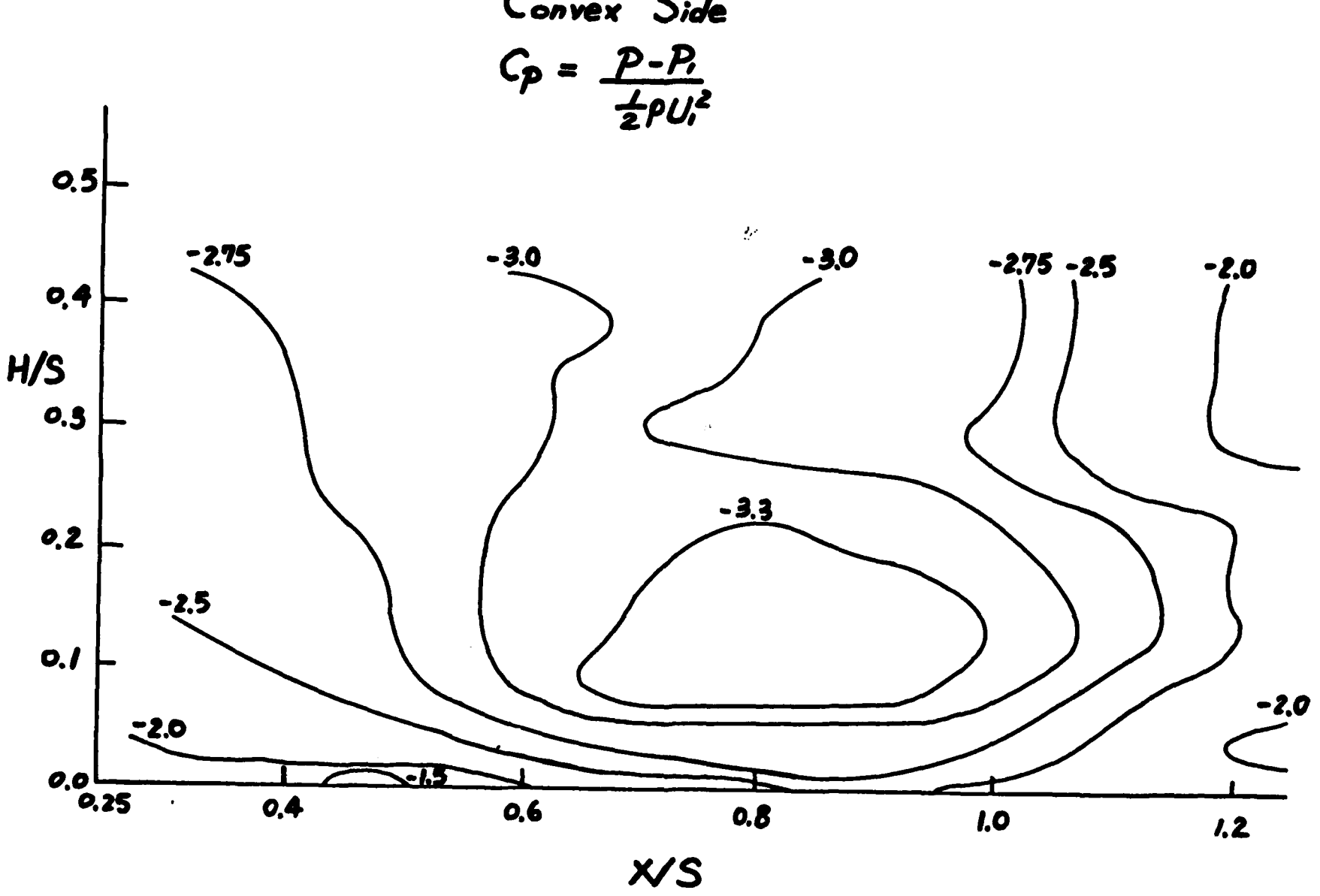

Fig. 5 Distribution of static pressure coefficient on the convex side of a blade

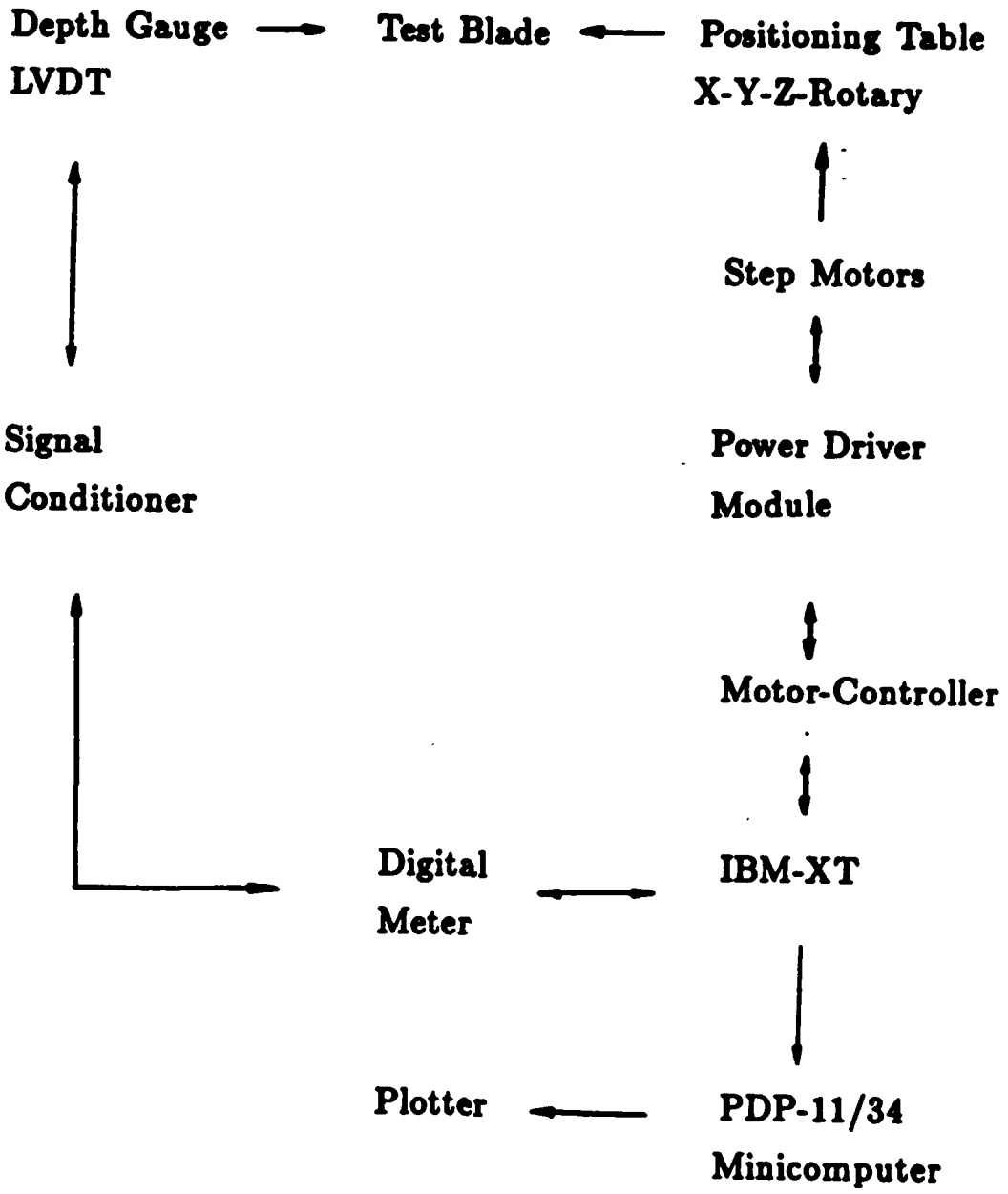

Fig. 6 Data acquisition system

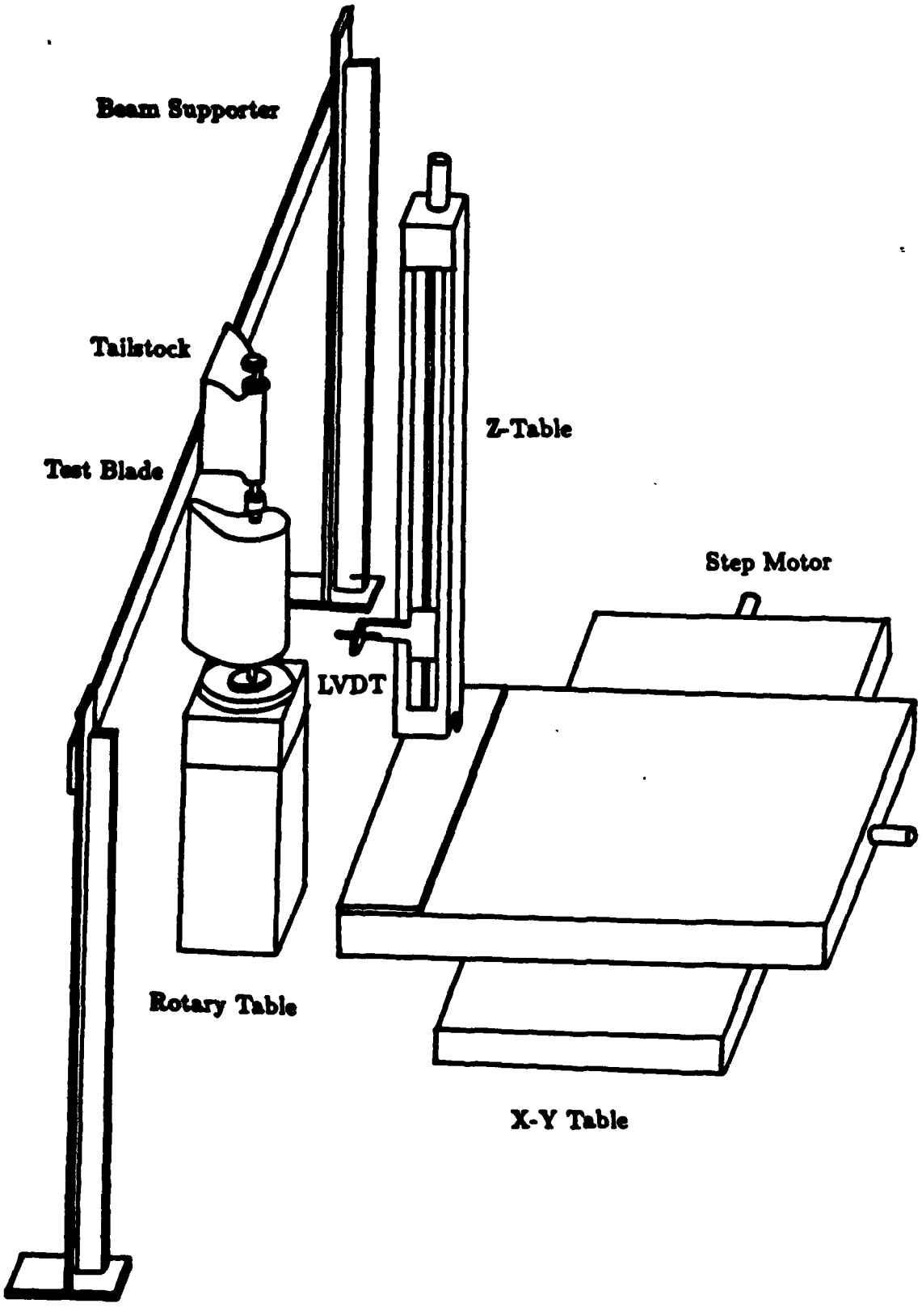

Fig. 7 Four-Axis Table

Proc. Eighth International Heat Transfer Conference, San Francisco, CA., Vol. 3, pp. 1089-1094 (1985).

BOUNDARY LAYER HEAT TRANSFER AND FLUID MECHANICS MEASUREMENTS ON A MILDLY-CURVED CONVEX WALL

S. M. You, T. W. Simon, and J. Kim

Mechanical Engineering Department, University of Minnesota
Minneapolis, MN 55455-0111 U.S.A.

Previous studies have demonstrated that even mild streamwise curvature has a marked effect on turbulence structure, heat transfer, and skin friction. This effect was further investigated in the present experiment where two cases of different radii of convex curvature were tested. An attached fully-turbulent boundary layer, grown on a flat plate was introduced to a constant radius of curvature convex wall followed by a flat recovery wall. The strength of curvature, the ratio of boundary layer thickness to radius of curvature, δ/R, was 0.013 and 0.03 for the two cases. Both cases were taken with the same test wall, bent to two radii of curvature and the same curvature entry conditions. In the curve, Stanton numbers and skin friction were reduced by 10% and 20% below flat plate values for $\delta/R = 0.013$ and 0.03, respectively. Recovery was slow. Turbulent Prandtl numbers were increased by 20-25% returning rapidly to flat-wall values on the recovery wall. Shear stress profiles responded quickly to curvature, reducing to about 65% of the upstream flat plate values for $\delta/R=0.03$.

1. INTRODUCTION

A better understanding of transport processes for flow over streamwise curved surfaces is required for many practical applications. One representative application is in gas turbines where accurate prediction of the heat transfer rates is critical to a successful gas turbine design. Because curvature has a significant influence on turbulent boundary layers, high performance turbomachinery design models must appropriately include its effects. Presently, the experimental data base is not sufficiently complete to develop and qualify such models. Heat transfer with sustained weak curvature, $\delta/R = 0.01$, can be predicted with the corrector proposed by Bradshaw [1], but this model fails when curvature becomes substantially greater than $\delta/R = 0.01$. The recovery process on a downstream flat wall and the effect of curvature on turbulent Prandtl number are presently not adequately modeled, even under weak curvature conditions.

The objective of the present curved boundary layer study is to broaden the data base for model development. For this study, strength of curvature, δ/R, was changed by changing the radius of curvature, R, holding the entry boundary layer thickness essentially constant The flexible wall design of the present facility allows such a study.

Previous Work

In a comprehensive survey of literature documenting the effects of streamline curvature, Bradshaw [1] pointed out that streamline curvature effects on shear stress and heat transfer are significant even for cases of δ/R~0.01. Some important findings published after the 1968 Bradshaw survey are discussed next. In 1973, So and Mellor [2], showed that normal and shear stress profiles develop self-similar shapes shortly downstream of entry to a strongly curved section. In 1979, Simon and Moffat [3] published heat transfer results for strong convex curvature and, for the first time, a flat recovery wall. Though the effect of curvature was substantial, they found little difference between cases with $\delta/R = 0.05$ and 0.08. Recovery of Stanton number differed from that of skin friction coefficient indicating a curvature effect on turbulent Prandtl number. Mayle, et al. [4] measured local heat transfer coefficients with $\delta/R = 0.01$; 120 boundary layer thicknesses downstream of the start of curvature, the Stanton number was 20% less than the flat-wall correlation on the convex surface and 33% greater on the concave surface.

In 1982 and 1984, Gibson et al. [5, 6, 7] concluded that, with $\delta/R = 0.01$, the Stanton number responds more rapidly than the skin friction coefficient to curvature change. The increase of turbulent Prandtl number was 21%. The heat transfer results of Simon and Moffat [8] and the fluid mechanic measurements of Gillis and Johnston [9] showed the effects of strong streamwise curvature and recovery from curvature on a downstream flat surface. Shear stress profiles within the curved region for two strengths of curvature (0.05 and 0.10) collapsed upon one another when plotted in $-u'v'/U_\tau^2$ vs. y/R coordinates. They concluded that cases with $\delta/R > 0.05$ were fundamentally different than weaker curved cases; the weak cases have evolving shear stress profiles while shear stress profiles for stronger curved cases have reached their asymptotic curved state.

The present study adds weaker curved heat transfer and fluid mechanics data, with recovery, to the data base. Since previous studies attained various δ/R values by varying δ, the present program was designed to change δ/R by varying R, thus testing the robustness of the strength of curvature parameter, δ/R.

2. THE EXPERIMENTAL APPARATUS

The experiment was conducted in an open-circuit, blown-type wind tunnel constructed with an upstream developing section, a curved section and a downstream recovery section (Fig. 1). Details of this wind tunnel are given in [10]. The test channel is rectangular, 68 cm in span and 11.4 cm deep. The heated test wall consists of a 1.4 m long developing section, a 1.4 m long curved section of either 0.9 m or 2.1 m radius of curvature, and a 1.4 m long recovery section.

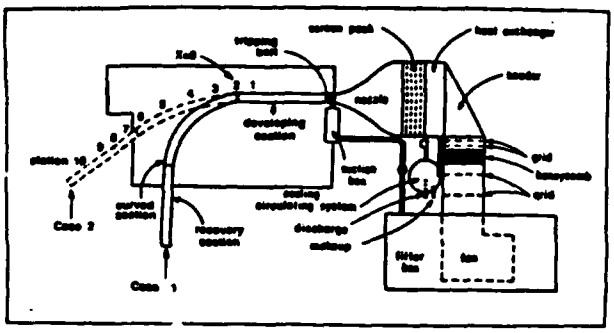

Fig. 1. Plan view of the curved boundary layer facility

The test wall (convex for this study) was heated to nominally 8°C above the free-stream air temperature with a uniform heat flux of 255 W/m^2. Static pressure on the test wall was uniform. The three sections of the channel were of similar construction except that the curved section could be bent to various radii of curvature. This gave the opportunity to systematically investigate curvature effects with a single wall. The entry section provided a mature turbulent boundary layer in the measurement area. Boundary layers entering the curved section were similar for the two cases. Stanton number data was corrected for back-side heat losses, radiation losses, streamwise conduction loss, recovery effects and the effects of temperature and humidity on fluid properties. The uncertainty of the Stanton number data was 5%.

Static pressures were measured through 0.64 mm diameter taps in the opposite walls and end-walls. In the curved region, these pressures were used to estimate the static pressure at the test wall by assuming potential flow. Mean velocity profiles were measured with a 0.34 mm ID pitot tube. Mean temperature profiles were measured with a 2-D boundary layer thermocouple probe. Turbulence measurements were taken in an isothermal flow with a constant temperature hot-wire anemometer; a horizontal wire for normal stress measurements and a cross-wire for shear stress measurements. The digitized anemometer signals were computer-linearized and processed. Signals from the cross-wire probe were digitized simultaneously. Averages were taken over a period of 40 seconds.

2.1 Qualification Test

The mean velocity measured in the potential core of the developing section, nominally 16 m/s, was uniform to 0.2% and the mean temperature, nominally 26°C was uniform to 0.03°C. Heat flux on the test wall was uniform to within 1% and the potential velocity was uniform to 3% in C_p. Free-stream turbulence intensity, normalized by U_{pw} was 0.65%. Spanwise variations of the Stanton number, measured within the central span of 30 cm, were typically less than 5%. Secondary flow measurements, taken with a Conrad probe, showed skew angles of less than 2 degrees within the curve and 3 degrees within the recovery section. Energy and momentum balances over the full test region showed closure to within 5% and 3%. From the above, it was felt that the boundary layer was sufficiently two-dimensional and that secondary flow effects were minimal.

3. RESULTS AND DISCUSSION

Descriptors for the two cases discussed herein are listed in Table 1. As shown, Cases 1 and 2 have similar flow conditions upon entry to the curve; they differ only in radius of curvature.

Table 1. Descriptors of Cases 1 & 2 and locations of stations

Case	R (cm)	U_{pw} (m/s)	T.I. (%)	δ/R (θ/R) Beginning of curvature	δ/R (θ/R) End of curvature
1	90	16.32	0.65	0.03 (0.0036)	0.04 (0.0054)
2	210	17.12	0.65	0.013 (0.0016)	0.019 (0.0025)

Case	STA.	1	2	3	4	5
1	X(cm)	-29.9	---*	26.2	52.8	79.8
	Re_θ	2737	---	3987	4287	4602
2	X(cm)	-29.9	0.0	27.9	56.1	85.3
	Re_θ	2916	3565	3814	4539	4661

Case	STA.	6	7	8	9	10
1	X(cm)	106.7	133.4	150.6	178.6	208.5
	Re_θ	5056	5140	5589	6146	6580
2	X(cm)	113.5	141.0	158.8	186.7	214.6
	Re_θ	5622	5738	6022	6417	7010

*No data taken due to proximity to a 0.025 mm step.

3.1 The Base Case: R = 90 cm; δ/R = 0.03-0.04

The Reynolds number based on the momentum thickness was 2740 and the shape factor was 1.42 at Station 1 indicating a mature turbulent boundary layer.

Fig. 2 shows mean velocity profiles plotted in inner coordinates. Skin friction coefficients were deduced from the velocity profile (the Clauser technique [11]) and the Van Driest relationship. The stabilizing effect of convex-curvature reduces the length of the log-linear region slightly and enhances the wake greatly. One sees that curvature affects only the outer region, $Y^+>150$. The existence of the log-linear region within $Y^+<150$ indicates that the near-wall layer has normal structure. This lends support to the use of the Clauser technique. No direct measurements of wall shear stress were taken. At Station 10 in the recovery section, the log-linear region appears to have recovered completely, but the wake is not growing normally. In fact, the wake is decreasing slightly in strength. This indicates that recovery is not complete.

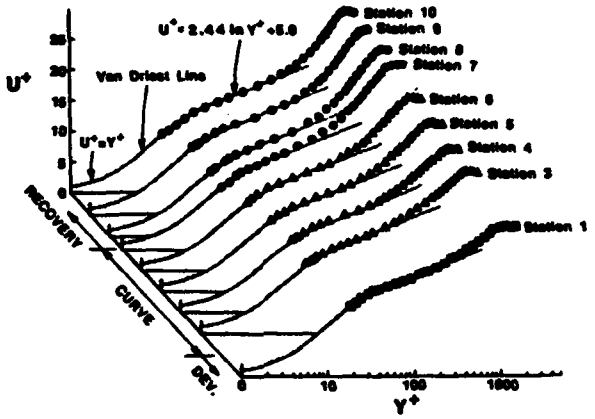

Figure 2. Mean velocity profiles, Case 1, the base case.

The rates of growth of the boundary layer parameters, δ, δ^*, and θ, were reduced by curvature, resuming in the recovery region. The shape factor increased from 1.42 to 1.52 by the end of the curved section, then decreased slowly within the recovery section. The reduced rate of growth of the momentum thickness and the increasing shape factor within the curve are associated with a more laminar-like shape of the velocity profiles characterized by the growth of the wake. These are the effects of a decrease in turbulent transport in the outer (wake) regions due to curvature.

Fig. 3 shows mean temperature profiles plotted in wall coordinates. They show a response to curvature that is similar to that observed in the velocity profiles. The mean temperature data is expected to follow $T^+ = Pr \cdot Y^+$ near the wall and $T^+ = (Pr_t/0.41)\ln(Y^+/Y_{C1}^+)+Pr \cdot Y_{C1}^+$ in the log-linear region. The mean temperature profiles were fit using this turbulent log-linear correlation assuming Pr_t and Y_{C1}^+ are free parameters to determine their values. The effective average turbulent Prandtl number deduced from the profiles were increased about 25% by curvature, then quickly returned to 0.88 (Fig. 7).

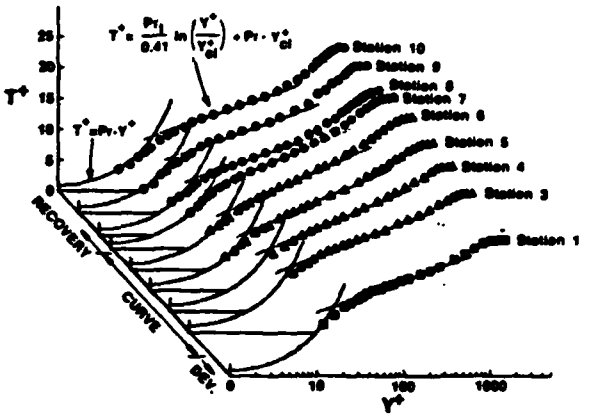

Figure 3. Mean temperature profiles, Case 1, the base case.

Fig. 4 shows the local Stanton number and skin friction coefficient values comparing the curved-wall results to flat-wall values predicted by the boundary layer code STAN5 [12]. The effects of curvature are dramatic. Stanton number responds immediately upon entry to the curve, decreasing about 15% by x = 30 cm and continuing to decrease slowly thereafter. The same trend can be observed for the skin friction coefficient. Recovery of the skin friction coefficient is slower than that of the Stanton number, as was observed in [8] and [9]. Stanton numbers increase to within 13% of the flat-plate value 80 cm downstream of the end of curvature while skin friction coefficients remain 20% below. The rapid decrease of effective average Pr_t is consistent with this increase of $2St/C_f$ in the recovery section.

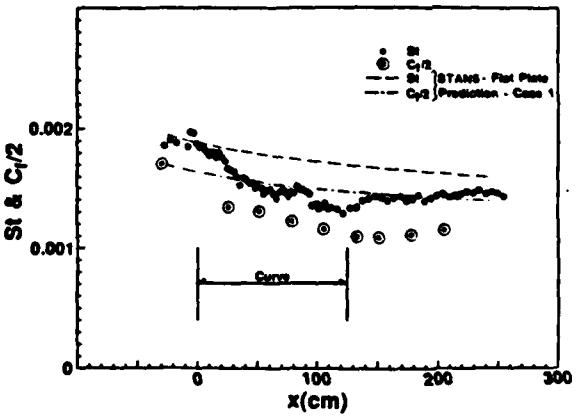

Figure 4. Stanton number and skin friction coefficient vs. streamwise distance, Case 1, the base case.

Turbulence intensity profiles are shown in Fig. 5. The upstream flat-wall profile (Re_θ~2700) was found to lie between the two profiles given by Klebanoff (Re_θ~7500), [13, 14] and compared well with previous researchers' results. Between Stations 1 and 3 the near-wall peak dramatically falls while the remainder of the profile

(y/δ > 0.1) is less affected. The response to the introduction of convex curvature is complete by Station 4 and a self-similar shape continues through the remainder of the curve. The u' profiles, then, indicate an immediate response of turbulence quantities upon entry to curvature followed by a more gradual adjustment within the curve; this is consistent with the St and $C_f/2$ trends in Fig. 4. The return to flat-plate profiles on the recovery wall is different. A peak appears at y/δ = 0.1-0.2 at the beginning of the recovery process and diffuses slowly outward. By Station 9, the recovery of turbulence is complete beyond y/δ = 0.2, but the near-wall data shows no change from profiles taken at the beginning of recovery. The slow near-wall recovery is consistent with the slow response of skin friction coefficient observed in Fig. 4. It is expected that the profile eventually returns to the Station 1 shape as $C_f/2$ returns to flat-wall values. The recovery length of the present experiment was too short to observe this, however.

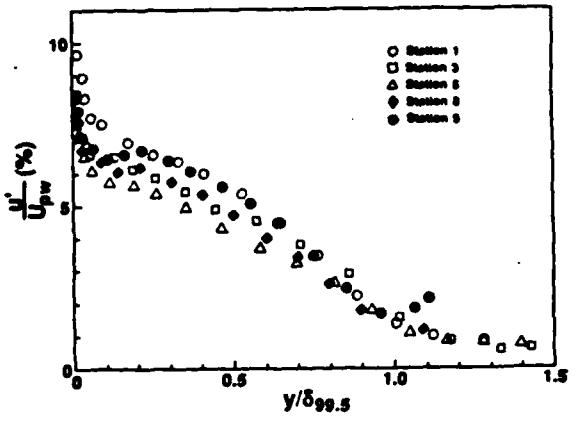

Figure 5. Streamwise-normal turbulence intensity profiles, Case 1, the base case.

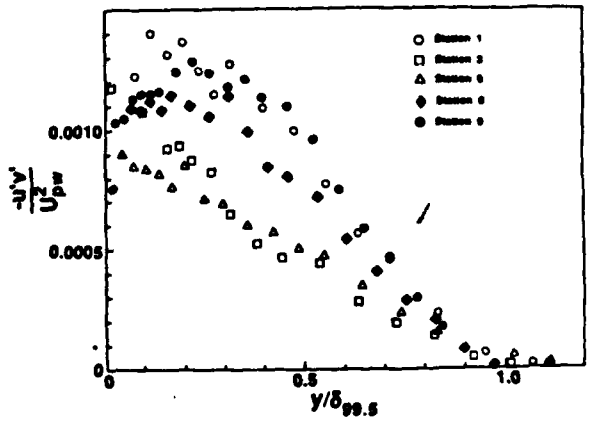

Figure 6. Reynolds shear stress profiles, Case 1, the base case.

Shear stress profiles are shown on Fig. 6. They respond quickly to curvature but do not change appreciably after Station 3. The u' profiles also respond quickly to the introduction of curvature but continue to evolve until Station 4. Curvature reduces shear stress by about 45% throughout the boundary layer. Recovery is slow and continuous through Station 9, where the magnitudes of the shear stress are comparable to, or greater than, the magnitudes at Station 1 for the outer 75% of the boundary layer thickness. A maximum shear stress in the recovering profiles occurs away from the wall, moving to larger values of y/δ as recovery proceeds. The near-wall shear stress is affected by recovery very little. This is consistent with the observed trends in $C_f/2$.

3.2 The Effect of Radius of Curvature: Introduction of a Comparison Case with R = 210 cm; δ/R = 0.013-0.019

The comparison case, one of weaker curvature than the base case, was achieved by bending the wall to a larger radius of curvature. A momentum thickness Reynolds number of 2920 and a shape factor of 1.42 at Station 1 indicate similar flow conditions with those of the base case. Mean and turbulence profiles for Station 1 were also nearly identical. Stanton number values on the pre-plate were only about 2.5% lower than those of Case 1; skin friction values were about 1% lower. Evolution of mean velocity and temperature profile integral parameters and shape factor confirm the same trends discussed for the base case. A comparison of Pr_t for the two cases is shown on Fig. 7. Less of an effect on Pr_t for the weaker-curved case is observable. Local Stanton number data (Fig. 8) show a 10% reduction from plane-wall values for this case compared to a 20% reduction for the base case (which has approximately twice the value of δ/R). The comparison of these two cases supports the conclusion that δ/R is an appropriate scaling parameter over this range of δ/R.

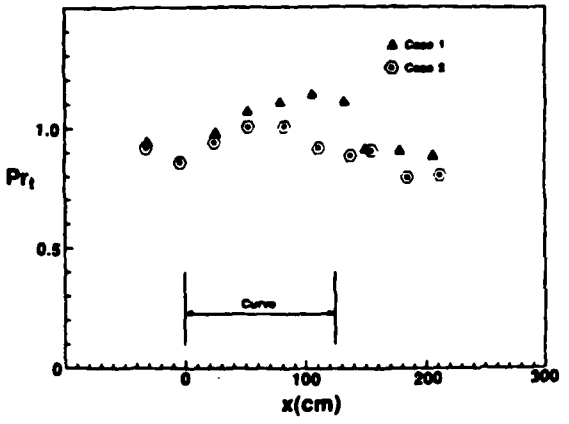

Figure 7. Turbulent Prandtl number vs. streamwise distance, Cases 1 and 2.

The comparison of turbulence intensity profiles for the two cases, at Station 5 (Fig. 9) shows that the profiles are similar but that the Case 2

profile is still evolving while the Case 1 profile has reached an asymptotic shape (by Station 4 as shown in Fig. 5). A comparison of turbulence intensity profiles for Station 9

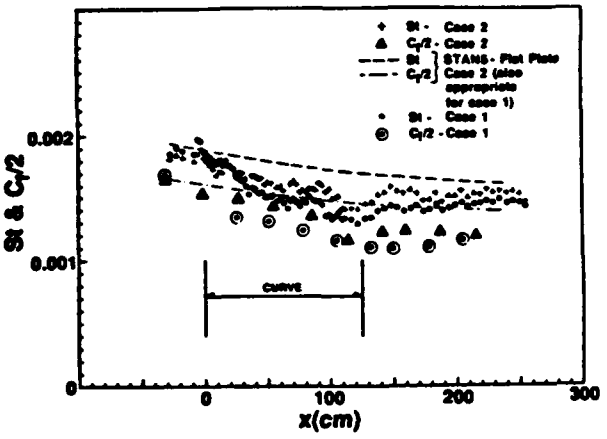

Figure 8. Stanton number and skin friction coefficient vs. streamwise distance (comparison between Cases 1 and 2).

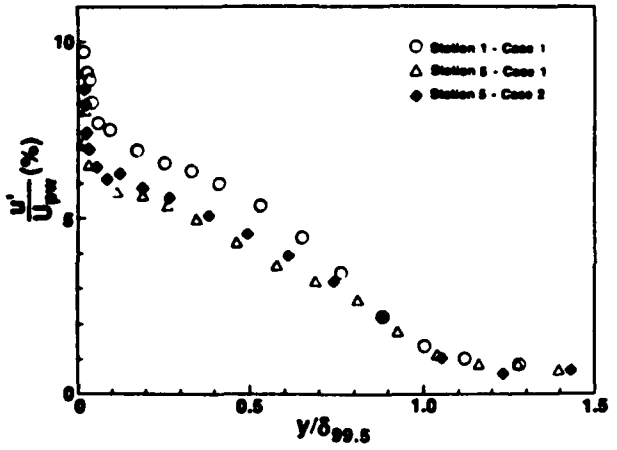

Figure 9. Streamwise-normal turbulence intensity profiles at Station 5 (near the end of the curved section), comparison between Cases 1 & 2.

(Fig. 10) shows that the Case 2 profile recovery is more complete; only the near-wall portion differs from the Station 1 flat-wall profiles. Profiles of shear stress plotted in $-u'v'/U_\tau^2$ vs. y/R coordinates for two cases are given on Fig. 11. The solid line is the "asymptotic profile" ($\delta/R > 0.05$) suggested by Gillis and Johnston [9], while the dashed line is a mild curvature profile measured by Hoffmann and Bradshaw [15]. The base case (Case 1) results support the suggestion by Gillis and Johnston that the appropriate scaling parameter for turbulent structure for strongly curved flows is the radius of curvature, rather than boundary layer thickness. The base case data show that the flow approaches this same asymptotic profile for $\delta/R > 0.04$. Though the base case profiles appear to be approaching an asymptotic shape, it is clear that the weaker-curved Case 2 profiles are more characteristic of those observed in previous, mild-curvature experiments. The two cases, therefore, represent examples of weak and moderate-to-strong curvature cases, as viewed in these coordinates.

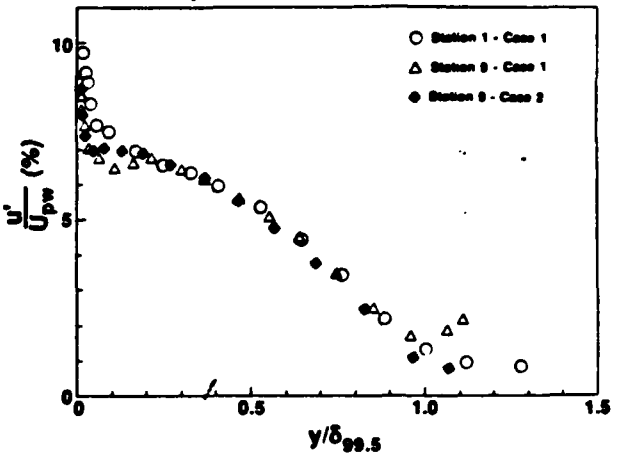

Figure 10. Streamwise-normal turbulence intensity profiles at Station 9 (near the end of the recovery section), comparison between Cases 1 & 2.

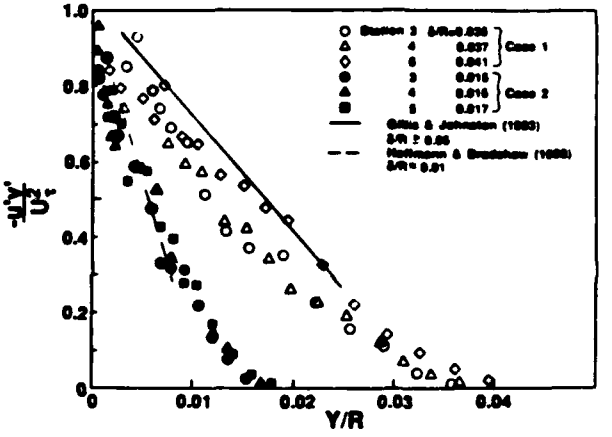

Figure 11. Turbulent shear stress profiles within the curved section, comparison between Cases 1 & 2.

4. SUMMARY AND CONCLUSIONS

Significant additions to the data base are:
1) The recovery process with heat transfer was investigated for cases of milder curvature than previously studied.
2) The radius of curvature was varied from case to case in the same study and data was taken for two δ/R values representing mild and moderately strong curvature using the same apparatus.

Conclusions are:
1) Profiles of mean velocity and temperature show shortened log-linear regions and enhanced wake regions in the curve. The recovery of these mean profiles in the log-linear region is complete by about 80 cm of recovery length.
2) Curvature increases turbulent Prandtl number by about 20-25% for the cases studied.
3) A rapid decrease of St and $C_f/2$ at the beginning of the curve is observed followed by a

slow decrease within the curve. Decreases of about 20 and 10% from expected flat-wall values are observed for Cases 1 ($\delta/R = 0.03$) and 2 ($\delta/R = 0.013$), respectively. Recovery is extremely slow with St recovery leading $C_f/2$ recovery, resulting in an increase of $2St/C_f$.

4) Normal stress profiles show a fast response to the beginning of curvature. During recovery an increase of turbulence intensity originates near the wall at $y/\delta \sim 0.1$-0.2 propagating slowly to the outer layers.

5) Shear stress profiles respond quickly to curvature, reducing to about 55% of the upstream flat-plate values for $\delta/R = 0.03$. Recovery occurs slowly, with the wake recovering faster than the near-wall flow.

6) Asymptotic behavior is observed for flows with $\delta/R > 0.04$.

ACKNOWLEDGEMENTS

This study was supported by the Air Force Office for Scientific Research grant number F 49620-83-C0062. The grant monitor is Dr. James D. Wilson. Additional support was provided by the Graduate School of the University of Minnesota and by the AMOCO Foundation.

NOMENCLATURE

$C_f/2$	Skin friction coefficient
C_p	Static pressure coefficient, $(P_{sw}-P_{sw,ref})/(\frac{1}{2}\rho U_{pw}^2)$
M	Mach number
R	Radius of curvature
Re	Reynolds number (using U_{pw} as characteristic velocity)
T^+	Normalized mean temperature, $(T_w-T)\rho C_p U_\tau/q_w$
U	Streamwise mean velocity
U^+	Normalized streamwise velocity, U/U_τ
U_τ	Shear velocity, $\sqrt{\tau_w/\rho}$
u'	Root-mean-square of fluctuating streamwise velocity
v'	Root-mean-square of fluctuating velocity normal to the test wall
-u'v'	Reynolds shear stress
x	Streamwise distance
y	Distance normal to the test wall
Y^+	Normalized distance normal to the test wall, yU_τ/ν
Y_{cl}^+	Conduction layer thickness in inner coordinates

Greek Letters

δ	Boundary layer thickness based on 99.5% of potential flow velocity
δ^*	Displacement thickness
θ	Momentum thickness

Subscripts

p	Potential flow
pw	Potential flow value at the wall
ref	At the reference station (Station 1)
s	Static
sw	Static conditions on the test wall
w	Wall value
∞	Free-stream value

REFERENCES

1. Bradshaw, P., Effects of Streamline Curvature on Turbulent Flow, AGARDograph No. 169, 1972.
2. So, R. M. C., and Mellor, G. L., Experiment on Convex Curvature Effects in Turbulent Boundary Layers, JFM, Vol. 60, pp. 43-62, 1973.
3. Simon, T. W., and Moffat, R. J., Turbulent Boundary Layer Heat Transfer Experiments: A Separate Effects Study on a Convexly Curved Wall, J. of Heat Transfer, 81-HT-78, Feb. 1982.
4. Mayle, R. E., Blair, M. F., and Kopper, F. C., Turbulent Boundary Layer Heat Transfer on Curved Surfaces, J. of Heat Transfer, Vol. 101, No. 3, Aug. 1979.
5. Gibson, M. M., Verriopoulos, C. A. and Nagano, Y., Measurements in the Heated Turbulent Boundary Layer on a Mildly Curved Convex Surface, Proc. 3rd Symp. on Turbulent Shear Flows, 1982.
6. Gibson, M. M., Verriopoulos, C. A., and Vlachos, N. S., Turbulent Boundary Layer on a Mildly Curved Convex Surface, Part 1: Mean Flow and Turbulence Measurements, Exp. Fluids 2, pp. 17-24, 1984.
7. Gibson, M. M., and Verriopoulos, C. A., Turbulent Boundary Layers on a Mildly Curved Convex Surface, Part 2: Temperature Field Measurements, Exp. Fluids 2, pp. 73-80, 1984.
8. Simon, T. W., and Moffat, R. J., Convex Curvature Effects on the Heated Turbulent Boundary Layers, Proc. 7th Int. Heat Transfer Conf., Vol. 3, pp. 295-301, 1982.
9. Gillis, J. C., and Johnston, J. P., Turbulent Boundary-Layer Flow and Structure on a Convex Wall and its Redevelopment on a Flat Wall, JFM, Vol. 135, pp. 123-153, 1983.
10. You, S. M., Turbulent Boundary Layer Heat Transfer and Fluid Mechanics Measurements on a Curved Convex Wall, M.S.M.E. Thesis, University of Minnesota, Minneapolis, MN, March 1986.
11. Clauser, F. G., Advances in Applied Mechanics, Vol. IV, Academic Press, pp. 1-151, 1956.
12. Crawford, M. E., and Kays, W. M., STAN5—A Program for Numerical Compuation of Two-Dimensional Internal and External Boundary Layer Flows, NASA CR-2742, Dec. 1976.
13. Klebanoff, P. S., and Diehl, Z. W., Some Features of Artificially Thickened Fully Developed Turbulent Boundary Layers with Zero Pressure Gradient, National Bureau of Standards Rep. 1110, Sept. 1950.
14. Klebanoff, P. S., Characteristics of Turbulence in a Boundary Layer with Zero Pressure Gradient, National Bureau of Standards Rep. 1247, 1953.
15. Hoffmann, P. H., and Bradshaw, P., Turbulent Boundary Layers on Surfaces of Mild Longitudinal Curvature, Imperial College, Aero. Rept. 78-04, Dec. 1978.

THE AMERICAN SOCIETY OF MECHANICAL ENGINEERS
345 E. 47 St., New York, N.Y. 10017

86-WA/HT-46

Free-Stream Turbulence Effects on Convexly Curved Turbulent Boundary Layers

YOU, S. M., SIMON, T. W., and KIM, J.
University of Minnesota
Minneapolis, Minnesota

ABSTRACT

Free-stream turbulence intensity effects on the convex-curved turbulent boundary layer are investigated. An attached fully turbulent boundary layer, grown on a flat plate, is introduced to a convex wall of constant radius of curvature. Two cases with free-stream turbulence intensities of 1.85% and 0.65%, taken in the same facility with moderate curvature, $\delta/R = 0.03$-0.045, are compared. The two cases have similar flow conditions upon entry to the curve, thus separating free-stream turbulence effects within the curve from the other effects. The higher turbulence case shows stronger curvature effects on $C_f/2$ and on streamwise normal and shear stress profiles than those observed in the lower turbulence case. The case with increased turbulence has a higher ($\sim 5\%$) $C_f/2$ value upstream of the curve than the $C_f/2$ value of the lower turbulence case, as expected, but this increase disappears by the end of the curve where nearly identical $C_f/2$ values are found. Similarly, streamwise turbulence intensity profiles, differing upstream of the curve for the two cases, are found to be similar near the end of the curve; this indicates a dominating effect of curvature over the effect of turbulence intensity. Many effects of curvature observed in the lower turbulence intensity case, e.g., a dramatic response to the introduction of curvature, are also seen in the higher turbulence case.

NOMENCLATURE

$C_f/2$	Skin friction coefficient
C_p	Static pressure coefficient, $2(P_{s,w} - P_{s,ref})/\rho U^2_{pw,ref}$
c_p	Specific heat
H	Shape factor
P	Pressure
Pr	Prandtl number
Pr_t	Turbulent Prandtl number
$\dot{q}''$	Heat flux
R	Wall radius of curvature
Re	Reynolds number
St	Stanton number
T	Mean temperature
T^+	Normalized mean temperature, $(T_w - T_\infty)U_\tau/(\dot{q}''_w/\rho c_p)$
T.I.	Turbulence intensity
U	Streamwise mean velocity
U^+	Normalised streamwise velocity, U/U_τ
U_τ	Shear velocity, $\sqrt{\tau_w/\rho}$
u'	Fluctuating component or root-mean-square of fluctuating streamwise velocity
$-\overline{u'v'}$	Reynolds shear stress
v'	Fluctuating component of velocity normal to the test wall
x	Streamwise distance
y	Distance normal to the test wall
Y^+	Normalised distance normal to the test wall, yU_τ/ν
Y^+_{Ci}	Conduction layer thickness in inner coordinates

Greek Letters

δ	Boundary layer thickness based on 99.5% of potential flow velocity
θ	Momentum thickness
κ	Karman constant, 0.41
ν	Kinemetic viscosity
ρ	Density
τ	Shear stress

Subscripts

pw	Potential flow value at the wall
ref	Reference
s	Static
w	Wall value
∞	Free-stream value

1. INTRODUCTION

The present experimental study was conducted to enhance the knowledge of curved turbulent flows and to expand the data base used for development of computational models, particularly those applied to gas turbine design. Despite the considerable work on the effects of curvature, the present study is the first showing the effect of turbu-

Presented at the Winter Annual Meeting
Anaheim, California — December 7-12, 1986

lence intensity on convex-curved turbulent boundary layer flows. It is important to investigate the effect of turbulence intensity with curvature since accurate predictions of skin friction and heat transfer, under the combined effects of curvature and free-stream turbulence intensity, are needed in the design of fluid machinery where the blades are operated in highly turbulent environments. Free-stream turbulence intensity can be as high as 20% in the gas turbine. The present study is a continuation of the convex curvature turbulent boundary layer study presented by You, et al. [1] in which two lower turbulence cases of different radii of convex curvature were tested ($\delta/R = 0.013$ and 0.03). The stronger curved case of the two is the base case for the present study which isolates the turbulence intensity effect.

1.1 Previous Work

Bradshaw [2] published a comprehensive survey of the literature on the effects of streamwise curvature in 1973 showing that the ratio of boundary layer thickness to radius of wall curvature, δ/R, was an appropriate descriptor for the strength of curvature. Experimental studies [3,4,5] published after the Bradshaw survey confirmed earlier findings that streamwise curvature has a marked effect on turbulence structure, heat transfer, and skin friction.

Carefully controlled and detailed experiments on mild ($\delta/R = 0.01$) and strong ($\delta/R > 0.05$) convex-curved boundary layers were performed by Gibson [6,7,8], Simon [9,10,11,12], and Gillis [13,14] and their co-workers.

In 1986, You, et al. [1] added heat transfer and fluid mechanics data on a mildly-curved convex surface, with recovery from curvature, to the data base. This test was designed so that δ/R could be changed by varying R in a single test facility from mild ($\delta/R = 0.013$) to moderately strong ($\delta/R = 0.03$). Though both cases show the same trends, the effects of the different strengths of curvature are clearly observable. Some observations were:

(1) The percentage decrease in St and $C_f/2$ from expected flat-wall values is almost an order of magnitude greater than the value of δ/R; 10% decrease for $\delta/R = 0.013$ and 20% for $\delta/R = 0.03$.

(2) The turbulent Prandtl number deduced from the mean velocity and temperature profiles increases within the curve about 20% for $\delta/R = 0.013$ and 25% for δ/R =0.03.

(3) Shear stress profiles, plotted in $-\overline{u'v'}/U_{pw}^2$ vs. y/δ show a self-similar shape within the curve, even for the weaker curvature case.

More details of recent studies on the effects of streamwise curvature are given in [15].

Many investigations have been reported on the effect of free-stream turbulence; some of the recent ones are Meier and Kreplin [16], Simonich and Bradshaw [17] and Blair [18,19]. Meier and Kreplin [16] concluded that increased free-stream turbulence levels increase skin friction and boundary layer growth rate and that mean velocity profiles become similar in shape to those of pipe flow. They also suggested that, for turbulence levels less than 1%, $C_f/2$ changes proportionally to $(u'/U)_\infty^2$ and for turbulence levels higher than 1%, $C_f/2$ changes proportionally to $(u'/U)_\infty$.

Simonich and Bradshaw [17] investigated the effect of free-stream turbulence on heat transfer. Their measurements, with turbulence intensities up to 7%, showed that Stanton numbers increased with increasing free-stream turbulence.

In 1983, several tests were conducted by Blair [18,19] in a zero pressure gradient two-dimensional channel, with turbulence intensities varying from 0.25% to 7%, showing the effects of free-stream turbulence on turbulent boundary layer heat transfer and hydrodynamics. He concluded that a free-stream turbulence intensity of 6% increased skin friction and heat transfer rates approximately 14% and 18%, respectively. He also found that the Reynolds analogy factor ($2St/C_f$) increased by just over 1% for each 1% increase in free-stream turbulence intensity.

2. EXPERIMENTAL APPARATUS

The present experiment was conducted in an open-circuit, blown-type wind tunnel constructed with an upstream developing section, a curved section and a downstream straight section (Fig. 1). Details of this wind tunnel are given in [15]. The test channel is rectangular, 68 cm in span and 11.4 cm deep. The heated test wall consists of a 1.4 m long developing section and a 1.4 m long curved section of 0.9 m radius of curvature followed by a straight section.

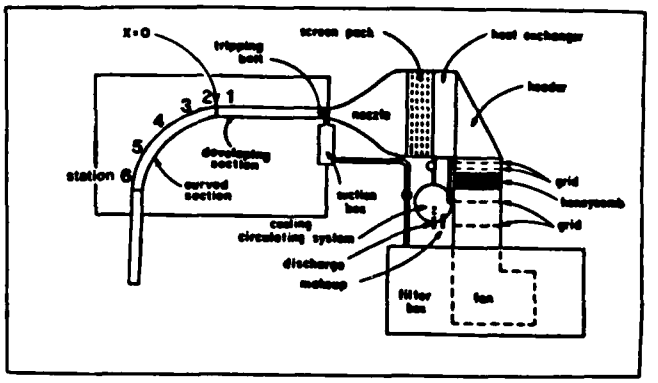

Fig. 1 Plan View of the Curved Boundary Layer Facility.

The laminar boundary layer was tripped in the lower-turbulence case, with a 1.0 mm high, 12.7 mm wide strip beginning 10 cm downstream of a suction slot — a mature turbulent boundary layer was established in the measurement area. Higher turbulence levels were obtained by inserting a coarse grid constructed of 2.5 cm aluminum strips in a square array on 10 cm centers at the entrance of the nozzle. A turbulence intensity, normalized by U_{pw}, of 1.85% was achieved in the test region. In the higher turbulence case, the trip was removed and the boundary layer was allowed to pass naturally through transition. Stanton numbers were spanwise uniform to within 4% upstream of the curve in both cases. It was previously shown that spanwise uniformity is maintained during natural transition with 2% turbulence intensity [20,21].

The test wall was heated to nominally 8°C above the free-stream temperature with a uniform heat flux of 255 W/m^2. Static pressure on the test wall was uniform. Stanton number data was corrected for back-side heat loss, radiation loss, streamwise conduction loss, recovery effects and the effects of temperature and humidity on fluid properties. The uncertainty in the Stanton number data was approximately 5%.

Static pressures were measured through 0.64 mm diameter taps in the opposite wall and end walls. In the curved region, these pressures were used to estimate the static pressure at the test wall assuming potential flow. Mean velocity profiles were measured with a 0.34 mm ID pitot tube. Mean temperature profiles were measured with a 2-D boundary layer thermocouple probe. Turbulence measurements were taken in an isothermal flow with constant temperature hot-wire anemometry; a horizontal wire for normal stress measurements and a cross-wire for shear stress measurements. The digitized anemometer signals were computer-linearized and processed. Signals from the

cross-wire probe were digitized simultaneously. Averages were taken over a period of 40 seconds.

2.1 Qualification Test

The mean velocity measured in the potential core of the developing section, nominally 16 m/s, was uniform to 0.2% and the mean temperature, nominally 20°C, was uniform to 0.05°C. Heat flux on the test wall was uniform to within 1% and C_p was uniform to within 3%. Free-stream turbulence intensity values, normalized by U_{pw} were 0.65% and 1.85% in the test region. Spanwise variations of Stanton numbers, measured within the central span of 30 cm, were typically less than 5%. Secondary flow measurements, taken with a Conrad probe, showed skew angles of less than 2 degrees within the curve. Energy and momentum balances over the full test region showed closure to within 5% and 3%, respectively. This ensured that the boundary layer was sufficiently two-dimensional and that secondary flow effects were minimal.

3. RESULTS AND DISCUSSION

Descriptors of the two cases and locations of the profile measurement stations are listed in Tables 1 and 2. Measurements of mean velocity profiles and streamwise turbulence intensity profiles at station 1, which served to characterize the state of each boundary layer, are presented in Figs. 2 and 3, respectively. These profiles were compared with the measurements of Hama [22] and Schultz-Grunow [23]. It was concluded from the excellent agreement with case 1 that the boundary layer achieved by artificial tripping has the characteristics of a turbulent boundary layer with zero pressure gradient on a smooth wall. The mean velocity profile of case 2 differs from that of the other cases, showing the effect of turbulence intensity. Turbulence intensity profiles at station 1 for the two cases were compared to show the effect of the higher free-stream turbulence intensity. The upstream flat-wall turbulence intensity profiles (Re_θ = 2737) for the lower turbulence case lie between the two profiles given by Klebanoff (Re_θ = 7500, Ref. 24 and 25) and compare well with previous researchers' results, e.g., Gillis and Johnston [13].

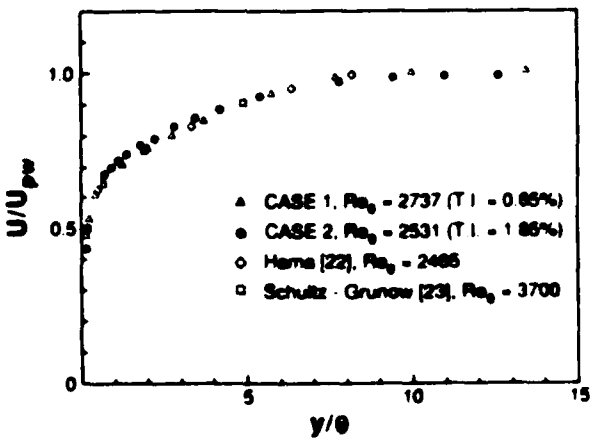

Fig. 2 Comparison of Mean Velocity Distributions at Station 1 (Cases 1 and 2).

Table 1 Descriptors of CASES 1 & 2

	CASE 1	CASE 2	
R	90	90	(cm)
U_{pw}	16.32	15.83	(m/s)
T.I.	0.65	1.85	(%)
δ/R at B.O.C.*	0.03†	0.039†	
δ/R at E.O.C.*	0.04†	0.045†	
Re_θ at B.O.C.*	3405†	3030†	

*B.O.C.—Beginning of Curvature (s=0 cm)
*E.O.C.—End of Curvature (s=125 cm)
†Estimated Values

Table 2
Locations of Stations

Stations	x (cm)*	Case 1 Re_θ (T.I.) [H]	Case 2 Re_θ (T.I.) [H]
1 (Dev.)	-29.9	2737 (0.74) [1.42]	2531 (1.85) [1.37]
3 (Cur.)	26.2	3987 (0.65) [1.47]	3468 (1.86) [1.42]
4 (Cur.)	52.8	4287 (0.64) [1.48]	3814 (1.82) [1.43]
5 (Cur.)	79.4	4602 (0.68) [1.51]	4131 (2.10) [1.48]
6 (Cur.)	106.7	5056 (0.75) [1.52]	4290 (2.55) [1.51]
End of Curve	125.0		

* Mean velocity and temperature profiles were measured at these stations; corresponding turbulence measurements stations were 10.2 cm (4 in) downstream.

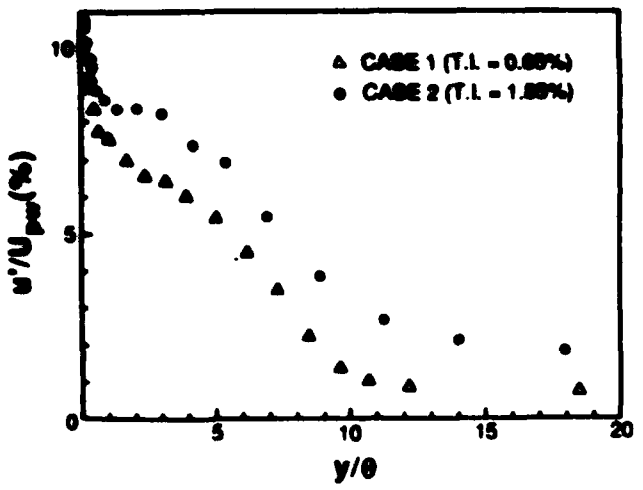

Fig. 3 Comparison of Streamwise-normal Turbulence Intensity Profiles at Station 1 (Cases 1 and 2).

A Summary of the Base Case (Case 1)

The effects of streamwise convex curvature on a turbulent boundary layer, as seen in the base case, are:

(1) Mean velocity and temperature profiles show shortened log-linear regions and enhanced wake regions in the curve.

(2) Curvature increases the turbulent Prandtl number, deduced from the mean velocity and temperature profiles, by about 25%.

(3) Reduced momentum thickness growth rate and increased shape factor, H, within the curve are observed.

(4) A rapid decrease of St and $C_f/2$ at the beginning of the curve is observed followed by a slow decrease within the curve. They become 20% lower than the expected flat-wall values.

(5) Streamwise-normal turbulence intensity profiles show a fast response to the introduction of curvature with a large reduction of the near-wall peak. A self-similar shape is attained mid-way through the curve and continues throughout the curve.

The effect of varying the radius of curvature on curved 2-D boundary layers, including the process of recovery from curvature, was previously investigated and reported in [1]. In [1] and [15], the base case of the present study was discussed in detail. The present paper uses this base case and a higher-turbulence comparison case to discuss the effect of turbulence intensity on curved turbulent boundary layer flows.

The Effect of Turbulence Intensity : Introduction of a comparison case with R = 99 cm; δ/R = 0.099 – 0.045 and T.I. = 1.85% (Case 2)

The comparison case has similar flow conditions with the base case except that the turbulence intensity, normalized on the free-stream velocity, was 1.85% instead of 0.65% (see Table 1). Though measurements were taken and could have been reported for the straight section downstream of the curve, rapid growth of the boundary layers resulted in the disappearance of the potential core in this region. Therefore, a comparison of the two cases in this region to show the free-stream turbulence intensity effect would not have been meaningful. For this reason, no data downstream of the curve is discussed in the present paper.

Mean velocity profiles at station 1 for the two cases (T.I. = 0.65% and 1.85%) are presented in Fig. 4. They demonstrate that free-stream turbulence mainly affects the outer part of the boundary layer (wake region). Despite the considerable depression of the wake region of case 2, the log-linear regions of the two velocity profiles are similar and obey the law of the wall. At station 1, the Reynolds number based on the momentum thickness is 2531 and the shape factor is 1.37 for case 2, while the case 1 Reynolds number and shape factor are 2737 and 1.42, respectively. The momentum thickness Reynolds numbers therefore match to within 10% for the two cases. The shape factors are expected to differ due to the effect of turbulence intensity on the profile shape. The streamwise evolutions of mean velocity and temperature profiles are shown in Figs. 5 and 6. One can observe the effects of curvature — the enhanced wake regions and the shortening of the log-linear regions. It is interesting that the enhancement of the wake region due to curvature (δ/R = 0.099) is more influential than the depression of the wake due to turbulence intensity (T.I. = 1.85%). This can be observed by comparing the data for the two cases at stations 1 (Fig. 4) and 6 (Fig. 7) — the mean velocity profiles of both cases at station 6 are similar; a contrast to the flat-plate profiles (station 1, Fig. 4) where the effect of turbulence intensity is quite visible. The value of the shape factor at station 1 for the higher turbulence intensity case is about 3.6% lower than that of the lower turbulence intensity case (Fig. 8). The shape factor for case 2 increases faster than that of the base case within the curved region and becomes comparable to the base case value at the end of the curve. This indicates a vanishing of the turbulence intensity effect — also seen in the velocity profiles.

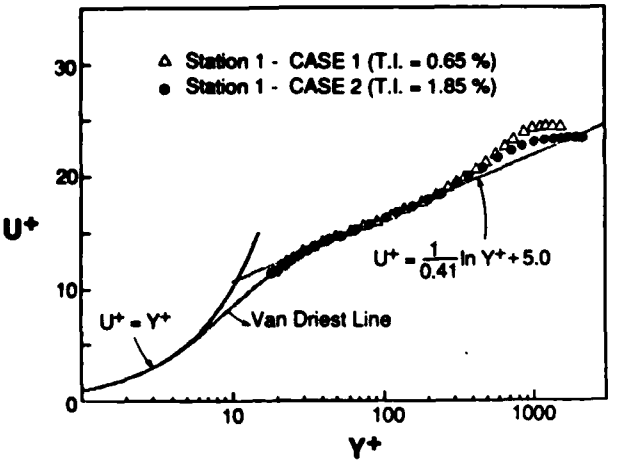

Fig. 4 Comparison of Mean Velocity Profiles at Station 1 (Cases 1 and 2).

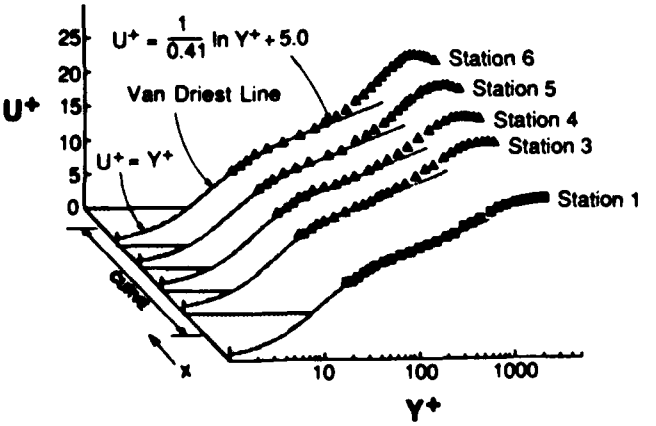

Fig. 5 Mean Velocity Profiles, Case 2 (T.I.=1.85%).

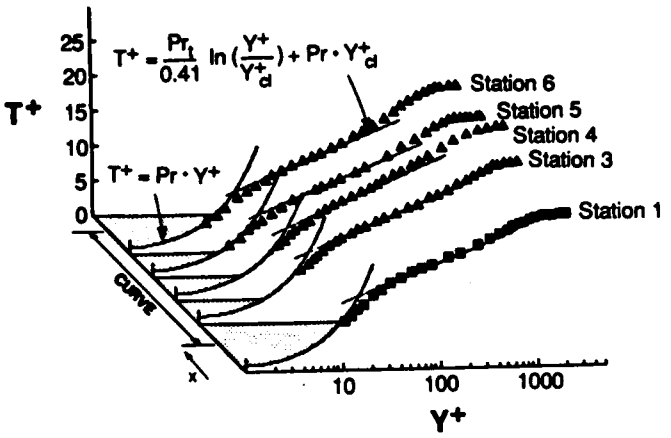

Fig. 6 Mean Temperature Profiles, Case 2 (T.I.=1.85%).

Stanton numbers and skin friction coefficients are compared in Fig. 9. St and $C_f/2$ for the higher turbulence case (T.I. = 1.85%) measured at station 1 are about 5% larger than those of case 1. Curvature is seen to affect the higher free-stream turbulence data more than the corresponding lower turbulence data, as evidenced by the $C_f/2$ values; although $C_f/2$ is higher for the higher T.I. case at the entrance to the curve, there is no difference in the values by the end of the curve. Stanton numbers for both cases showed similar reductions in spite of the enhanced curvature effect on $C_f/2$ for the higher turbulence intensity case. Turbulent Prandtl numbers deduced from the mean velocity and temperature profiles (Fig. 10) support the same trend as observed in Fig. 9. They decrease near the end of the curved region in case 2, while in case 1 they increase continuously throughout the curve. This is consistent with the increase of $2St/C_f$ at stations 5 and 6 in case 2 due to a larger effect on $C_f/2$ than on St. Turbulent Prandtl numbers are found by forcing the mean temperature profile to obey the thermal law of the wall. The curve and data are matched by choosing the appropriate values of Pr_t and Y^+_{cl}, as discussed in [15].

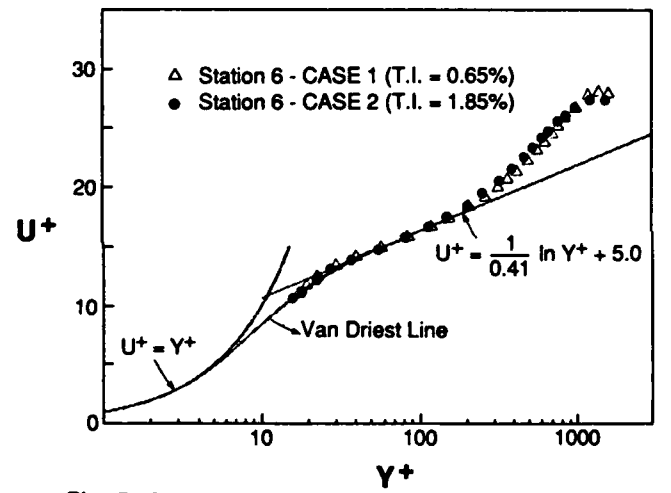

Fig. 7 Comparison of Mean Velocity Profiles at Station 6 (Cases 1 and 2).

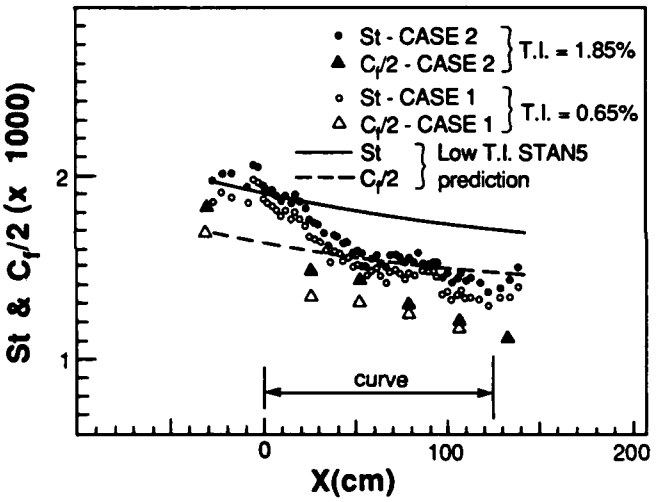

Fig. 9 Stanton Number and Skin Friction Coefficient vs. Streamwise Distance, Comparison Between Cases 1 and 2.

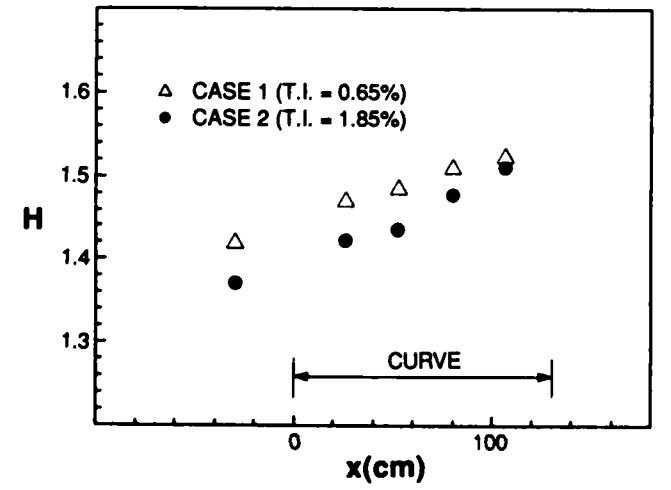

Fig. 8 Shape Factor vs. Streamwise Distance (Cases 1 and 2).

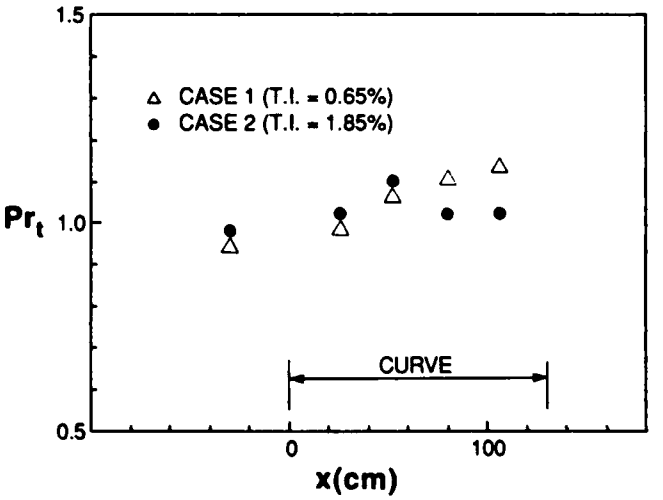

Fig. 10 Turbulent Prandtl Number vs. Streamwise Distance (Cases 1 and 2).

Streamwise-normal turbulence intensity profiles in case 2 are shown in Fig. 11. The response to the introduction of convex curvature shows the same trends as in the base case. The reduction of turbulence in the inner half of the boundary layer from the flat plate profile to the curved self-similar profile for case 2 is about twice that of case 1 (Fig. 12). Even though the shapes of the turbulence intensity profiles at station 1 are different, the curved self-similar profiles for cases 1 and 2 are nearly equal; this shows that the stabilizing curvature effect dominates the free-stream turbulence intensity effect (see Fig. 12).

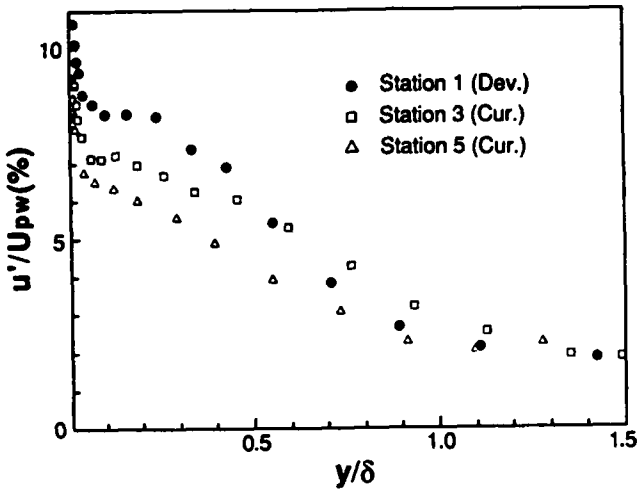

Fig. 11 Streamwise-normal Turbulence Intensity Profiles, Case 2 (T.I.=1.85%).

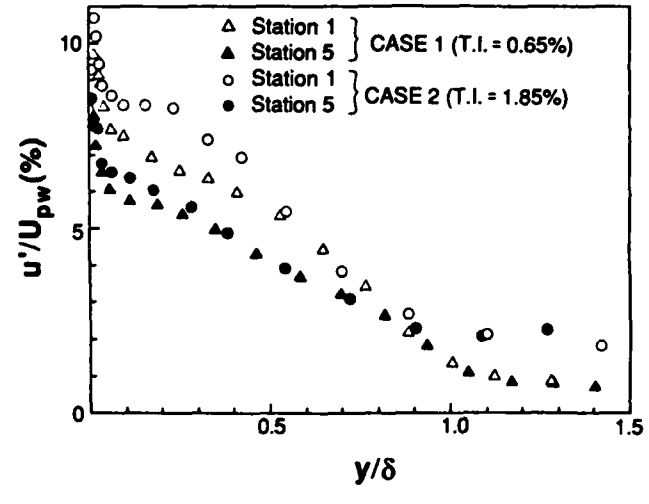

Fig. 12 Streamwise-normal Turbulence Intensity Profiles at Stations 1 and 5, Comparison Between Cases 1 and 2.

Reynolds shear stress data is plotted in Fig. 13. The dramatic response to the introduction of curvature and the appearance of an asymptotic profile are similar to those observed in case 1. The shear stress profile at station 1 in case 2 shows an extended "tail" — turbulent shear stress extends well beyond δ. The effect of curvature on shear stress profiles within the curve is dramatic. In the outer 30% of the boundary layer, the Reynolds shear stress reverses in sign downstream of station 3—this was not observed in the lower turbulence case (case 1). Similar profiles, including reversal of sign, were previously reported for more strongly curved cases [14]. It is interesting that there is a self-similar profile for $y/\delta < 0.5$ at stations 4 and 5 in this higher turbulence intensity case (Fig. 13), while the outer part of the boundary layer shows a reversal in sign of $\overline{u'v'}$. In Fig. 14, the shear stress data ($-\overline{u'v'}/U_\tau^2$ vs. y/R) approaches the "asymptotic" line for strong curvature suggested by Gillis and Johnston [14], as δ/R grows. The shear stress profile at $\delta/R = 0.042$ (station 6) is close but not on this line. The data also closely approached this line in case 1 (low free-stream turbulence intensity) when $\delta/R \approx 0.04$ [1].

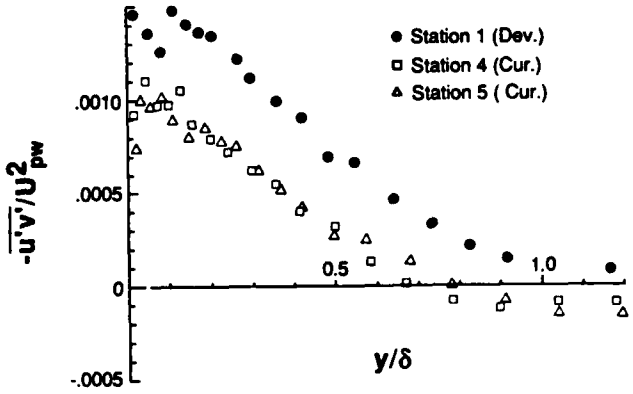

Fig. 13 Reynolds Shear Stress Profiles, Case 2 (T.I.=1.85%).

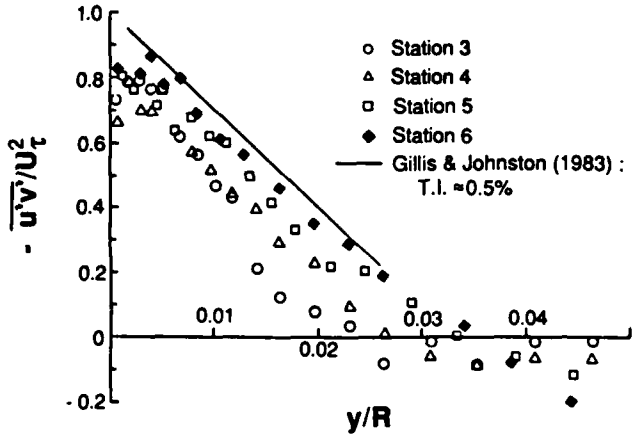

Fig. 14 Turbulent Shear Stress Profiles within the Curved Section, Case 2 (T.I.=1.85%).

4. SUMMARY AND CONCLUSIONS

Two different free-stream turbulence intensity cases were studied to investigate the effect of free-stream turbulence intensity on boundary layers over convex-curved surfaces.

The main conclusions about the effect of free-stream turbulence are:

(1) The curvature effect dominates the free-stream turbulence effect for the cases studied.

(2) Flat plate data upstream of the curve with 1.85% turbulence intensity show reduced wake strength and about a 5% increase in St and $C_f/2$ compared to the lower turbulence intensity case (0.65%).

(3) The skin friction coefficient decreases more for the higher turbulence case than for the lower turbulence case within the convex-curved section. This relative change was not so obvious with the Stanton number; this is consistent with the lower Pr_t of the higher turbulence case than of the lower turbulence case near the end of the curved section.

(4) Profiles of turbulence intensity show the same trends for the two cases: dramatic response to the introduction of curvature and the appearance of asymptotic turbulent shear stress profiles.

(5) Similar streamwise normal turbulence intensity profiles for the two cases were found near the end of the curve in spite of the different profiles upstream of the curve.

(6) Reynolds shear stress profiles for the higher turbulence case are dramatically influenced by curvature — shear stress reverses sign for $y/\delta > 0.7$ within the curve. This was also reported in strongly-curved convex-wall cases by Gillis and Johnston [14]. A self-similar shear stress profile in $-\overline{u'v'}/U^2_{ps}$ vs. y/δ coordinates on the curved wall was realized for both cases inside 50% of the boundary layer thickness.

ACKNOWLEDGEMENTS

This study was supported by the Air Force Office for Scientific Research grant number F49620-83-C0062. The grant monitor is Dr. James D. Wilson. Additional support was provided by the Graduate School of the University of Minnesota and by the AMOCO Foundation.

REFERENCES

1. You, S.M., T.W. Simon, and J. Kim, "Boundary Layer Heat Transfer and Fluid Mechanics Measurements on a Mildly-Curved Convex Wall," Proceedings of the VIIIth Int. Heat Trans. Conf., 1986.

2. Bradshaw, P., "Effects of Streamline Curvature on Turbulent Flow," AGARDograph No. 169, 1973.

3. So, R.M.C., and G.L. Mellor, "Experiment on Convex Curvature Effects in Turbulent Boundary Layers," JFM, Vol. 60, Part 1, pp. 43-62, 1973.

4. Hoffmann, P.H., and P. Bradshaw, "Turbulent Boundary Layers on Surfaces of Mild Longitudinal Curvature," Imperial College, Aero. Rept. 78-04, Dec. 1978.

5. Mayle, R.E., M.F. Blair, and F.C. Kopper, "Turbulent Boundary Layer Heat Transfer on Curved Surfaces," J. of Heat Transfer, Vol. 101, No. 3, Aug. 1979.

6. Gibson, M.M., C.A. Verriopoulos, and Y. Nagano, "Measurements in the Heated Turbulent Boundary Layer on a Mildly Curved Convex Surface," Turbulent Shear Flows 3, pp. 80-89, 1982.

7. Gibson, M.M., C.A. Verriopoulos, and N.S. Vlachos, "Turbulent Boundary Layer on a Mildly Curved Convex Surface, Part 1: Mean Flow and Turbulence Measurements," Exp. Fluids 2, pp. 17-24, 1984.

8. Gibson, M.M., and C.A. Verriopoulos, "Turbulent Boundary Layers on a Mildly Curved Convex Surface, Part 2: Temperature Field Measurements," Exp. Fluids 2,pp. 73-80, 1984.

9. Simon, T.W., R.J. Moffat, J.P. Johnston, and W.M. Kays, "Turbulent Boundary Layer Heat Transfer Experiments: Convex Curvature Effects Including Introduction and Recovery," NASA CR-3510, Feb. 1982.

10. Simon, T.W., and R.J. Moffat, "Heat Transfer Through Turbulent Boundary Layers - The Effects of Introduction of and Recovery from Convex Curvature," ASME, 79-WA/GT-10, 1979.

11. Simon, T.W, and R.J. Moffat, "Turbulent Boundary Layer Heat Transfer Experiments: A Separate Effects Study on a Convexly Curved Wall," ASME J. of Heat Transfer, 81-HT-78, Feb. 1982.

12. Simon, T.W., and R.J. Moffat, "Convex Curvature Effects on the Heated Turbulent Boundary Layer," Proceedings of the VIIth Int. Heat Trans. Conf., Vol. 3, pp. 295-301, 1982.

13. Gillis, J.C., and J.P. Johnston, "Turbulent Boundary Layer on a Convex, Curved Surface," NASA-CR3391, March 1981.

14. Gillis, J.C., and J.P. Johnston, "Turbulent Boundary-Layer Flow and Structure on a Convex Wall and its Redevelopment on a Flat Wall," JFM, Vol. 135, pp. 123-153, 1983.

15. You, S.M., "Turbulent Boundary Layer Heat Transfer and Fluid Mechanics Measurements on a Curved Convex Wall," M.S.M.E. Thesis, Dept. of Mech. Engrg., University of Minnesota, March 1986.

16. Meier, H.V., and H.P. Kreplin, "Influence of Freestream Turbulence on Boundary Layer Development," AIAA Journal, Vol. 18, No. 1, Jan. 1980.

17. Simonich, J.C., and P. Bradshaw, "Effect of Free-Stream Turbulence on Heat Transfer through a Turbulent Boundary Layer," ASME J. of Heat Transfer, Vol. 100, No. 4, pp. 671-677, Nov. 1978.

18. Blair, M.F., "Influence of Free-Stream Turbulence on Turbulent Boundary Layer Heat Transfer and Mean Profile Development, Part I - Experimental Data," ASME J. of Heat Transfer, Vol. 105, pp. 33-40, Feb. 1983.

19. Blair, M.F., "Influence of Free-Stream Turbulence on Turbulent Boundary Layer Heat Transfer and Mean Profile Development, Part II - Analysis of Results," ASME J. of Heat Transfer, Vol. 105, pp. 41-47, Feb. 1983.

20. Wang, T., Simon, T.W., and Buddhavarapu, J., "Heat Transfer and Fluid Mechanics Measurements in Transitional Boundary Layer Flows," J. Engr. for Gas Turbines and Power, Vol. 107, No. 4, pp. 1007-1015, Oct. 1985.

21. Wang, T., and Simon, T.W., "Heat Transfer and Fluid Mechanics Measurements in Transitional Boundary Layers on Convex-Curved Surfaces," ASME Paper No. 85-HT-60, 1985.

22. Hama, R., "Turbulent Boundary Layer Along a Flat Plate, I and II," Rep. Inst. Sci. and Technol., Tokyo Univ., Vol. 1, No. 1, pp. 13-16, Jan. 1947; Nos. 3-4, pp. 49-50, March 1947.

23. Schultz-Grunow, F., "New Frictional Resistance Law for Smooth Plate," NACA TM 986, 1941.

24. Klebanoff, P.S., and Z.W. Diehl, "Some Features of Artificially Thickened Fully Developed Turbulent Boundary Layers with Zero Pressure Gradient," National Bureau of Standards Report 1110, Sept. 1950.

25. Klebanoff, P.S., "Characteristics of Turbulence in a Boundary Layer with Zero Pressure Gradient," National Bureau of Standards Report 1247, 1953.

Measurements of the Turbulent Transport of Heat and Momentum in Convexly Curved Boundary Layers: Effects of Curvature, Recovery and Free-stream Turbulence

Kim, J. and Simon, T.W.

University of Minnesota, Minneapolis, MN

ABSTRACT

The effects of streamwise convex curvature, recovery, and free-stream turbulence intensity on the turbulent transport of heat and momentum in a mature turbulent boundary layer is investigated. A special three-wire hot-wire probe developed for this purpose is described. Two cases with free-stream turbulence levels of 0.68% and 2.0%, taken in the same facility with moderate strength of curvature, $\delta/R = 0.03$, are compared. Profiles of $\overline{u'v'}$, t', $\overline{u't'}$, and $\overline{v't'}$ are dramatically reduced within the curve, with asymptotic profiles being achieved quickly for the low T.I. case. Recovery occurs rapidly, with the profiles often overshooting flat-wall upstream values. Increased free-stream turbulence has the effect of increasing the profiles throughout the boundary layer on the flat developing wall. Profiles agreeing with the asymptotic profiles of the low T.I. case are observed by the end of the curve, however, illustrating the dominance of curvature over free-stream turbulence intensity. For the higher T.I. case, a reversal in the sign of $\overline{u'v'}$ in the outer half of the boundary layer is observed, leading to negative values of the turbulent Prandtl number in this region. This indicates a breakdown in Reynolds analogy.

NOMENCLATURE

b	offset
d	diameter of wire
H	shape factor
k	conductivity of air or correction coefficient of Champagne
l	active length of wire
m	slope
Nu	Nusselt number
OH	overheat ratio of wire based on free-stream temperature
P	Static pressure
Pr_t	turbulent Prandtl number
R	radius of curvature
Re	Reynolds number
St	Stanton number
t	instantaneous temperature
T	time-averaged temperature
TI	turbulence intensity
u	instantaneous streamwise velocity
U	time-averaged streamwise velocity
v	instantaneous cross-stream velocity
V	Voltage
w	instantaneous cross-span velocity
x	streamwise distance
y	distance normal to wall
α	angle between main flow direction and direction normal to wires
δ	boundary layer thickness based on 99.5% of free-stream velocity
ρ	density
μ	dynamic viscosity

Subscripts

ane	anemometer
eff	effective
pw	potential value at wall—reference value
sw	static value at the wall
∞	free-stream value
θ	momentum thickness
w	wire or wall value

Superscripts

$'$	fluctuating component or rms, depending on context
$''$	per unit area

· per unit time (overdot)
— time average (overline)

INTRODUCTION

Measurement Techniques

The following describes the development of a three-element hot-wire probe to measure the fluctuating components of velocity and temperature in 2-D boundary layers, and its use in a turbulent boundary layer over a convex surface. The probe is based on a design by Blair and Bennett (1984). These measurements are important to the gas turbine industry for they support the development of turbulent transport models used to predict the convective heat transfer to the turbine blades. These measurements are difficult and the data base is small. In fact, the effects of moderate-to-strong curvature, recovery, and turbulence intensity on the turbulent transport of heat has been studied here for the first time.

Previous investigators have measured fluctuating velocity and temperature. Representative examples of their work are reviewed below: A description of the use of multiple overheats in hot-wire anemometry to separate the temperature and velocity components in a flow was given by Corrsin (1947). He measured temperature fluctuations in the mixing of heated gas streams and concentration fluctuations in the mixing of different gases at constant temperature. His use of a single wire, however, precluded the possibility of simultaneous temperature/concentration and temperature/velocity measurements. Sakao (1973) used two parallel 5μm wires 0.2 mm apart operating at constant but different temperatures to simultaneously measure instantaneous streamwise velocity and temperature. A good response to frequencies to 300 Hz was reported. Hishida and Nagano (1978) used the same configuration but operated the front wire at constant current and the rear wire at constant temperature. No contamination from the front wire was reported and the frequency response was reported to be 6 kHz.

Chen and Blackwelder (1978) used a triple wire probe to measure two components of velocity, and temperature. The probe consisted of a conventional cross-wire with a resistance thermometer placed directly in front of the center of the cross-wires and in the plane perpendicular to them. The probe dimensions and frequency response were not presented. Smits and Perry (1981) used a technique similar to that used by Chen and Blackwelder (1978), but with the temperature sensing element placed in a plane next to and parallel with the cross wires. The methodology for separating the velocity and temperature components was presented, but no measurements were taken. A third configuration, used by Gibson and Verriopoulos (1984), consisted of a conventional cross-wire with a third "cold" wire positioned between and in a plane parallel to the planes of the cross-wires. A good response to frequencies to 6.5 kHz was reported.

A 4-wire probe designed to measure three components of velocity and temperature was described by Fabris (1978). Three wires were operated in the constant temperature mode, while the fourth was of constant current. All wires were 0.625 μm in diameter, minimizing contamination between the wires. The velocity components and temperature were found by simultaneously solving the four non-linear response equations for the sensors on a computer. A good response to frequencies to 2000 Hz was reported.

Blair and Bennett (1984) described a 3-wire probe for use in 2-D boundary layers. The probe consists of three wires located in three parallel planes. The two outer wires are orthogonal forming an X-array, while the third center wire is parallel to one of them. All three are operated at constant temperature with the center wire operated at a much lower temperature than the two outer wires. The instantaneous temperature is found from the two parallel wires, and the instantaneous velocity from the two orthogonal wires. A disadvantage to this design is that the measurement of temperature is not direct. The temperature must be determined by simultaneously solving two closely coupled non-linear equations. The advantages are numerous, however, for only constant temperature anemometers are used and frail sub-micron diameter constant current wires are avoided. A good response to frequencies to 50 kHz was reported. For this reason, the scheme of Blair and Bennett (1984) was chosen for the present study. The wire configuration of the probe used in this study is shown on Fig. 1.

Measurements

The probe was used to measure profiles of turbulence quantities in a zero pressure gradient, turbulent boundary layer influenced by convex curvature. Streamwise curvature is known to markedly affect the structure of turbulent boundary layers.

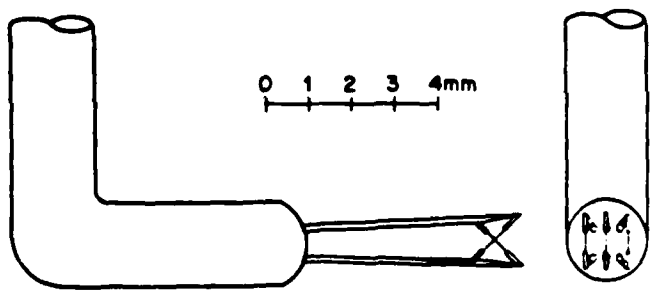

Fig. 1 -- Schematic of Wire Configuration

The changes in boundary layer turbulence intensity, wall skin friction, and Stanton number from the corresponding flat-wall values are generally an order of magnitude greater than the magnitude of the strength of curvature, δ/R. A number of studies concerning the effects of curvature on the mean flow and surface heat flux are described by You, Simon and Kim (1986a). Early work consists almost entirely of mean temperature profiles and surface heat flux measurements. Simon and Moffatt (1982a, 1982b) were the first to report heat transfer data in which the details of the velocity field were known—given by Gillis and Johnston (1980). They were also the first to document the recovery from curvature. Their strength of curvature was $\delta/R = 0.1$, indicating strong curvature. You, Simon and Kim (1986a) added heat transfer and fluid mechanics data on a mildly-curved convex surface, with recovery, to the

data base. Two strengths of curvature ($\delta/R = 0.013, 0.03$), obtained by bending the test wall, were investigated. This study by You, Simon, and Kim (1986a) is the basis for the present study. Some of their results were: 1). Profiles of the mean velocity and temperature showed shortened log-linear regions and enhanced wake regions in the curve. 2). Curvature increased the turbulent Prandtl number, deduced from the mean velocity and temperature profiles, by about 20-25%. 3). A rapid decrease in St and $C_f/2$ at the beginning of the curve was observed followed by a slow decrease within the curve. Decreases of about 20 and 10% from expected flat-wall values were observed for δ/R=0.03 and 0.13, respectively. Recovery was extremely slow, with St recovery leading $C_f/2$ recovery. 4). Normal stress profiles responded rapidly to the beginning of curvature. During recovery, an increase in turbulence intensity originated near the wall at $y/\delta \approx 0.15$ propagating slowly to the outer layers. 5). Shear stress profiles responded quickly to curvature, reducing to about 55% of the upstream flat-wall values for $\delta/R = 0.03$. Recovery occurred slowly, with the wake recovering faster than the near-wall flow. Asymptotic shear stress behavior (first observed by Gillis and Johnston—1980) was found when $\delta/R > 0.04$.

There are very few studies in which the effect of free-stream turbulence intensity on boundary layer heat transfer has been investigated. The study by You, Simon and Kim (1986b) was the first and only work to document free-stream turbulence effects (TI=0.68% and 1.85%) on heated curved flows. No recovery data was taken due to the disappearance of the potential core in recovery for the higher turbulence case. This turbulence intensity study by You, Simon and Kim (1986b) also provides a base for the present measurements. Some results were: 1). The curvature effect dominated the turbulence intensity effect. 2). The skin friction coefficient, deduced by use of the Clauser technique, decreased more within the curve than did Stanton number. 3). Similar streamwise normal turbulence intensity profiles for the two cases of different TI were found near the end of the curve in spite of the different profiles upstream of the curve. 4). Profiles of shear stress showed the same trend for both cases: a dramatic response to the introduction of curvature and asymptotic turbulent shear stress profiles by the end of the curve. A reversal in the sign of the shear stress was seen in the high TI case at the entry to the curve.

Gibson and Verriopoulos (1984) were the first and, until the present study, the only workers to take turbulence measurements in a heated curved ($\delta/R = 0.01$) flow. Their measurements indicated that $\overline{v't'}$ was affected by curvature more than was $\overline{u'v'}$. An initial sharp fall, then a continuous decrease of $\overline{v't'}$ was observed. $\overline{u't'}$ was less strongly affected by curvature. It responded more slowly to the step change in curvature. Its profiles at the last two stations in the curve were very nearly similar. Pr_t values were scattered, but the authors felt that a rise in Pr_t was observable. This is consistent with the values deduced from mean velocity and temperature profiles, and with the results of Simon and Moffatt (1982a, 1982b), and You, Simon, and Kim (1986a). A final conclusion was that turbulence in the boundary layer is modified by wall curvature such that heat transfer was stabilized more effectively than momentum transfer.

PROBE DESIGN AND DEVELOPMENT

In designing special purpose hot-wire arrays, consideration must be given to a multitude of factors, some of which are spatial averaging, prong and shaft interference, end conduction, sensor cross-talk, and survivability. The probe for the present study was constructed using the guidelines presented by Blair and Bennett (1984). The wires are 2.5 μm diameter platinum-plated tungsten with an active length-to-diameter ratio of 200 and a separation distance of 0.35 mm (Fig. 1). The ends of the wires are plated to reduce prong interference and end conduction loss.

The response equation of each sensor is assumed to be of the form

$$Nu = A_1 + B_1 Re^{0.435}$$

which is a slight variation on King's law. Substituting in the definition of Nu and Re, modelling the property variations as

$$\mu \sim t_\infty^{0.75}, \quad k \sim t_\infty^{0.80}, \quad \rho \sim t_\infty^{-1}$$

and re-arranging leads to the sensor response equation

$$u_\infty^{0.435} = A t_\infty^{0.76} + \frac{B}{(t_w - t_\infty)} V_{ane}^2$$

where A and B are assumed constant. This is the equation used by Blair and Bennett (1984) in modelling sensor response. The authors have found, however, that A and B are slight functions of temperature. This variation is incorporated into the response equation using a least-squares fit to the calibration data. The final response equation is given by

$$u_\infty^{0.435} = (m_A t_\infty + b_A) t_\infty^{0.76} + \frac{(m_B t_\infty + b_B)}{(t_w - t_\infty)} V_{ane}^2$$

The two assumptions made when reducing the data are 1). The boundary layer is two-dimensional, and 2). The instantaneous velocities seen by the two parallel wires are equal. The first assumption is needed since the third component of velocity (w) cannot be determined. If the probe is aligned with the flow, however, and if the boundary layer is two dimensional, the w-component makes only second-order contributions to sensor response and may be safely neglected. If the second assumption holds, the velocity term (u_{eff}) may be eliminated from the response equations for the two parallel wires, resulting in an equation in which the sole variable is the ambient temperature t_∞. The ambient temperature is found by iteratively solving for t_∞ using the Newton-Raphson method. The instantaneous velocities u and v may then be found from the signals of the

two outer orthogonal wires using Champagne's form of the k^2 relations:

$$u^2_{1,eff} = (u\ cos\alpha + v\ sin\alpha)^2 + k^2(u\ sin\alpha - v\ cos\alpha)^2$$

$$u^2_{2,eff} = (u\ cos\alpha - v\ sin\alpha)^2 + k^2(u\ sin\alpha - v\ cos\alpha)^2$$

Knowing the instantaneous values of u, v, and t, the rms fluctuation quantities (u', v', and t') and their cross correlations ($\overline{u'v'}$, $\overline{u't'}$, and $\overline{v't'}$) may be determined. The probe was calibrated as a function of both velocity and temperature.

Qualification of the probe was in a zero-pressure gradient flat-plate turbulent boundary layer with a momentum thickness Reynolds number of 2670 and a uniform wall heat flux of 160 W/m^2. The boundary layer thickness and free-stream velocity were 2.25 cm and 15.5 m/s, respectively. The probe was traversed across the boundary layer and measurements of $\overline{u'v'}$, t', $\overline{u't'}$, and $\overline{v't'}$ were made. These quantities, normalized on the free-stream velocity (U_∞) and the wall to free-stream temperature difference ($T_w - T_\infty$), were compared with the boundary layer data of Blair and Bennett (1984) and Gibson and Verriopoulos (1984). The three data sets agreed well except in the vicinity of the wall ($y/\delta < 0.25$) where the present data increased beyond those of other researchers. Insight into this discrepancy may be found from measurements of apparent t'. Apparent t' is the t' measured by the probe in an unheated boundary layer, and is a result of the two parallel wires not experiencing the same velocity. If the probe were perfect, the apparent t' across the boundary layer would, of course, be zero. A large apparent t' would indicate serious problems with the probe. Results of the measurements for TI=0.68% and TI=2.0%, shown on Fig. 2, show that the apparent t' values are a small percentage of the actual values in the outer part of the boundary layer, but rise rapidly as the wall is approached. This is expected since the eddy size decreases with decreasing normal distance from the wall, increasing the likelihood of the two parallel wires not seeing the same velocity. It may also be seen that turbulence intensity has little effect on apparent t', further suggesting that distance from the wall is the controlling parameter. The effect of apparent t' on the actual t' is smaller than the curves suggest since the apparent t' affects the actual data in a root-sum-square manner.

The turbulent Prandtl number (Pr_t) deduced from the measurements of $\overline{u'v'}$ and $\overline{v't'}$ were compared with the data of Blair and Bennett (1984) and Gibson and Verriopoulos (1984). There was some unavoidable scatter, but the three data sets agreed within their uncertainties ($\approx$ 20%).

The effect of overheat ratio (OH) on apparent t', presented in Fig. 3, shows that increasing OH increases t'. Furthermore, very low OH's are needed to achieve low apparent t'. Why this is the case is not presently known, but it is thought to be tied to the disappearance of the velocity dependence and the reduction of the solution matrix stiffness as the wire temperature is reduced. There was some worry that the low frequency response of the probe would affect the measurements, but, judging from the qualification data, the probe seems to follow fluctuations associated with important scales of the flow. A good response to frequencies as large as a few hundred hertz is expected.

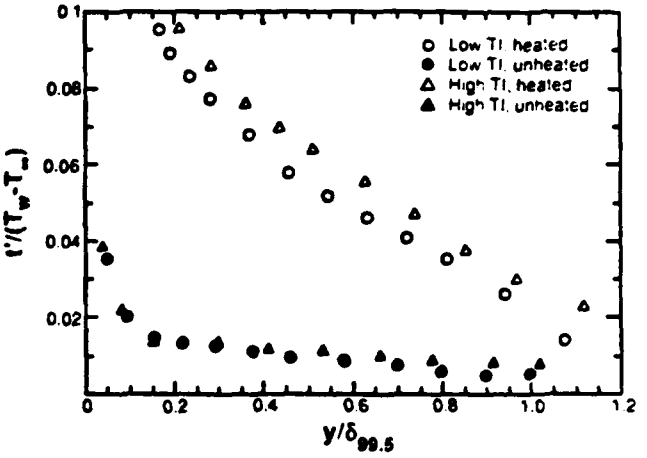

Fig 2 -- Comparison of apparent t' with the t' in a heated boundary layer

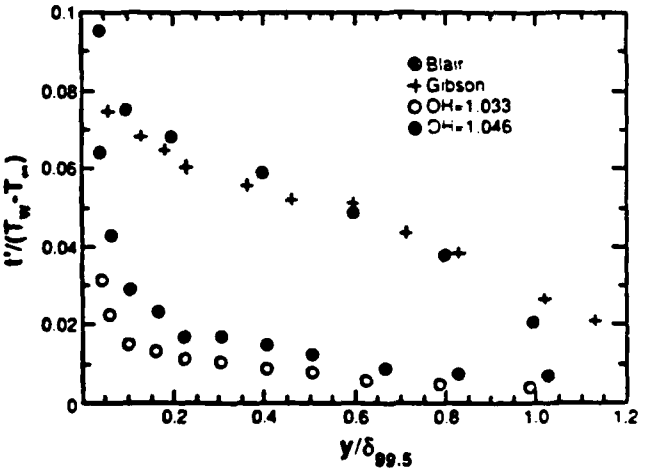

Fig 3 -- Effect of overheat ratio (OH) on apparent t'

As a last check on the probe, the measurements of shear stress were taken with the two outer orthogonal wires and again with the two inner orthogonal wires to check for prong interference and cross-talk. The difference in the two data sets was well within the uncertainty, and the curves agreed well with the data of Gibson and Verriopoulos (1984). No evidence of interference or other forms of contamination was evident.

In summary, the probe performs well except in the near vicinity of the wall. The uncertainty in the measurements is estimated at 15% for the correlations and 20% for Pr_t.

DESCRIPTION OF THE TEST FACILITY

The present experiment was conducted in an open-circuit, blown-type wind tunnel constructed with an upstream developing section, a curved section and a downstream recovery section. A

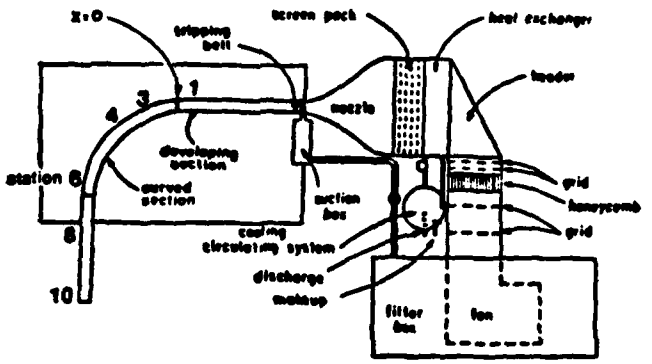

Fig 4 -- Plan view of the curved boundary layer facility

schematic of the test facility is shown on Fig. 4. Details of the tunnel are given in You, Simon, and Kim (1986a and 1986b). The test channel is rectangular, 68 cm in span and 11.4 cm deep. The heated test wall consists of a 1.4 m long developing section and a 1.4 m long curved section of 0.9 m radius of curvature followed by a 1.4 m long straight recovery section.

The laminar boundary layer was tripped in the lower-turbulence case, with a 1.0 mm high, 12.7 mm wide strip beginning 10 cm downstream of a suction slot—a mature boundary layer was established in the measurement area. The free-stream turbulence intensity, normalized on U_{pw}, was 0.68%. Higher turbulence levels were obtained by inserting a coarse grid constructed of 2.5 cm aluminum strips in a square array on 10 cm centers at the entrance of the nozzle. The boundary layer trip was removed and the boundary layer was allowed to pass naturally through transition. A turbulence intensity of 2.0% was achieved in the test section with the grid in place. Stanton numbers were spanwise uniform to within 4% of the centerline value upstream of the curve in both cases.

The test wall was heated to nominally 6°C above the free-stream temperature with a uniform heat flux of 160 W/m^2. Static pressure on the test wall was uniform. Static pressures were measured through 0.64 mm diameter taps in the opposite wall and end walls. In the curved region, these pressures were used to estimate the static pressure at the test wall assuming potential flow.

RESULTS AND DISCUSSION

Measurements of $\overline{u'v'}$, t', $\overline{u't'}$, and $\overline{v't'}$ were taken at the flat upstream developing station (station 1), three stations in the curve (stations 3, 4, and 6), and two stations in the recovery (stations 8 and 10). Data was not taken beyond station 6 in the high TI case due to merging of the test-wall and opposite-wall boundary layers. Descriptors for the two cases are presented on Table 1. The flexible outer walls were adjusted such that the pressure coefficient (C_p) defined as

$$C_p = \frac{P_{ow} - P_{ow,ref}}{\rho U_{pw}^2/2}$$

was adjusted to within 3% of the mean. The reference pressure was taken to be the static pressure at station 1.

Low TI Case (TI=0.68%)

Station	x(cm)	Reθ	H
1	-29.87	2696	1.42
3	26.16	3940	1.44
4	52.83	4784	1.54
6	106.68	5919	1.65
8	150.62	5633	1.52
10	206.50	6400	1.47

High TI Case (TI=2.0%)

Station	x(cm)	Reθ	H
1	-29.87	2640	1.35
2	26.16	4053	1.41
3	52.83	4155	1.42

Table 1 -- Summary of boundary layer parameters

Low TI Case (TI = 0.68%)

Shear stress profiles are shown on Fig. 5. The profiles are seen to respond quickly to curvature. A dramatic reduction at the onset of curvature and the appearance of what appears to be an asymptotic state in the curve occurs. Curvature is seen to reduce the shear stress by about 45% below the flat wall values throughout the curve. Recovery of shear stress is slow, with recovery seemingly complete in the wake by station 10 (See Fig. 4 for station locations). You, et al. (1986a) have shown that the near-wall values of $\overline{u'v'}$ recover very slowly. All

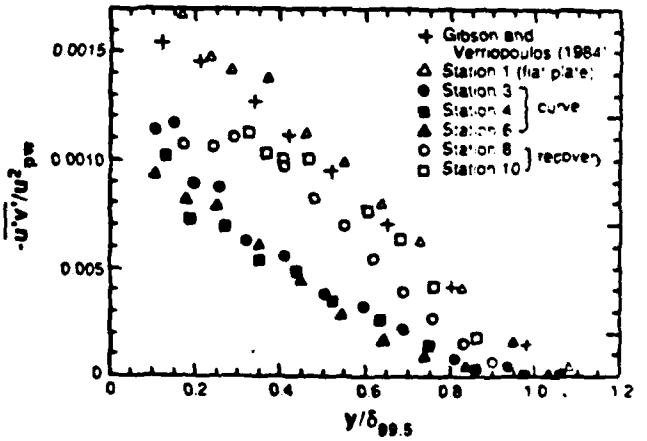

Fig 5 -- Effect of curvature and recovery on $\overline{u'v'}$, TI= 0.68%

the trends are consistent with the observations of Gillis and Johnston (1983) and You, et al. (1986a).

Profiles of t' are plotted on Fig. 6. The flat upstream values (station 1) agree with the measurements of Blair and Bennett (1984) and Gibson and Verriopoulos (1984) within the uncertainty of the measurement, except near the wall. The profiles within the curve assume an asymptotic shape for $y/\delta <$ 0.5. A slight evolution of the profiles for $y/\delta > 0.5$ is evident. Recovery has a dramatic effect on t'. Values at station 10 are seen to overshoot the station 1 values. It is believed that the profile eventually returns to the station 1 shape. The recovery length was too short to observe this in the present experiment, however.

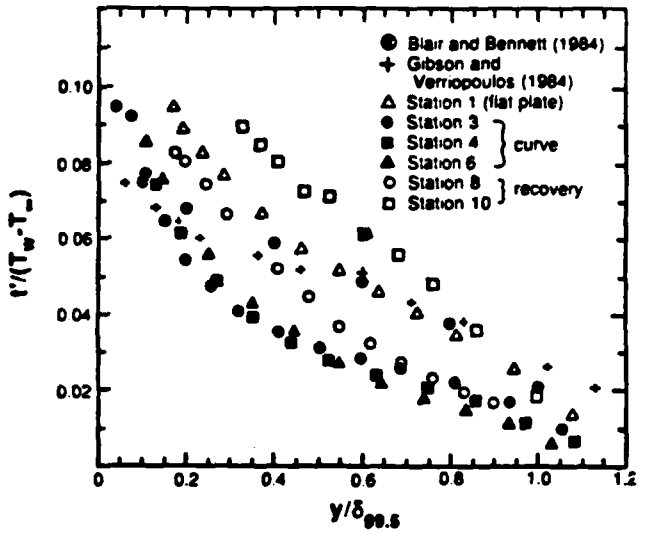

Fig. 6 -- Effect of curvature and recovery on t'. Ti=0.68%

The effects of curvature and recovery on the streamwise turbulent heat flux $\overline{u't'}$ are shown on Fig. 7. Station 1 values agree well with the data of Gibson and Verriopoulos (1984). The effect of curvature on $\overline{u't'}$ is dramatic. The profiles in the curve "snap" into an asymptotic shape for $y/\delta < 0.5$ while slow evolution of the profiles for $y/\delta > 0.5$ may be observed. Recovery is seen as an overshoot of $\overline{u't'}$ beyond the station 1 values, although the profile is expected to eventually return to the station 1 values.

Profiles of cross-stream turbulent heat flux $\overline{v't'}$ are shown on Fig. 8. The effects of curvature and recovery on $\overline{v't'}$ are very similar to those observed for $\overline{u't'}$—a dramatic reduction in the curve to an asymptotic shape, followed by an overshoot in the recovery. Values of an effective, extrapolated $\overline{v't'}$ at the wall as calculated from the wall heat flux measurements are located on the $y = 0$ axis in Fig. 8. The wall values and the profile measurements agree very well at station 1 and in the curve. The values of $\overline{v't'}$ in the recovery region, however, rise above the wall heat flux values, especially for station 10. This may be seen more clearly on Fig. 9 where $\overline{v't'}$ has been normalized on the wall heat flux. The profiles at station 1 and within the curve approach unity near the wall while the profiles in the recovery section rise above unity. It is believed that the profiles

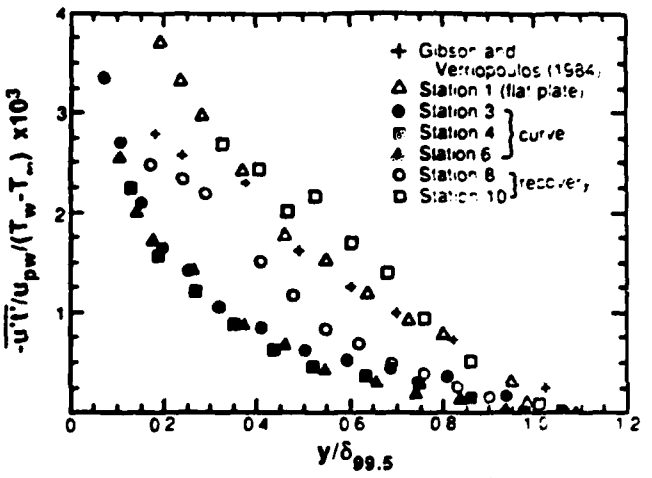

Fig 7 -- Effect of curvature and recovery on $\overline{u't'}$. Ti=0.68%

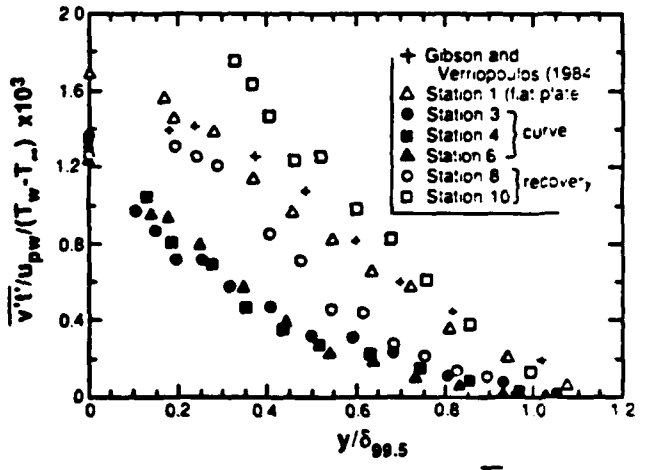

Fig 8 -- Effect of curvature and recovery on $\overline{v't'}$. Ti=0.68%

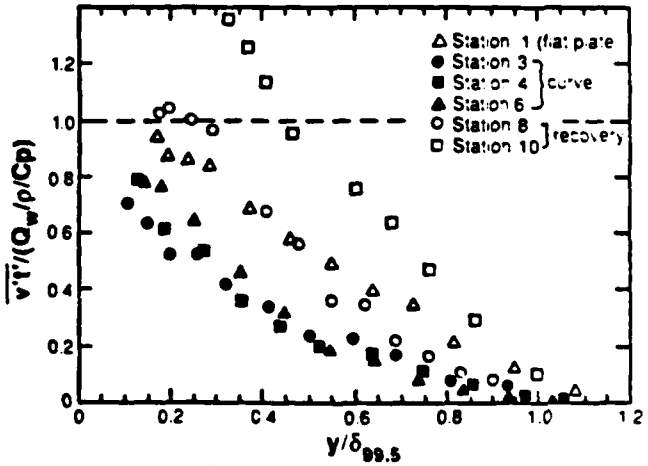

Fig 9 -- $\overline{v't'}$ normalized on wall heat flux. Ti=0.68%

turn down and approach unity as the wall is approached. The measurements cannot be taken this close to the wall, however. A positive slope in $\overline{v't'}$ suggests mixing of increasing intensity with increasing distance away from the wall.

Profiles of turbulent Prandtl number (Pr_t) are shown on Fig. 10. The data show some unavoidable scatter which makes it difficult to draw firm conclusions about the effect of curvature. Gibson and Verriopoulos (1984), You, et al. (1986a), and Simon and Moffatt (1982a, and 1982b) stated that Pr_t in the log-linear region rises due to convex curvature. The You, et al. (1986) and Simon and Moffatt (1982a, and 1982b) studies cite indirect Pr_t values deduced from mean temperature and velocity profiles which represent average values for the turbulent core. Because of scatter in Fig. 10 the only conclusion which can be drawn from this data is that the pre-plate and curved-flow Pr_t values are not vastly different (> 20%) from one another whereas the data at the end of the recovery section is lower.

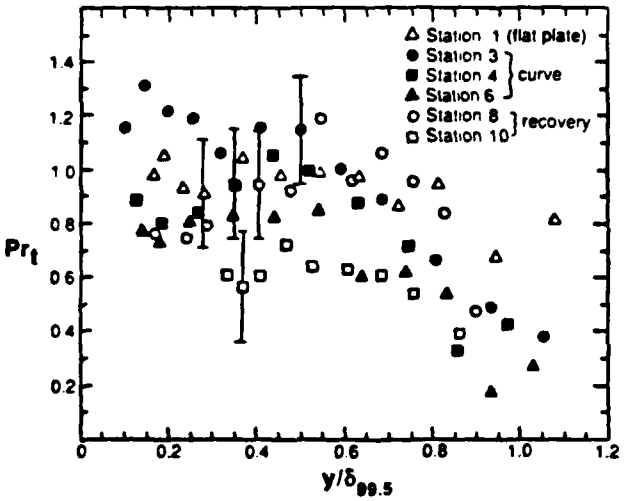

Fig. 10--Effect of curvature and recovery on Pr_t. TI=0.68%

A plot of the triple product $\overline{u'v'^2}$ representing the cross-stream flux of turbulent stress is presented on Fig. 11. The flat-wall data is compared to the data of Gibson and Verriopoulos (1984), and is seen to be higher throughout the boundary layer. Why this is the case is not presently known. The effect of curvature on $\overline{u'v'^2}$ is dramatic. Values of $\overline{u'v'^2}$ are reduced to 15% to 25% of the flat wall values by station 6, indicating that the transport of stress from the near-wall production layer to the outer flow is virtually shut off. A sharp drop at the introduction of curvature followed by a slow continued decrease is evident. The profiles are seen to recover slowly. The near-wall values remain low (which is consistent with the downturn in the shear stress profiles near the wall) within the recovery section, as discussed earlier. The peak in the profiles increases and is seen to move away from the wall with increasing streamwise distance. The profile appears to become negative for $y/\delta < 0.35$, indicating diffusion of stress toward the wall.

Profiles of the triple product $\overline{v'^2t'}$, the cross-stream flux of $\overline{v't'}$, is presented on Fig. 12. The flat-wall values are seen to be somewhat higher than the data of Gibson and Verriopoulos (1984), as was the case for $\overline{u'v'^2}$. Curvature is seen to affect $\overline{v'^2t'}$ in much the same way as with $\overline{u'v'^2}$. A sharp reduction

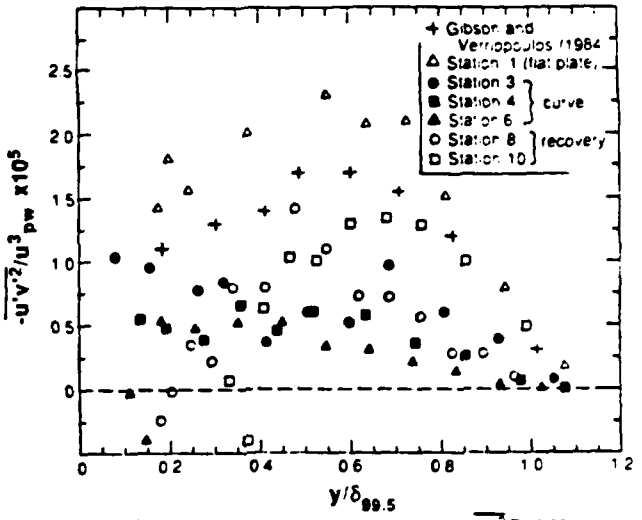

Fig. 11-- Effect on curvature and recovery on $\overline{u'v'^2}$. TI=0.68%

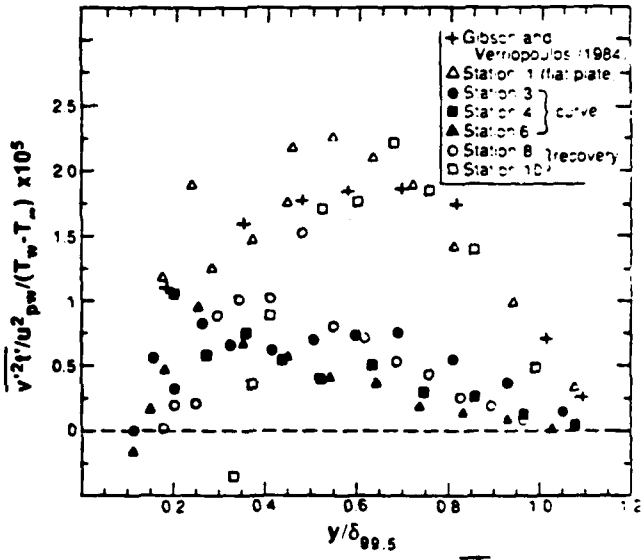

Fig. 12 -- Effect of curvature and recovery on $\overline{v'^2t'}$. TI=0.68%

in $\overline{v'^2t'}$ followed by a slow evolution to values 15 to 25% the magnitude of the upstream flat-wall values is evident. Recovery of the profiles with the peak moving away from the wall is again seen, and a reversal in sign of $\overline{v'^2t'}$ is seen for $y/\delta < 0.35$, as was seen for $\overline{u'v'^2}$. The latter indicates that the turbulent heat flux decreases as the wall is approached. This is consistent with the observed downturn in $\overline{v't'}$ upon recovery.

High TI Case (TI = 2.0%)

Shear stress profiles for the higher free-stream turbulence case are presented on Fig. 13. Higher turbulence intensity has the effect of increasing the shear stress throughout the boundary layer. This is expected. The profiles immediately assume an asymptotic shape within the curve for $y/\delta < 0.5$, as in the low TI case. The asymptotic profile for the low TI case is also plotted on Fig. 13 where it is seen to agree well with the high TI curved flow data. A reversal in the sign of the shear stress is seen to occur in the outer part of the boundary layer. This

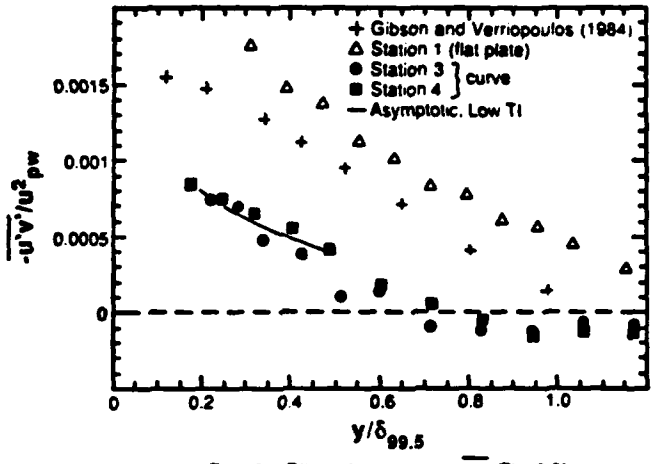

Fig. 13 -- Effect of curvature on $\overline{u'v'}$, TI = 2.0%

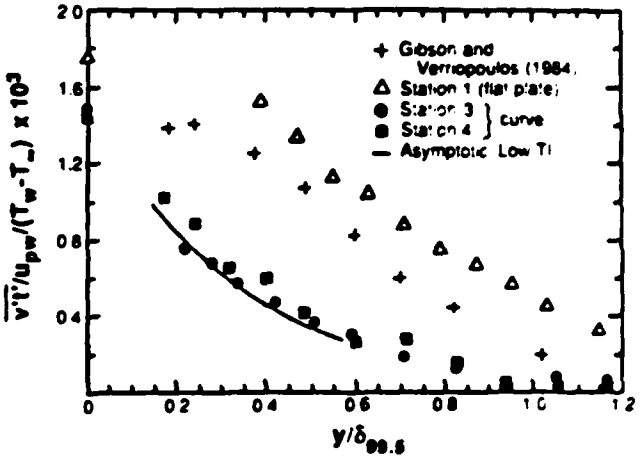

Fig. 14 -- Effect of curvature on $\overline{v't'}$, TI=2.0%

reversal in sign has also been observed by Gillis and Johnston (1983) for more strongly curved flows. An explanation for the reversal in shear stress given by Honami (1980) was presented in Gillis and Johnston (1983). Within the curve, the dominant production terms in the budget equation for shear stress are given by

$$P = \overline{v'^2}\frac{\partial U}{\partial y} - (2\overline{u'^2} - \overline{v'^2})\frac{U}{R}$$

For a flat wall, the second term on the right hand side is zero. As the flow enters the curve, however, the second term appears. Since $\overline{u'^2}$ is usually greater than $\overline{v'^2}$, the production rate is decreased by this term, and even goes negative, as shown by calculations performed for the high TI case. It is interesting to note that a large decrease in the production level in the study by Gillis and Johnston (1983) occurred due to the relatively small radius of curvature ($\delta/R = 0.1$), while a large decrease in the production level in the present study is obtained by increasing the turbulence intensity while keeping the radius of curvature large ($\delta/R = 0.03$).

Profiles of $\overline{v't'}$ are given on Fig. 14. Values of $\overline{v't'}$ higher than the corresponding low TI values are seen at station 1, while an asymptotic profile agreeing with the asymptotic profile for the low TI case is achieved in the curve. This dramatically illustrates the dominance of curvature over turbulence intensity. The profiles are seen to agree well with the wall heat flux measurements. Profiles of $\overline{v't'}$ normalized on the extrapolated, effective value computed from the wall heat flux are shown on Fig. 15. The values are expected to approach unity as the wall is approached.

The effect of turbulence intensity on t' and $\overline{u't'}$ is similar to its effect on $\overline{u'v'}$ and $\overline{v't'}$. The flat-plate values are greater than the corresponding low-turbulence values, but this increase is eliminated by the end of the curve where the values agree with the asymptotic profile of the low TI case.

Turbulent Prandtl number profiles are shown on Fig. 16. It is interesting that, with high TI, values of Pr_t become negative in the wake region of the boundary layer due to the sign

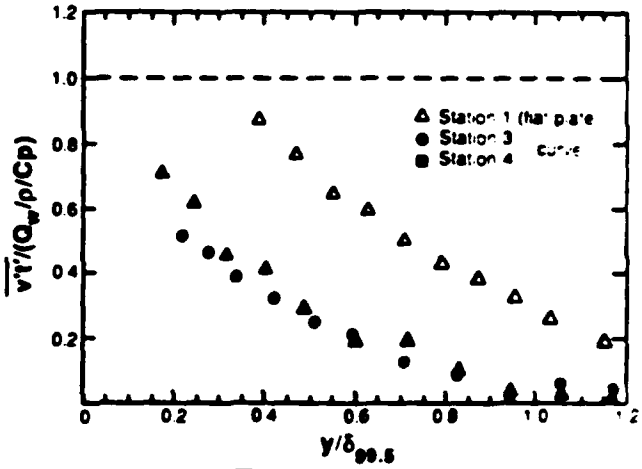

Fig. 15 -- $\overline{vt}$ normalized on wall heat flux, TI=2.0%
Effect of curvature

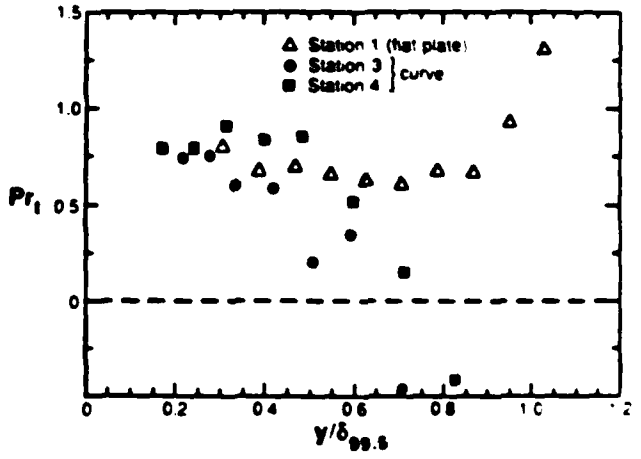

Fig. 16-- Effect of curvature on Prt, TI=2.0%

reversal in shear stress with no equivalent reversal in the sign of the turbulent heat flux, as discussed earlier. This strong variation in Pr_t indicates that Reynolds analogy is not valid.

Increasing the turbulence intensity was seen to greatly increase the values of $\overline{u'v'^2}$ and $\overline{v'^2v'}$. Inside the curve, the diffusion was reduced, reaching the order of the corresponding low Tl values by the end of the curve.

CONCLUSIONS

The effects of curvature, recovery and turbulence intensity on turbulent boundary layer heat transfer were studied. The main conclusions are:

1. Profiles of $\overline{u'v'}$, t', $\overline{u't'}$, and $\overline{v't'}$ are reduced in the curve with an asymptotic profile being achieved by station 4. Recovery in the wake region occurs quickly, with the profiles often overshooting the flat upstream (station 1) values.
2. A reversal of sign in shear stress is seen for the high Tl case (Tl=2.6%) for $y/\delta > 0.5$. A reversal of sign was also the observed by other researchers in strongly curved flows with lower turbulence intensity.
3. Because the measured turbulent Prandtl number profiles show considerable scatter, one can only conclude that the effect of curvature is no more than about 20%. But the data appear to show a decrease by the end of recovery from curvature. This does not refute Pr_t values deduced in earlier studies from mean velocity and temperature profiles, but does not provide support for the 20% increase noted by You, et al. (1986a). Negative turbulent Prandtl numbers were seen in the wake for the high Tl case, indicating a breakdown in Reynolds analogy.
4. Curvature effects dominate turbulence intensity effects for the cases studied.

ACKNOWLEDGEMENTS

This study was supported by the Air Force Office of Scientific Research grant number F49620-83-C0082. The grant monitor is Dr. James D. Wilson. Funding was also provided by the NASA-Lewis Research Center grant number NAG 3-286. The grant monitor is Dr. Raymond Gaugler. Additional support was provided by the Graduate School of the University of Minnesota and by the AMOCO Foundation.

REFERENCES

Blair, M.F., and Bennett, J.C. (1984) Hot wire measurements of velocity and temperature fluctuations in a heated turbulent boundary layer, 29th ASME International Gas Turbine Conference, Amsterdam.

Champagne, F.H., Sleicher, C.A., and Wehrmann, O.H. (1967) Turbulence measurements with inclined hot-wires, parts 1 and 2. JFM 28, pp. 153-182.

Chen, C.P., and Blackwelder, R. (1978) Large-scale motion in a turbulent boundary layer: A study using temperature contamination, JFM 89, Part 1, pp. 1-31.

Corrsin, S. (1947) Extended applications of the hot-wire anemometer, Review of Scientific Instruments, Vol. 18, No 7, pp 469-471.

Fabris, G. (1979) Probe and method for simultaneous measurements of "true" instantaneous temperature and three velocity components in turbulent flow, Review of Scientific Instruments, Vol. 50, No. 5, pp.645-654.

Gibson, M.M., and Verriopoulos, C.A. (1984) Turbulent boundary layer on a mildly curved convex surface, Expt in Fluids 2, Springer-Verlag, pp. 73-80.

Gillis, J.C., and Johnston, J.P. (1980) Experiments on the turbulent boundary layer over convex walls and its recovery to flat-wall conditions. Turbulent Shear Flows 2, pp. 116-128

Gillis, J.C., and Johnston, J.P. (1983) Turbulent boundary layer flow and structure on a convex wall and its redevelopment on a flat wall, JFM 135, pp. 123-153.

Hishida, M., and Nagano, Y. (1978) Simultaneous measurements of velocity and temperature in nonisothermal flows, J of Heat Transfer, Vol. 100, pp. 340-345.

Sahoo, F. (1973) Constant Temperature hot wires for determining velocity fluctuations in an airflow accompanied by temperature fluctuations, J. of Physics E, Scientific Instruments, Vol 6, pp. 913-916.

Simon, T.W., and Moffatt, R.J. (1982a) Turbulent boundary layer heat transfer experiments: A separate effects study on a convexly curved wall, J. of Heat Transfer, Vol 105, No 4, pp 835-840.

Simon, T.W., Moffatt, R.J. (1982b) Convex curvature effects on the heated turbulent boundary layer, Proc 7th Int Heat Transfer Conf., Vol. 3, pp. 295-301.

Smits, A.J., and Perry, A.E. (1981) A note on hot-wire anemometer measurements of turbulence in the presence of temperature fluctuations, J. of Physics E, Scientific Instruments, Vol 14, pp. 311-312.

You, S.M., Simon, T.W., and Kim, J. (1986a) Boundary layer heat transfer and fluid mechanics measurements on a mildly-curved convex wall, Proc. 8th Int. Heat Transfer Conf., Vol. 3, pp. 1089-1094.

You, S.M., Simon, T.W., and Kim, J. (1986b) Free-stream turbulence effects on convex-curved turbulent boundary layers. ASME Paper No. 86-WA/HT-46.

2nd ASME/JSME Joint Thermal Engineering Conference, 1987

A TEST OF THE M.L.H MODELS FOR PREDICTION OF CONVEX-CURVED TRANSITIONAL BOUNDARY LAYER HEAT TRANSFER BEHAVIOR

W. C. Park, Research Assistant
T. Simon, Associate Professor
Department of Mechanical Engineering
University of Minnesota
Minneapolis, MN 55455-0111

ABSTRACT

Computed transitional and turbulent boundary layer heat transfer results are compared to experimental data. Focus is on the appropriate choice of existing transition models and curvature corrections to the M.L.H turbulence model. The hypothesis tested is that only the turbulence model need be corrected for convex curvature--the transition model need not. First, the best transition model of the models tested is found by comparison to flat-wall data. The two M.L.H curvature modifications to the standard M.L.H turbulence closure model are next compared to a fully-turbulent, convex-curved data set to select the better one. The combined model, with transition and curvature modeling, is then shown to accurately predict convex-curved transition data when the free-stream turbulence intensity is large (2%). A curvature correction to the transition model is needed when the turbulence intensity is lower(0.6%), however.

NOMENCLATURE

C	Lag constant
C_f	Skin friction coefficient
K	Local acceleration parameter, $\frac{\nu}{U_e^2}\frac{dU_e}{dx}$
L	Length of transition region, $x_e - x_s$
L_0	Mixing length on a flat plate
L_c	Mixing length on a curved wall
M	Local Mach number
R	Wall radius
Ri	Richardson number
Re_L	Transition length Reynolds number, $U_e L/\nu$
Re_x	x-Reynolds number
Re_δ	Boundary layer thickness Reynolds number
Re_θ	Momentum thickness Reynolds number
S	Stability parameter
St	Stanton number
Tr	Vorticity Reynolds number
T_1	Local free-stream turbulence intensity, $\sqrt{u^2}/U_e$
T_3	Local free-stream turbulence intensity, $\sqrt{(u^2+v^2+w^2)/3}/U_e$
$\bar{T}_3$	Average free-stream turbulence intensity, $0.5(T_{3,0} + T_3)$
U	Mean velocity in the stream direction
U_e	Local free-stream velocity
u,v,w	Fluctuation velocities in x, y, z directions
x	Streamwise distance from the leading edge
y	Cross-stream distance from the wall
β	Empirical constant
γ	Intermittency factor--fraction of the time the flow is turbulent-like
δ	Boundary layer thickness
η	Dimensionless distance in the transition region, $(x - x_s)/L$
Λ	Instantaneous Pohlhausen parameter, $\frac{\theta^2}{\nu}\frac{dU_e}{dx}$
$\bar{\Lambda}$	Mean value of Pohlhausen parameter
λ	Pressure gradient parameter, $\frac{\theta^2}{\nu}\frac{dU_e}{dx}$
θ	Momentum thickness
μ_t	Eddy viscosity
ν	Kinematic viscosity
ρ	Fluid density

Subscripts

e	End of transition
s	Start of transition
0	Leading edge

INTRODUCTION

Methods presently exist for predicting laminar-to-turbulent transition. One method employs empirically derived mixing-length-hypothesis (M.L.H) models for transition start, length and path. Another employs multi-equation low-Reynolds-number turbulence closure models assuming that the models accurately capture the propagation and amplification of external disturbances with the turbulence production term. This second method has shown some success recently when disturbances are large; but more development is

needed before it can be put into general use. Multi-equation models require the solution of several diffusion equations, e.g. momentum, enthalpy, turbulence kinetic energy and turbulence dissipation. This can be expensive and cumbersome. Presently there is no assurance that transition will be predicted more accurately with multi-equation models than with simpler models. MLH modeling of transition, on the other hand, is inexpensive and convenient, but highly empirical. Being empirical, it is trustworthy within the domain of experimental support, but not outside. Because MLH modeling is inexpensive and has vast experimental support, it has its place. One conclusion of the AFOSR/Stanford Conference on Complex Turbulent Flows (Kline et al., 1982) was that no turbulence closure model (including higher-order models) is sufficiently general and accurate to merit dominance over the others.

The present paper investigates the use of existing MLH models to predict transition on convex-curved boundary layer flows undergoing laminar-to-turbulent transition. First, present flat-wall transition models are tested against recently-taken data to determine what combination of transition start, length and path models appears to be the best for this data set. Next, existing curvature corrections to the MLH turbulence closure model are tested against recent convex-curved, fully-turbulent boundary layer data to determine the preferred correction for this data set. Finally, predictions from a combined transition-with-curvature model are compared to recent curved-flow transition data. The combined model has no curvature correction term to the transition model; therefore, the comparison indicates whether such a correction is necessary.

Objectives of the present investigation are:
(1) to choose the best MLH flat-wall transition model, based on the data chosen for comparison,
(2) to choose the best curvature correction to the MLH turbulence closure model, based on the data chosen for comparison, and
(3) to test the combined model against the curved-wall transition data.
The primary motivation of this work is to test present empirical correlations which would be used as submodels for design methods for predicting external heat load on the suction surface of a highly-contoured gas turbine airfoil in the vicinity of boundary layer transition.

Mixing Length Hypothesis Transition Models

MLH modeling of transition consists of empirically-based submodels for specifying transition start, transition region length and the transition path which is usually expressed as an intermittency factor. Existing expressions for these submodels are given below.

Transition Start Models

van Driest and Blumer (1963) assumed that breakdown of laminar flow occurs when the local vorticity within the boundary layer is sufficiently strong sufficiently far from the wall. The local vorticity Reynolds number is given by $Tr = (y^2/\nu)(dU/dy)$. If the streamwise variation of Tr vs. y profiles were monitored in a laminar boundary layer, one would find that the magnitude of the peak of the profile and the y-location of the peak value increase with the square root of the streamwise distance. When transition begins, these two quantities begin to increase more rapidly, with streamwise distance, than in the laminar boundary layer. This observation supports the van Driest and Blumer hypothesis that transition occurs when the local vorticity Reynolds number becomes sufficiently large sufficiently far from the wall. van Driest and Blumer(1963) next applied the Pohlhausen theory to find the following relationship between Tr (at the profile maximum), Reynolds number based upon boundary layer thickness and the instantaneous Pohlhausen pressure gradient parameter, $Tr/Re_\delta = A + B A$. This equation was then used as the basis for an empirical fit of experimental data with the inherent assumption that transition occurs at a sufficiently large value of vorticity Reynolds number, dependent upon pressure gradient and free-stream turbulence intensity. They proposed the relationships:

$$\frac{1690}{Re_{x,s}^{0.5}} = 1 + 1.96\, Re_{x,s}^{0.5}\, T_1^2 \qquad \bar{A}=0.,$$

$$\frac{9860}{Re_{\delta,s}} = 1 - 0.0485\,\bar{A} + 3.36\, Re_{\delta,s} T_1^2 \qquad \bar{A}= 0.$$

Brown and Martin (1979) noted that the van Driest and Blumer model predictions compare well with data when the pressure gradient is zero or adverse but results were not found to agree well when there are favorable pressure gradients. This is in contrast to the findings of Blair (1982) who stated that the agreement with his zero and positive pressure gradient data was excellent.

Seyb (1967) empirically found the following expression for the start of transition:

$$Re_{\theta,s} = \frac{1000}{1.2 + 70\, T_1} + 10\left(\frac{0.09 + \lambda}{0.0106 + 3.6\, T_1}\right)^{2.62}.$$

It is based upon flat-wall data with $-0.09 < \lambda < 0.10$. Note that $Re_{\theta,s}$ approaches zero as T_1 approaches infinity, whereas the Tollmien-Schlichting limit of stability based upon linear-stability theory suggests a lower limit of 163. Brown and Martin (1979) stated that, of the van Driest and Blumer (1963), Seyb (1967) and Hall and Gibbings (1972) models, only the Seyb model compared favorably to data for adverse, zero and favorable pressure gradients. Gaugler (1981) found that results for both the Seyb (1967) and Dunham (1972) models agree with turbine blade data of Lander (1969). Hylton et al. (1983) selected the Seyb model as the best choice because it predicted transition only on the suction surface of their airfoil, as was true according to the data.

Hall and Gibbings (1972) later correlated experimental measurements to form the relationship: $Re_{\theta,s} = 190 + \exp(6.88 - 103\, T_3)$. This model does not include the effect of streamwise acceleration, which was added in later models by Dunham (1972) and Abu-Ghannam and Shaw (1980); therefore, the Hall and Gibbings model was not incorporated into the present study.

Dunham (1972) suggested the following empirical expression for the start of transition:

$$Re_{\theta,s} = [0.27 + 0.73 \exp(-80\,\bar{T}_3)](550 + 680/D),$$

where, $D = 1 + 100\,\bar{T}_3 - 21\lambda$

This model is an extension of the Hall and Gibbings (1972) model with the effect of pressure gradient added. Gaugler (1981) found favorable agreement between the results of the Dunham model and turbine blade data of Lander(1969).

Abu-Ghannam and Shaw (1980) modified the Hall and Gibbings model so that, as free-stream turbulence intensity increases to infinity, transition Reynolds number based upon momentum thickness asymptotes to 163. They stated that this modification was needed to make the model agree with the Tollmien-Schlichting limit of stability. They also extended the Hall and Gibbings (1972) model to account for the effects of pressure gradient. Their available data was more substantial than that of Dunham (1972) with free-stream turbulence intensities over the range $0.1 < T_3 < 5\%$ and pressure gradients over the range $-0.09 < \lambda < 0.06$. The resulting form of their model is:

$$Re_{\theta,s} = 163 + \exp\left[F(\lambda) - \frac{F(\lambda)}{0.0691}\bar{T}_3\right]$$

where $F(\lambda) = 6.91 + 12.75\lambda + 63.64\lambda^2$ when $\lambda \leq 0$

and $F(\lambda) = 6.91 + 2.48\lambda - 12.27\lambda^2$ when $\lambda > 0$

Priddy and Bayley (1985) noted that predictions with the Abu-Ghannam and Shaw model compared well with their turbine airfoil measurements on the suction surface, but that the model predicted a much larger $Re_{\theta,s}$ value than observed in the experiment on the pressure surface. They felt that the discrepancy on the pressure surface was due to the destabilizing concave curvature effect. It appears that the premise of this paper, that no convex curvature correction is needed in the start model, is born out by the Priddy and Bayley data set.

Other transition start models include those of Michel (1951), Granville (1953), Smith and Gamberoni (1956), van Ingen (1956), Crabtree (1958) and Jaffe et al. (1970). These models were not included in the present study partially because of their age and partially because of the recommendations of Hall and Gibbings (1972), Brown and Martin (1979), Gaugler (1981), Blair (1982) and Hylton et al. (1983) presented above. The McDonald and Fish (1973) model was not included in the present study because it requires solving the turbulent kinetic energy equation; therefore, the McDonald and Fish model was considered to not be of the form chosen for the present study.

Transition Length Models

Dhawan and Narasimha (1958) showed that data for transition length can be correlated with: $Re_\ell = 5.0\, Re_{x,s}^{0.8}$, where Re_ℓ is a Reynolds number based upon transition length, ℓ, and $Re_{x,s}$ is the x-Reynolds number of the start of transition given by an appropriate start model. The length, ℓ, is the streamwise distance between the positions where the intermittency is 0.25 and 0.75. Consistent with this is a modified relationship for 0.0 to 0.99 intermittency presented by Dunham (1972):

$$Re_\ell = 16.8\, Re_{x,s}^{0.8}.$$

Brown and Martin (1979) showed that the Dhawan and Narasimha model predictions compared well with the measurements of Brown and Burton (1978) over airfoils and was better than the Debruge (1970) model. Hylton et al. (1983) selected the Dhawan and Narasimha length model as the best, by comparison against their turbine blade data.

Debruge (1970) presented the following empirical relationship using the form of the Dhawan and Narasimha model along with the expanded data base at that time:

$$Re_\ell = 0.0168\, Re_{x,s}^{1.28}.$$

Chen and Thyson (1971) expanded the above form to include the local free-stream Mach number finding, empirically:

$$Re_\ell = (60 + 4.68\, M^{1.92})\, Re_{x,s}^{0.67}.$$

Brown and Martin (1979) suggested the following empirical relationships:

$$Re_\ell = 0.41\, Re_{x,s} \qquad T_1 < 0.001$$

$$Re_\ell = 0.62\, Re_{x,s} \qquad T_1 > 0.006$$

No other M.H transition length models are known by the authors.

Transition Path Models

Dhawan and Narasimha (1958) measured the intermittency, the time-fraction that the flow is turbulent-like, during transition and found a universal function of intermittency versus dimensionless transition length:

$$\gamma = 1 - \exp(-0.412\,\eta^2)$$

where η is $(x - x_s)/(x_e - x_s)$ and x_s and x_e are for transition start and end based upon 0.25 and 0.75 intermittency, respectively. From these results, one can write a relationship for the intermittency range $0.0 < \gamma < 0.99$, following Dunham (1972), as:

$$\gamma = 1 - \exp(-4.65\,\eta^2).$$

This path model was selected as the best model by Hylton et al. (1983) after comparison with their airfoil data.

Chen and Thyson (1971) drew from the theory of Emmons (1951) to develop their transition path model. Emmons found that random turbulent spots grow while keeping their shape as they move downstream; finally they merge and form turbulent boundary layers. He presented an intermittency factor based upon this reasoning:

$$\gamma = 1 - \exp\left(-\int_V g\,dV'\right)$$

where g is the source rate density and V is the influence volume at a given point for the resultant turbulent spot. The influence volume at a given time can be calculated knowing the locations of the boundaries of turbulent spots for times earlier than the time at which the intermittency is being evaluated. Chen and Thyson extended this equation by evaluating V in terms of transition length. A form of their result, which accounts for variations in free-stream velocity, as given by Bradshaw et al. (1981) is:

$$\gamma = 1 - \exp\left[-G(x - x_s)\int_{x_s}^{x}\frac{dx}{U_e}\right]$$

where G is the spot formation parameter. They found that the formation rate of turbulent spots depends not only on the transition Reynolds number but also on the local Mach number. With the data available to them, they formulated:

$$G = 3\,U_e^3 / \left[\nu^2(60 + 4.68\,M^{1.92})^2 Re_{x,s}^{1.34}\right].$$

Note that the pressure gradient affects the Chen and Thyson path model whereas the Abu-Ghannam and Shaw (1980) indicated no pressure gradient effect.

Abu-Ghannam and Shaw (1980) empirically found the intermittency relationship:

$$\gamma = 1 - \exp(-5\eta^3).$$

Their measurements, supported by those of Schubauer and Klebanoff (1955), showed that intermittency grows more slowly for smaller distances beyond the transition start and more rapidly for larger distances. Matching this behavior requires a larger exponent than in the Dhawan and Narasimha model.

No other path models are known to the authors.

Turbulent Flow Curvature Modifications

It is generally known that convex curvature suppresses turbulence activity in a turbulent boundary layer whereas concave curvature enhances activity (e.g. Simon and Moffat (1983), and You et al. (1986a and 1986b), So and Mellor (1975)). The curvature effect on turbulent transport must therefore be included into the modeling. This effect is expected to be visible soon after the beginning of transition when the intermittency factor begins to turn on the turbulent transport model. The curvature effect is introduced as a correction to the standard flat-wall mixing length turbulence closure model. The corrections discussed herein take the form of multipliers on the mixing length distribution such as the distribution given by Kays and Crawford (1980).

Bradshaw (1973) modified the mixing length for the effect of streamline curvature by using an analogy with atmospheric flows. He suggested that, for small curvature, the modification of the mixing length is linearly related to a particular form of the Richardson number:

$$\ell_c = \ell_o(1 - \beta Ri),$$

where Ri, the Richardson number, is $2U/(R\ \partial U/\partial y)$, R is the radius of wall curvature--positive for convex curvature, β is an empirical constant, ℓ_c is the curved-flow mixing length and ℓ_o is the flat-wall mixing length. Bradshaw recommended values for β of 4.5 and 7.0 for concave and convex curvature, respectively. His recommendation is based on data with mild streamwise curvature, $\delta/R \sim 0.01$. Later, Johnston and Eide (1976) recommended a β value of 6.0 for both concave and convex curvature based on compressor blade conditions. In the present study, a value of 5.0 was found to be optimum, as will be discussed.

Adams and Johnston (1983) suggested a modification to the mixing length for convex curvature in both the log-linear region and the outer region. They found that in the outer layer the mixing length normalized on wall radius becomes invariant with streamwise distance when the curvature is sufficiently strong. They cast this statement into the form:

$$\ell_o/R = 0.0025 \tanh (34.5\ \delta/R).$$

Their proposed form of the near-wall modification for strong curvature was given as:

$$\ell_c = \ell_o/(1 + \beta Ri)$$

where Ri, the Richardson number, is given as $S(1 + S)$. The stability parameter, S, is computed as $2U/(R\ \partial U/\partial y - U)$. Adams and Johnston recommended a β value of 5.0 for the inner region model and employed a lag on the outer region model for situations where the strength of curvature, δ/R, decreases abruptly with streamwise distance. This model imposes a first-order lag on the outer-layer modifier:

$$\frac{d(\ell_c/\delta)}{d(x/\delta)} = C\left(\frac{\ell_c}{\delta} - \left(\frac{\ell_o}{\delta}\right)_{eq.}\right)$$

where $(\ell_o/\delta)_{eq.}$ is the local equilibrium outer-layer mixing length as given by the above ℓ_c/R equation. A value of 0.06 was used for the lag constant, C, following their recommendation.

Curvature Modifications to Transition Models

There is no appropriate curvature modification for M.L.H transition modeling. The three experimental programs discussed below lend information about this rather complex situation, however.

Clauser and Clauser (1937) measured transition locations on concave and convex walls. They concluded that the transition start x-Reynolds number changes linearly with x_s/R. From their data a relationship can be formulated as:

$$Re_{x,s} = (\ 4.50 + 0.25\ x_s/R\ )\ x10^5.$$

The relationship gives a delay of transition on the convex wall and an early transition on the concave wall. The free-stream turbulence level, now known to be an important parameter, was not given; but, from their data and flat-wall information now available, one would deduce that their turbulence intensity was around one percent. One criticism of their conclusion is the near linearity which they claim--one would expect the transition mechanism on the concave wall to be fundamentally different than that on the convex wall and, therefore, the effect on transition start would be different. Also, their experiment does not incorporate the cross-effects of curvature, free-stream turbulence intensity and streamwise acceleration. The cross-effect of curvature and free-stream turbulence intensity was shown by Wang and Simon (1985) to be significant.

Liepmann (1943) measured transition start locations on concave and convex walls. The documented free-stream turbulence level was 0.1 percent. He found a strong effect of concave curvature and no effect of convex curvature on transition. The finding that convex curvature has no influence on the transition start location for lower turbulence intensity runs is contrary to the findings of Clauser and Clauser (1937) and Wang and Simon (1985). Liepmann notes that in his curved-flow runs, turbulence from the opposite (concave) wall is spread to the convex wall raising the "free-stream" turbulence intensity value from 0.1 percent at the beginning of the test plate to 0.75 percent at the end. This increased turbulence intensity over that of the Liepmann straight-wall measurements would result in an earlier transition on both convex and concave walls. This earlier transition, superposed with a retarding effect of convex curvature and an enhancing effect of concave curvature may have led to an incorrect conclusion about the curvature effect--the conclusion that convex curvature has no effect on the transition start location and concave curvature has a large effect.

Wang and Simon (1985) made transition boundary layer heat transfer and fluid mechanics measurements on a wall that was straight, then bent to two different radii of convex curvature. Tests were run at 0.68 percent and 2 percent free-stream turbulence intensity. They found a doubling of the transition

start location from the flat wall case to a mildly curved case when the turbulence intensity was 0.68 percent, but no further increase in the effect of curvature as the curvature strength was increased further. They also found only a minor effect of curvature on the transition start position at the higher free-stream turbulence level.

Because of the strong cross-correlation of free-stream turbulence effects and curvature effects, as documented by Wang and Simon (1985), and because of the conflicting conclusions from the above three experiments, it is difficult to consolidate the above results into a curvature correction for tansition models. The higher turbulence case of Wang and Simon suggests that for higher turbulence levels, a curvature correction to the transition model may not be necessary, however. This is a hypothesis which the present paper tests.

SOLUTION PROCEDURE

The transition start, length and path models and the turbulent curvature modifications discussed above were incorporated into the boundary layer code STAN5 (Crawford and Kays, 1976). Laminar velocity and total enthalpy profiles were given at the starting location 1 mm downstream of the leading edge of the test plate. For cases which were initiated as turbulent boundary layers, measured velocity and total enthalpy profiles were supplied for the beginning of computation. The measured wall surface heat flux variation with streamwise distance was used as the thermal boundary condition. Most cases were run assuming uniform properties across the boundary layer after test cases were run to verify that variable property effects were insignificant. The turbulence closure model used was the mixing length model employing a standard mixing length distribution as discussed in Kays and Crawford (1980). Turbulence closure in the energy equation was by use of specified turbulent Prandtl numbers. Those turbulent Prandtl numbers were the measured values, except in the cases of Blair and Werle (1981, 1982) where a constant turbulent Prandtl number of 0.90 was used.

The transition start models used different free-stream turbulence intensity definitions, T_1 and T_3. When available, T_3 was used; when necessary, T_1 was substituted. The local free-stream turbulence intensity was linearly interpolated from the data points.

RESULTS AND DISCUSSION

Selection of Test Cases

Three experimental studies (Wang et al., 1985, You et al.,1986a and 1986b and Wang and Simon, 1985), all done at the Heat Transfer Laboratory of the University of Minnesota, were chosen as the primary comparison cases. These three were done on the same facility using the same experimental procedures. They, therefore, represent a coherent data set where curvature and transition effects are first isolated, then combined. These tests are familiar to the authors and detailed data from the tests are available to the authors.

Six cases of Blair and Werle (1981,1982) were also chosen to investigate the effects of free-stream turbulence intensity and streamwise pressure gradient on the transition start.

The Test Cases

An experimental study of transition on a flat wall by Wang et al. (1985) was chosen as a test case for determining the best transition start, length and path submodels. In their study, data for 0.68 percent and 2 percent turbulence intensities with zero streamwise pressure gradient were presented. The wall heat flux was nearly uniform. The 2 percent turbulence intensity case was selected as the primary case for comparison. It was shown to be two-dimensional throughout the test length and good momentum and energy balances on the test wall were achieved. The measured turbulence intensity varied from 2.3 percent at the leading edge to 1.9 percent at the downstream end. Though the skin friction was measured at only nine streamwise locations, local heat transfer coefficient data was taken at more than 50 streamwise positions making the transition path clearly discernable. Comparison runs were also made using the 0.68 percent turbulence intensity case of Wang et al. (1985) and with the data of Blair and Werle (1981, 1982) with and without favorable pressure gradients and for several values of free-stream turbulence intensity using the submodels selected.

The curvature correction to the turbulent mixing length was chosen by comparison with the experimental data of You et al. (1986a, 1986b) measured in a fully turbulent flow of moderate convex curvature strength ($0.013 < \delta/R < 0.03$). In this experiment a turbulent boundary layer was grown on a flat wall followed by a constant-radius curved section and a downstream flat wall. The data, therefore, tests the model's response to both the introduction of and recovery from convex curvature. Two values for the strength of curvature were achieved by bending the test wall to two different radii. Comparisons were made with cases of 0.65 percent and 1.85 percent turbulence intensity.

The combined model, with the chosen transition start, length and path submodels as well as the curvature modification to the turbulence model, was tested against the transitional flow data of Wang and Simon (1985) taken on a convex wall. Comparisons were made for 0.68 percent and 2 percent turbulence intensities, each at two radii of streamwise curvature.

Transition on Flat Walls

A comparison of predicted streamwise variations of Stanton number on a flat wall using the transition start models discussed earlier is shown on Figure 1(a). Each run was made with the same transition length and path models. Shown also is the data from the comparison experiment discussed above. The Abu-Ghannam and Shaw (1980) start model accurately predicted the location of the onset of transition whereas the other three models gave a later transition than the data indicate. A comparison of further test results of the start models against various degrees of free-stream turbulence intensity and streamwise pressure gradient is shown in Table 1. The Abu-Ghannam and Shaw (1980) start model appears to be better than the other start models. Based upon these comparisons, and favorable results of subsequent comparisons using the Abu-Ghannam and Shaw start model and the chosen length and path models, the Abu-Ghannam and Shaw start model was chosen.

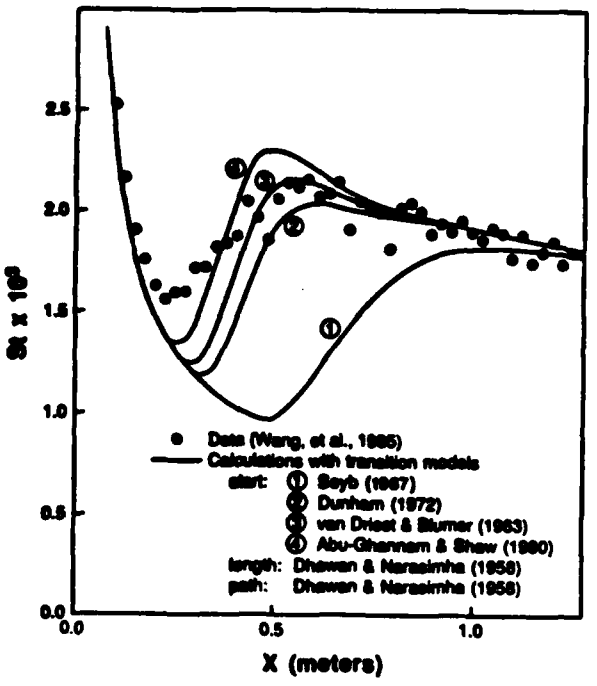

Fig. 1(a) Comparison of transition start models
U_e = 13 m/s, T_1 = 2 %, flat plate

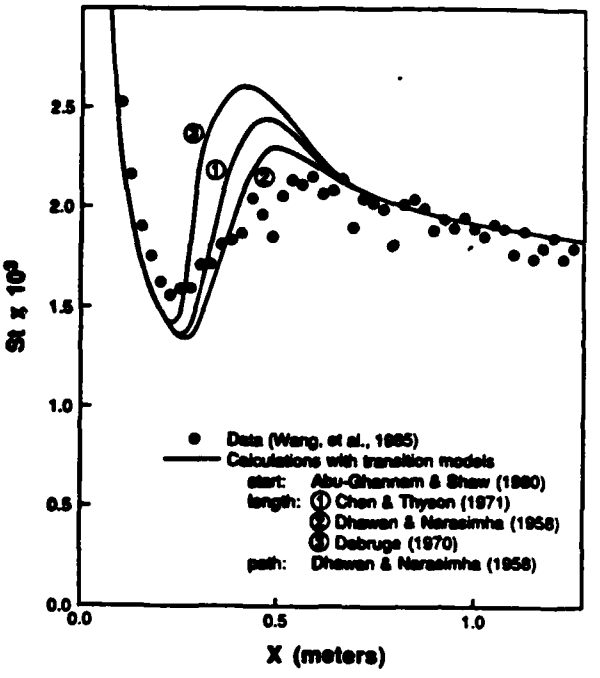

Fig 1(b) Comparison of transition length modes
U_e = 13 m/s, T_1 = 2 %, flat plate

Table 1

Comparison of transition start models--locations of the onset of transition (minimum Stanton number)

transition length: Dhawan & Narasimha (1958)

transition path : Dhawan & Narasimha (1958)

(distance from the leading edge in meters)

	data	van Driest & Blumer (1963)	Seyb (1967)	Dunham (1972)	Abu-Ghannam & Shaw (1980)
Wang et al. (1985)					
T_1 = 0.6%, K = 0	0.40	0.397	0.336	0.475	0.475
2.0 %, 0	0.25	0.295	0.400	0.225	0.263
Blair & Werle (1982)					
$T_{1,e}$ = 1%, K = 0	0.25	0.270	0.204	0.210	0.210
2%, 0	0.14	0.170	0.229	0.157	0.135
4%, 0	-	0.064	0.102	0.074	0.064
Blair & Werle (1981)					
$T_{1,e}$=0.1%, K= 0.2×10^{-6}	0.27	0.220	0.635	0.240	0.257
2.2%, 0.72×10^{-6}	0.64	-	-	-	0.622
2.2%, 0.72×10^{-6}	0.17	0.127	0.220	0.211	0.160

- No onset of transition noted.

Figure 1(b) shows the same data and predictions using the Abu-Ghannam and Shaw start model and the various length models discussed earlier. All three predictions employ the same transition path model. All three models predict a shorter transition length than the data indicate. The Brown and Martin (1979) model gave almost the same results as the Debruge (1970) model. The Dhawan and Narasimha (1958) model gives the best results, however. Based on this comparison and favorable results of subsequent comparisons using the Abu-Ghannam and Shaw start model, the Dhawan and Narasimha length model and the chosen path model, the Dhawan and Narasimha length model was chosen.

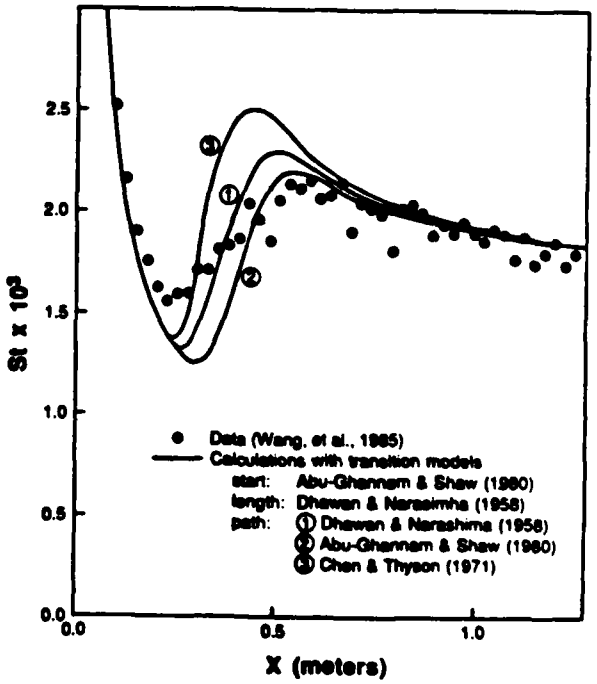

Fig. 1(c) Comparison of transition path models
U_e = 13 m/s, T_1 = 2 %, flat plate

Results of predictions of the same data set using the three transition path models are shown on Fig. 1(c). The comparison cases were all computed with the Abu-Ghannam and Shaw start model and the Dhawan and

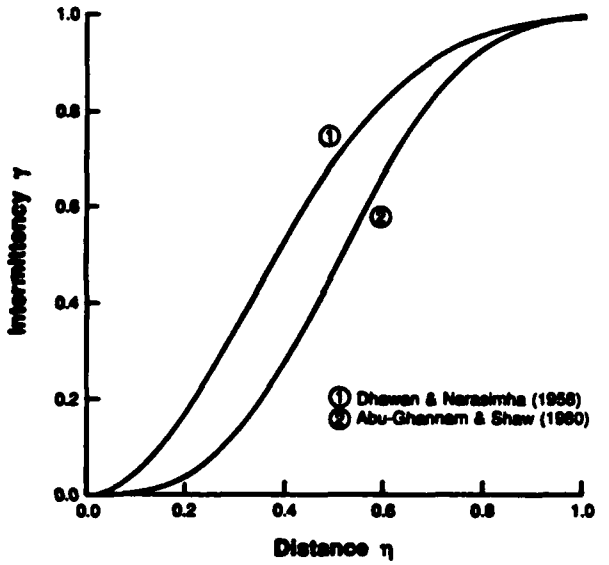

Fig. 2 Intermittency vs. Non-dimensional Distance

Narasimha length model. The Chen and Thyson (1971) model is clearly passing to turbulent-like flow too quickly. The Dhawan and Narasimha (1958) and Abu-Ghannam and Shaw (1980) models show somewhat the same path but predicted Stanton numbers from the Abu-Ghannam and Shaw model are slower to change with downstream distance than those of the Dhawan and Narasimha model. This slower early response of the Abu-Ghannam and Shaw model is seen in the intermittency versus distance functions shown on Fig. 2. Because of this earlier rise in intermittency and because of favorable subsequent comparisons of the results of the combined model to experimental data, the Dhawan and Narasimha (1958) model was chosen.

The transition start, length and path models have now been selected. Computed flat-wall, transition skin friction and Stanton number results are compared to the data of the comparison test on Fig. 3. In Fig. 4, results from the chosen combination of transition submodels are compared to 1 percent, 2 percent, and 4 percent turbulence intensity data, respectively, from Blair and Werle (1982). Fig. 5 shows predictions, by the same model, of the Blair and Werle (1981) data for combinations of free-stream turbulence intensity and streamwise favorable pressure gradient. A favorable pressure gradient, $dp/dx < 0$, stabilizes the flow delaying transition; an adverse pressure gradient has the opposite effect. Of all the boundary layer fluid, the low-momentum near-wall flow tends to be most affected by pressure gradient. This is also the region of maximum vorticity Reynolds number and the region most likely to amplify small disturbances eventually leading to transition. A comparison of the data of Fig. 5 shows the stabilizing effect of a favorable pressure gradient. Sensitivity to pressure gradient would be greatly reduced if the near-wall flow possessed more streamwise momentum. This can be effected by increasing the free-stream turbulence intensity. A comparison of Figs. 4(c) and 5(c) shows a much reduced effect of acceleration from that of the previous comparison (Figs. 5(b) and 4(b)). In the experiment of Abu-Ghannam and Shaw (1980), the effect of pressure gradient nearly disappeared for turbulence intensities larger than 5 percent. The pressure gradient and turbulence intensity effects of the Blair and Werle (1981) data are captured reasonably well by the chosen model.

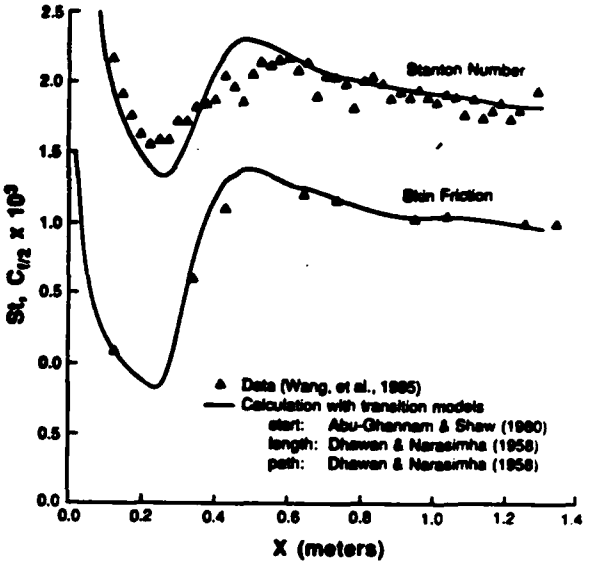

Fig 3 Calculation of a transitional flow over a flat plate with selected transition models
U_e = 13 m/s, T_1 = 2 %

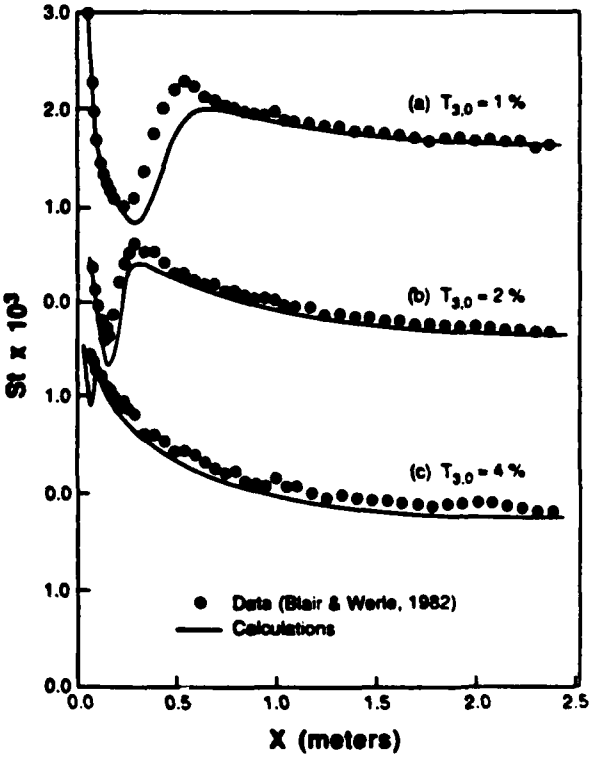

Fig. 4 Transition with zero pressure gradient (flat plate)

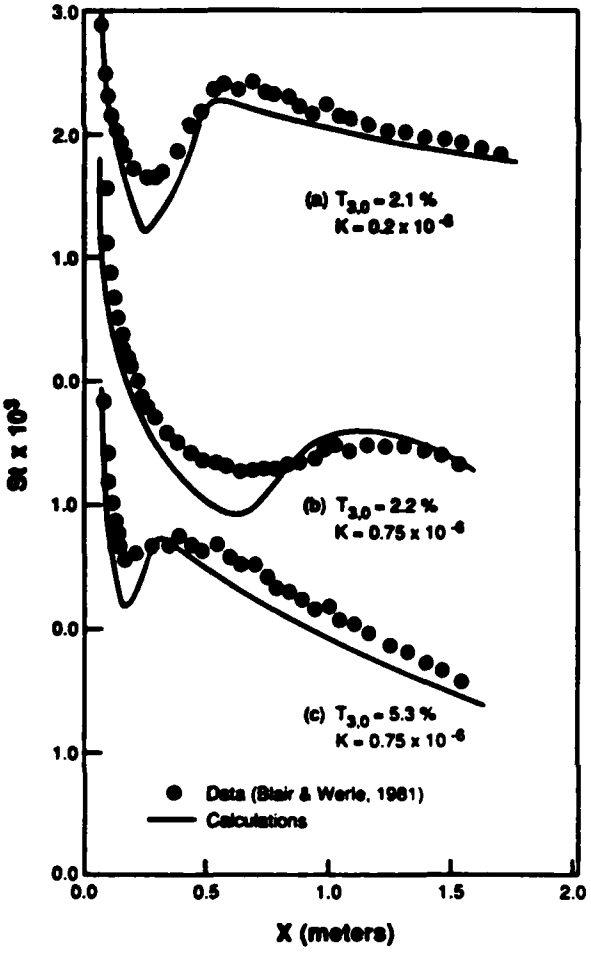

Fig. 5 Transition with pressure gradient (flat plate)

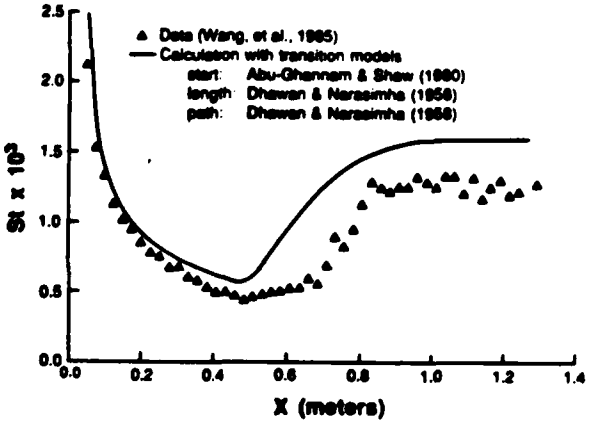

Fig. 6 Transition over a flat plate
U_e = 34 m/s, T_1 = 0.68 %

Figure 6 shows a comparison of predictions and the Stanton number data of the flat-wall, lower turbulence intensity (0.68%) case of Wang et al. (1985). The predicted onset of transition agrees well with the measurements but a large discrepancy is seen between the transition path data and predictions. Wang, et al. noted that the momentum and energy balances used to verify the test began to degrade at the start of transition due to the development of three-dimensionality caused by earlier transition on the side-walls. This is thought to not account for the full discrepancy between the data and the predictions, however. To the authors' knowledge, no detailed transition path data in addition to the Wang et al. (1985) case are available in this turbulence intensity range.

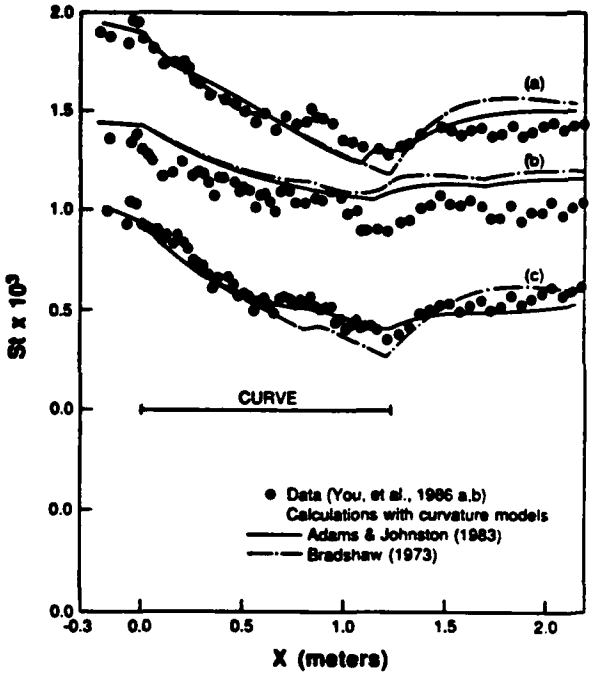

Fig. 7 Comparison of turbulent curvature modifications
(a) T_1 = 0.65 %, R = 90 cm (convex)
(b) T_1 = 0.65 %, R = 210 cm (convex)
(c) T_1 = 1.85 %, R = 90 cm (convex)

Turbulent Flow on Convex-Curved Walls

The two curvature modification models previously discussed were tested against the experimental data of You et al. (1986a, 1986b). The results are shown in Fig. 7. Both models predict the three cases reasonably well but the Adams and Johnston (1983) model is somewhat better, particularly in its performance against the recovery data on the flat wall downstream of the curve. The Adams and Johnston curvature modifier was therefore chosen.

Transition on Convex-Curved Walls

The combined model, consisting of the Abu-Ghannam and Shaw (1981) start model, the Dhawan and Narasimha (1958) length and path models and the Adams and Johnston (1983) curvature modifier was next tested against curved-wall transition data. The comparison cases were the experiments of Wang and Simon (1985) taken with two radii of curvature, each with two levels of turbulence intensity (0.68 and 2%). The comparisons with the two percent turbulence cases,

shown on Fig. 8, are quite favorable. Under these conditions, it appears that there need not be a curvature correction to the transition start model--the curvature modifier to the turbulence model, which would alter the transitional and turbulent flow data but not the transition start location, seems to account for the entire curvature effect. The comparison against the low turbulence intensity data (Fig. 9) is not so favorable, however. Clearly, for low turbulence intensity, a different transition model, which includes a curvature correction, is needed. Though the turbulence intensity value at which such correction to the model is needed is not precisely known, it would appear to be somewhere around one to two percent. The conclusion, then, is that the model chosen in the present study can be used to predict transition on curved walls, provided that the free-stream turbulence intensity value is about two percent or greater. This is useful because gas turbine suction surface design conditions would generally not violate this requirement.

CONCLUSIONS AND RECOMMENDATIONS

The following conclusions can be drawn from the present study:

1. A transition model based on the Abu-Ghannam and Shaw transition start submodel, and the Dhawan and Narasimha length and path submodels is the best transition model of thr models tested above for computing the behavior of the chosen flat-wall, transition comparison case data. Predictions with this model were shown to also be favorable when compared to transition data that included various levels of free-stream turbulence and favorable streamwise pressure gradient especially when the free-stream turbulence intensity value remained higher than about one percent.
2. The curvature modification to the mixing length model proposed by Adams and Johnston was the preferred model for predicting the effect of convex curvature as displayed in the chosen turbulent curved flow case.
3. The combined (transition and curvature) model predicts the convexly curved wall transition data well for the high turbulence intensity case (2%), but a curvature correction to the transition model is needed for the low turbulence case (0.68%).

In general, more comparison data from curved transitional flows would be useful for continued model development. More remains to be done on predicting convexly curved transitional flows with various degrees of turbulence intensity. Data is needed to support the present paper's preliminary finding that no curvature correction to the transition model is needed when the free-stream turbulence intensity is high (≥2%), and for modeling transitional flows with low turbulence intensity. The effect of concave curvature on transition is presently not well understood--more, detailed transition path data in this very complex flow is needed.

ACKNOWLEDGMENTS

This work was partially supported by the Air Force Office for Scientific Research under grant number F49620-85-C0049. The grant monitor is Dr. James D. Wilson. Additional support came from the AMOCO Foundation. Funds from these two sources are gratefully acknowledged. The authors also thank Dr. Raymond E. Gaugler of NASA Lewis Research Center for making his version of STAN5 available.

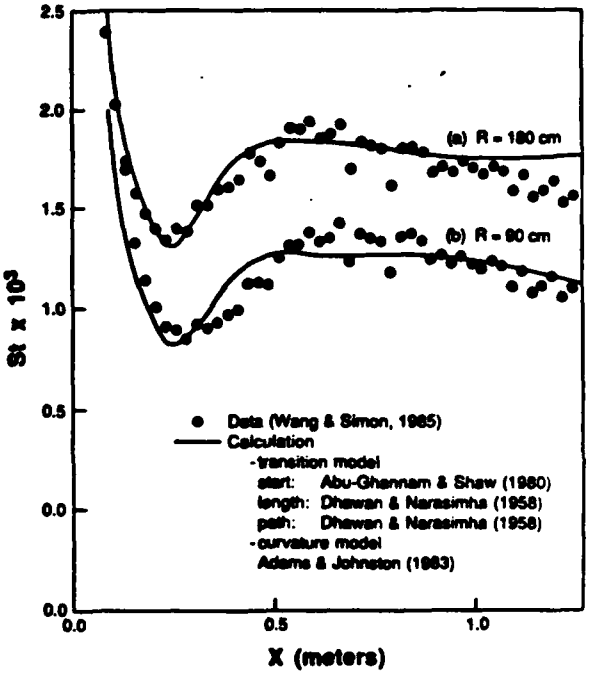

Fig. 8 Calculation of a transitional flow over a convex-curved wall with transition-curvature combined model
U_e = 14.5 m/s, T_1 = 2 %

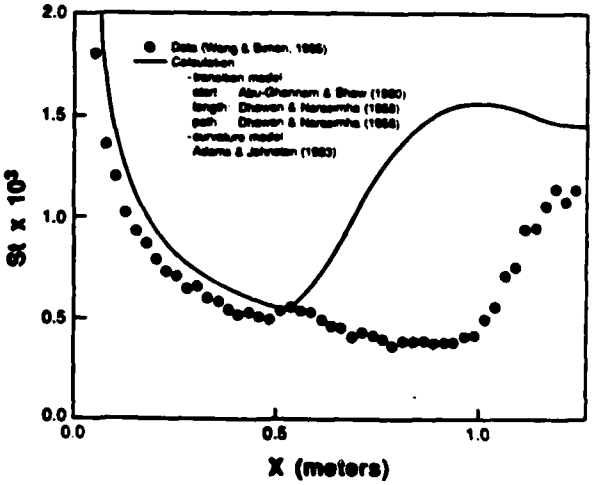

Fig. 9 Calculation of a transitional flow over a convex-curved wall with transition-curvature combined model
U_e = 34 m/s, T_1 = 0.68 %, R = 180 cm

REFERENCES

Abu-Ghannam, B. J. and Shaw, R., 1980, "Natural Transition of Boundary Layers—The Effects of Turbulence, Pressure Gradient, and Flow History," J. Mech. Engr. Sci., Vol. 22, No. 5, pp. 213-228.

Adams, E. W. and Johnston, J. P., 1983, "A Mixing Length Model for Prediction of Convex Curvature Effects on Turbulent Boundary Layers," ASME Paper No. 83-GT-80.

Blair, M. F., 1982, "Influence of Free-Stream Turbulence on Boundary Layer Transition in Favorable Pressure Gradients," J. Engr. for Power, Trans. ASME, Vol. 104, pp. 743-750.

Blair, M. F. and Werle, M. J., 1981, "Combined Influence of Free-Stream Turbulence and Favorable Pressure Gradients on Boundary Layer Transition and Heat Transfer," United Technologies Research Center, East Hartford, Rep-No. R81-914388-17.

Blair, M. F. and Werle, M. J., 1982, "The Effects of Free-Stream Turbulence on the Turbulence Structure and Heat Transfer in Zero Pressure Gradient Boundary Layers," United Technologies Research Center, East Hartford, Rep-No. R82-915634-2.

Bradshaw, P., 1973, "Effects of Streamline Curvature on Turbulent Flow," AGARD-AG-169.

Bradshaw, P., Cebeci, T. and Whitelaw, J. H., 1981, Engineering Calculation Methods for Turbulent Flow, Academic P., London, pp. 111.

Brown, A. and Burton, R. C., 1978, "The Effects of Free Stream Turbulence Intensity and Velocity Distribution on Heat Transfer to Curved Surfaces," J. Engr. for Power, Trans. ASME, Vol. 100, pp. 159-168.

Brown, A. and Martin, B. W., 1979, "Heat Transfer to Turbine Blades, with Special Reference to the Effects of Mainstream Turbulence," ASME Paper No. 79-GT-26.

Chen, K. K. and Thyson, N. A., 1971, "Extension of Emmons' Spot Theory to Flows on Blunt Bodies," AIAA J., Vol. 9, No. 5, pp. 821-825.

Clauser, M. and Clauser, F., 1937, "The Effect of Curvature on the Transition from Laminar to Turbulent Boundary Layer," NACA Tech. Note No. 613.

Crabtree, L. F., 1958, "Prediction of Natural Transition in the Boundary Layer on an Aerofoil," J. Royal Aeronaut. Soc., Vol. 62, pp. 525-528.

Crawford, M. E. and Kays, W. M., 1976, "STAN5--A Program for Numerical Computation of Two-Dimensional Internal and External Boundary Layer Flows," NASA CR-2742.

Debruge, L. L., 1970, "A Theoretical Determination of Convection Heat-Transfer Coefficients During Transition on the Suction Side of Turbine Airfoils,"" AFAPL-TR-69-95.

Dhawan, S. and Narasimha, R., 1958, "Some Properties of Boundary Layer Flow During the Transition from Laminar to Turbulent Motion," J. Fluid Mech., Vol. 3, pp. 418-436.

Dunham, J., 1972, "Predictions of Boundary Layer Transition on Turbomachinery Blades," AGARD-AG-164, pp. 55-71.

Emmons, H. W., 1951, "The Laminar-Turbulent Transition in a Boundary Layer, Part 1," J. Aero. Sci., Vol. 18, No. 7, pp. 490-498.

Gaugler, R. E., 1981, "Some Modification to, and Operational Experiences with, the Two-Dimensional, Finite Difference, Boundary-Layer Code, STAN5," ASME Paper No. 81-GT-89.

Granville, P. S., 1953, "The Calculation of Viscous Drag of Bodies of Revolution," David Taylor Model Basin Rep. 849.

Hall, D. J. and Gibbings, J. C., 1972, "Influence of Stream Turbulence and Pressure Gradient on Boundary-Layer Transition," J. Mech. Engr. Sci., Vol. 14, No. 2, pp. 134-146.

Hylton, L. D., Mihelc, M. S., Turner, E. R., Nealy, D. A. and York, R. E., 1983, "Analytical and Experimental Evaluation of the Heat Transfer Distribution over the Surfaces of Turbine Vanes," NASA-CR-168015.

Jaffe, N. A., Okamura, T. T. and Smith, A. M. O., 970, "Determination of Spatial Amplification Factors and Their Application to Predicting Transition," AIAA J., Vol. 8, pp. 301.

Johnston, J. P. and Eide, S. A., 1976, "Turbulent Boundary Layers on Centrifugal Compressor Blades: Prediction of the Effects of Surface Curvature and Rotation," J. Fluids Engr., Trans. ASME, Vol. 98, pp. 374-381.

Kays, W. M. and Crawford, M. E., 1980, Convective Heat and Mass Transfer, Second edition, McGraw-Hill.

Kline, S. J., Cantwell, B. J. and Lilley, G. M. (ed.), 1982, Complex Turbulent Flows, The 1980-81 AFOSR-HTTM-STANFORD Conference on Complex Turbulent Flows, Vol. 2, Stanford University, California.

Lander, R. D., 1969, "Evaluation of the Effect of Free-Stream Turbulence on the Heat Transfer to Turbine Airfoils," PWA-3713, Pratt & Whitney Aircraft, East Hartford, Conn. (AFAPL-TR-69-70, AD-857303).

Liepmann, H. W., 1943, "Investigations of Laminar Boundary-Layer Stability and Transition on Curved Boundaries," NACA Wartime Report W-107.

McDonald, H. and Fish, R. W., 1973, "Practical Calculations of Transitional Boundary Layers," Int. J. Heat and Mass Transfer, Vol. 16, No. 9, pp. 1729-1744.

Michel, R., 1951, "Etude de la transition sur les profiles d'aile; etablissement d'un critère de détermination du point de transition et calcul de la trainée de profile incompressible," O.N.E.R.A. Report 1/1578A.

Priddy, W. J. and Bayley, F. J., 1985, "Effects of Free-Stream Turbulence on the Distribution of Heat Transfer around Turbine Blade Sections," Int. J. Heat and Fluid Flow, Vol. 6, No. 3, pp. 181-192.

Schubauer, G. B. and Klebanoff, P. S., 1955, "Contribution to the Mechanism of Boundary-Layer Transition," NACA T.N. No. 3489.

Seyb, N. J., 1967, "A Simplified and Practical Method of Determining the External Heat Transfer Coefficient around a Turbine Blade," ARC Report 29398.

Simon, T. W. and Moffat, R. J., 1983, "Turbulent Boundary Heat Transfer Experiments: A Separate Effects Study on a Convexly Curved Wall," J. Heat Transfer, Trans. ASME, Vol. 105, pp. 835-840.

Smith, A. M. O. and Gamberoni, N., 1956, "Transition, Pressure Gradient and Stability Theory," Proc. 9th Int. Congr. Appl. Mech. (John Wiley and Sons, Chichester).

So, R. M. C., and Mellor, G. L., 1975, "Experiment on Turbulent Boundary Layers on a Concave Wall," The Aeronautical Quarterly, Vol. 16, pp. 25.

van Driest, E. R. and Blumer, C. B., 1963, "Boundary Layer Transition: Free-Stream Turbulence and Pressure Gradient Effects," AIAA J., Vol. 1, No. 6, pp. 1303-1306.

van Ingen, J. L., 1956, "A Suggested Semi-Empirical Method for the Calculation of the Boundary Layer Transition Region," Report Nos. V.T.H. 71, V.T.H. 74, Delft, Holland.

You, S. M., Simon, T. W. and Kim, J., 1986(a), "Boundary Layer Heat Transfer and Fluid Mechanics Measurements on a Mildly-Curved Convex Wall," Proc. Eighth Intl. Heat Transfer Conf.

You, S. M., Simon, T. W. and Kim, J., 1986(b), "Free-Stream Turbulence Effects on Convex-Curved Turbulent Boundary Layers," Gas Turbine Heat Transfer Session, 1986 ASME Winter Annual Meeting.

Wang, T. and Simon, T. W., 1985, "Heat Transfer and Fluid Mechanics Measurements in Transitional Boundary Layers on Convex-Curved Surfaces," ASME Paper No. 85-HT-60.

Wang, T., Simon, T. W. and Buddhavarapu, J., 1985, "Heat Transfer and Fluid Mechanics Measurements in Transitional Boundary Layer Flows," J. Eng. Gas Turbines and Power, Trans. ASME, Vol. 107, No. 4, pp. 1007-1015.

Film Cooling of a Turbine Blade with Injection through Two Rows of Holes in the Near-Endwall Region

by

R. J. Goldstein and P. H. Chen
Mechanical Engineering Department
University of Minnesota
Minneapolis, Minnesota 55455

ABSTRACT

Measurements of film cooling on a simulated turbine blade are conducted using a mass transfer technique. Under the influence of the endwall, dramatic changes of film cooling performance occur on the convex surface of the blade as compared to the region where the flow is two-dimensional. The result is a triangular region, where coolant is swept away from the surface by the passage vortex present between adjacent blades. In order to predict the area of this unprotected region, the influence of several parameters including density ratio, blowing rate and number of rows of injection holes are studied. The presence of the endwall affects the film cooling performance on the concave surface only slightly.

Introduction

To improve the performance of a gas turbine engine, the temperature of combustion gas entering the first stage turbine has increased to as high as 1750 K which is above the allowable limit for present alloys, used as turbine materials. An effective cooling system is required to protect the gas turbine blade from high-temperature failure. Surface film cooling combined with internal convection cooling and impingement cooling is widely used in the aircraft industry. A better understanding of this cooling system can improve the design of gas turbine engines. The present work focuses on film cooling using a plane simulated turbine blade cascade. Particular attention is directed to the influence of the endwall on the adiabatic wall effectiveness.

Adiabatic wall effectiveness is defined by:

$$\eta_{aw} = \frac{T_{aw} - T_r}{T_2 - T_r} \qquad (1)$$

Based on the definition of the adiabatic wall temperature, the heat transfer is defined by the equation:

$$q_w = h\,(T_w - T_{aw}) \qquad (2)$$

Values of the heat transfer coefficient are generally close to those without coolant injection if the region near the injection holes is excluded.

The present study applies the heat-mass transfer analogy to investigate the film cooling effectiveness. Detailed discussion about heat-mass transfer analogy is available in ref[1]. A gas mixture containing a tracer is injected into the mainstream. The concentrations of the tracer are measured in samples drawn through taps which are located on the surface of a blade. The local impermeable wall effectiveness, η_{iw}, is defined by:

$$\eta_{iw} = \frac{C_{iw} - C_\infty}{C_2 - C_\infty} \qquad (3)$$

As the concentration of the tracer in the mainstream is zero, the impermeable wall effectiveness can be calculated from the equation:

$$\eta_{jw} = \frac{C_{jw}}{C_2} \qquad (4)$$

Early studies [2, 3] of the film cooling on a turbine blade were conducted in the central space of the blade to minimize the influence of the endwall. The effect of blade-wall curvature to the performance of the film cooling was reported. However, the span of most blades is not long compared to the chord length. The flow field as well as the film cooling are strongly affected by the presence of the endwall. A recent work [4] found that there is a close relation between the flow field in the endwall region and the film cooling. Measurements of the film cooling in a plane cascade show that a passage vortex travelling from the adjacent blade sweeps the coolant from the convex surface and produces a triagular region without film cooling protection. An understanding of the flow field in the near endwall region is essential when conducting a study of film cooling. Studies of the three-dimensional flow field within a turbine cascade passage have been described by others [5, 6, 7, 8]. A review of invesitigations of the flow field for past decade was reported in ref. [9].

The present work is an extension of an earlier study done with a single row of holes, a single blowing rate and a single density ratio. Here the effect of density ratio, two rows of injection holes and blowing rate on film cooling near an endwall are considered.

Experimental System and Test Conditions

Measurements are conducted in an open cycle, low speed wind tunnel using a plane cascade of six turbine blades [1]. Two central blades with injection holes face each other. Four others are solid. Figure 1(a) shows the location of the injection holes and sampling taps. Two staggered rows of injection holes inclined at an angle of 35° are used. The angles of flow inlet and outlet with respect to the blades are shown in Fig. 1(b). To assure uniform flow though each hole, the injection hole half embedded in the endwall is plugged. The lateral positions of each of the four rows of sampling taps are Z/D = 0.0, 0.5, 1.0, and 1.5, respectively. Each row has seven sampling taps distributed at various positions downstream. The central two blades can be moved in or out of the endwall using a positioning mechanism underneath the blades. For any single run, the blades are positioned at a fixed distance from the endwall, that is, the lowest hole of the second row is centered on the endwall. For each position, samples are drawn from all four rows of sampling taps. These represent the regions between different paired holes, that is, only one row of sampling taps lie inside the shaded area where the measurement region is. To get data for results between a given pair of holes (at fixed H/D), four different positionings of the blades are required. For a given blowing rate and a density ratio, the blades will be positioned into a dozen different locations to conduct a series of measurements before the two-dimensional flow region is reached. Note that the shaded area only covers half the space between a given pair of holes as the sampling taps are designed for a study in the central span of the blades where the flow is symmetrical around the injection hole.

The injected flow is produced by mixing refrigerant-12 or helium and air. Two density ratios, R = 2.0 and 0.96, are used. For the measurments on a

convex surface, three blowing rates, M = 0.5, 1.0, and 1.5, are used for both density ratios. On the concave surface, the blowing rates are 1.38 and 1.5 corresponding to the density ratio of 0.96 and 2.0, respectively.

The sampled gases are analyzed using a gas chromatograph. The velocity profile is measured 14 cm upstream of the leading edge of the blades. The free stream velocity is 10.2 $^{m}/_{s}$. The boundary layer is turbulent with a thickness, δ_{99}, of 10 mm corresponding to $^{H}/_{D}$ = 4.2. The turbulent intensity of the free stream is 1.2%. The momentum thickness is 1.2 mm and the displacement thickness is 1.8 mm. By calculating a virtual origin of the turbulent boundary layer and assuming a variation of a turbulent boundary layer on a flat plate, the boundary layer thickness at the location of the stagnation line of the blade would be about 6% larger than the value measured 14 cm upstream of the leading edge of the blade. The mainstream velocity near the injection holes of the first row is 17.8 $^{m}/_{s}$ on the convex surface and 4.2 $^{m}/_{s}$ on the concave surface. The uncertainty of measuring impermeable wall effectiveness is 6% as the value of the effectiveness is greater than 10%. The uncertainty is 7% in calculating the blowing rate and 4% in calculating the density ratio.

Flow Field

Because of a strong relation between film cooling and the flow field, a detailed description of the flow field is essential to explain the results of the film cooling measurements. A sketch of the flow field, based on results of flow visualization [3], is shown in Fig. 2. The main structure is clear

but, without more investigations, some details, especially close to the blade, are still ambiguous. In Fig. 2, the attachment (stagnation) line, indicated by a1 - a2, extends from the stagnation point on the blade into the mainstream. The separation line, indicated by s1 - s2, lies in front of the leading edge of the blade. A saddle point, Ss1, is a singular separation point and is located at the intersection of the attachment line and the separation line. Several flow regions are bounded by these two separation lines and two attachment lines. When the mainstream approaches the leading edge of the blade, the inlet boundary layer separates and a horseshoe vortex is generated behind the separation line. After the mainstream travels into the blade passage, a pressure variation is produced, high pressure near the concave surface and low pressure near the convex surface. Behind the separation line, one leg of the horseshoe vortex on the concave side travelling downstream is driven by the pressure difference in the blade passage and becomes part of the passage vortex. The other leg of the horseshoe vortex, on the convex side, is confined near the blade wall and rolls up when it encounters the passage vortex from the the adjacent blade. On the endwall, a boundary layer is driven by the pressure difference from the concave side to the convex side.

Essentially, the passage vortex is formed from the concave side leg of the horeshoe vortex and fed from the cross flow on the endwall and the mainstream in the blade passage. It grows bigger as it travels downstream. When the passage vortex encounters the convex surface of the adjacent blade, it apparently lifts up the convex side leg of the horseshoe vortex from that blade. Also, a counter vortex is generated underneath the passage vortex.

Near the endwall, the limiting streamlines near the blade surface are not two-dimensional. On the concave surface, the limiting streamlines are skewed downward because fluid feeds into the crossflow on the endwall. On the convex surface, the limiting streamlines are pushed up by the passage vortex. Initial work on film cooling near the endwall [4] indicates that the passage vortex sweeps the coolant flow from the convex surface and there is a triangular area in which the coolant is essential absent.

Impermeable Wall Effectiveness

Convex surface

For M = 1.0 and R = 2.0, iso-effectiveness lines of the convex surface are shown in Fig. 3. These lines are constructed in the measurement regions which start at X/D = 1.88 and end at at H/D = 70.93. Note that these measurement regions only cover half area between two adjacent injection holes. For the region of $31.5 > H/D > 30$, the coolant jet is symmetric around the injection hole centerline as can be seen from the periodicity of local effectiveness of two adjacent measurement regions, $28.5 > H/D > 27.0$ and $31.5 > H/D > 30$. Secondary flow in the blade passage has little effect on the film cooling performance at distances over 30 diamters from the end wall.

For the region of $H/D < 30$, the variation of local effectiveness of two adjacent measurement regions is no longer periodic. For $H/D < 18$, local effectiveness over approximately half of this region is under 0.1. The blade surface is not effectively protected by the film cooling. Much lower effectiveness is found in the region, $H/D < 1.5$. Two reasons are believed to

cause this phenomenon. First, lower mainstream velocity in this region results in a higher blowing rate and coolant blows away from the surface instead of covering the surface. Also, the hole half embedded in the endwall is blocked which diminishes the coolant flow for a given span.

Due to limited numbers of sampling taps, it is hard to determine the downstream location at which the local effectiveness just reaches zero. Because the locations of iso-effectiveness lines are calculated by interpolation, the iso-effectiveness lines with a value of 0.1 involve some degree of error.

Figs. 4 and 5 show the spanwise-average effectiveness $\overline{\eta_{fw}}$, as a function of the dimensionless distance H/D. Results for two density ratios are presented. Solid symbols on the right axis represent $\overline{\eta_{fw}}$ in the two-dimensional flow region, at $H/D = 69$. These values compare well with results in Ref. [3]. The data at each downstream position (x), have a similar trend. As H/D decreases the average effectiveness at first deviates only slightly from that in the two-dimensional flow region. At a certain distance, marked by a plus symbol in Figs. 4 and 5, the values of the average effectiveness start to decrease approximately linearly to zero.

For each specified downstream location, the results can be approximated by two straight lines. One extends from the value in the two-dimensional flow region and is parallel to the horizontal axis. The slant line fits data which decreases linearly with H. Both lines intersect at the location shown by a plus symbol, which indicates where the value of the average effectiveness starts to decrease linearly. The star symbols represent the locations on the

horizontal axis intersected by the slant straight lines. The region between the location of the star symbol and $H/D = 0$ has no film cooling protection. Note that these plus and star symbols are not data points.

The plus and star symbols can be mapped on the convex surface of a blade. Figure 6 presents the ranges of the average effectiveness in the near endwall region on the convex surface of a blade. Note that the location at a value of $X/D = 0$ is at the downstream edge of the injection holes of the second row. The leading edge of a blade is at $X/D = -14.5$. The star symbols (in fig. 4 or 5) construct the upper boundary of the region C. The upper boundary of the region B is formed by the corresponding plus symbols. The dashed line shows the extropolated boundary thickness, $\delta 99$, of the mainstream on the endwall at the leading edge of a blade.

Region C is the unprotected area where coolant flow is swept away by the passage vortex from the adjacent blade. The span of this unprotected area grows as the location moves toward the trailing edge because the passage vortex becomes bigger as it travels downstream. In region B, the values of the average effectiveness vanish linearly to zero as measurements are conducted toward the endwall. In this region, the coolant flow mixes with the passage vortex but is not totally absent. Above the region B, the performance of the film cooling is slightly affected by skewed streamlines and is close to the two-dimensional flow value at $H/D \cong 30$.

The flow field near the end wall significantly affects the performance of the film cooling on the convex surface of a blade. The passage vortex is so significant that a large area of a blade surface could be exposed to hot gas

without coolant protection. It may be helpful to add coolant to the end wall to protect the lower convex surface of the blade. It is however uncertain that the coolant so injected would be carried up by the passage vortex to the blade surface.

The effect of some key parameters on the size of the unprotected region were studied. Fig. 6 shows the effect of the density ratio on boundaries between the regions. At a blowing rate of unity, the unprotected area is smaller with the lower density ratio but the change is slight. Figs. 7 and 8 show the effect of the blowing rate on the three regions. Results for the two density ratios studied are presented. Higher blowing rate might be expected to decrease the size of the unprotected area. However, the upper boundary of region B is not affected by the change of the blowing rate and there is very little affect on the lower boundary of B (upper boundary of region C) as well. Figure 9 shows the effect of the number of rows of injection holes on the regions. Results of the one-row configuration are from ref. [4]. There is little difference between the two sets of results in terms of the size of the regions. Outside region C, the values of the average effectiveness of the two-row configuration are of course higher than those for one-row injection, but the locations of the boundaries are not very different for the different geometries.

Concave surface.

For M = 1.5 and R = 2.0, iso-effectiveness lines on the concave surface are shown in Fig. 10. Measurement regions start at X/D = 1.10 and end at X/D = 38.86. Because streamlines near the concave surface are bent toward the

endwall, periodicity between two adjacent measurement regions is not present close to the endwall. The influence of the endwall on local effectiveness can be neglected for $H/D > 30$. Values of the average effectiveness are shown in Figs. 11 and 12; results for two density ratios are presented. Values of the average effectiveness are almost independent of H except very close to the endwall. The presence of the endwall does not greatly affect the performance of the film cooling on the concave surface.

Fig. 13 shows a comparison of the average effectiveness between one-row and two-row configurations on the concave surface. Although the blowing rate has a 10% difference, a comparison is still acceptable. As expected, effectiveness with two-row injection is higher than with one-row injection. In the region $H/D < 3$, one might expect that the values of the average effectiveness should be higher than those of the two-dimensional flow region for two reasons. The first is that coolant is washed toward the endwall. The other is that the values of average effectiveness on the concave surface generally increase with a higher blowing rate excluding the region close to the injection hole. From Fig. 13, this is true for one-row configuration but not for two-row configuration. Due to the blockage of the lowest hole of the second row, the region of $H/D < 3$ is not fully covered by two rows of injection holes.

Conclusion

The presence of the endwall has a significant effect on the performance of the film cooling on the convex surface of a blade. A triangular region, where the coolant is swept from the convex surface by a passage vortex from

the adjacent blade, has no film cooling protection at all. Moving away from this unprotected area, the values of the average effectiveness increase linearly from zero to a value close to that in the two-dimensional mid-span region. The boundaries of these regions are only slightly changed by varying blowing rate, density ratio, and number of rows of injection hole. On the concave surface, the performance of the film cooling is not significantly altered by the presence of the endwall but the periodicity of the local effectiveness is changed due to skewing of the streamlines toward the endwall.

The film cooling effectiveness is closely related to the mainstream flow field. The incoming flow condition and the geometry of the turbine blade can play important roles in affecting the dimensions of the different regions of effectiveness variation on the convex surface. To protect the region where coolant is washed away, it may be necessary to further cool the end wall itself.

References

1. Petersen, D.R., Eckert, E.R.G., and Goldstein, R.J., "Film Cooling with Large Density Difference Between the Mainstream and the Secondary Fluid Measured by the Heat-Mass Transfer Analogy," Journal of Heat Transfer, 99, 620-627 (Nov. 1977).

2. Ito, S., Goldstein, R.J., and Eckert, E.R.G., "Film Cooling of a Gas Turbine Blade," ASME Journal of Engineering for Power, 100, 476-480 (July 1978).

3. Goldstein, R.J., Kornblum, Y., and Eckert, E.R.G., "Film Cooling Effectiveness on a Turbine Blade," Israel Journal of Technology, 20, 193-200 (1982).

4. Goldstein, R.J., Chen, H.P., "Film Cooling on a Gas Turbine Blade Near the Endwall," ASME Journal of Engineering for Gas Turbines and Power, 107, 117-122 (Jan. 1985).

5. Langston, L.S., Nice, L.M., and Hopper, R.M., "Three-Dimensional Flow within a Turbine Cascade Passage," ASME Journal of Engineering for Power, 99, 21-28 (Jan. 1977).

6. Langston, L.S. "Crossflows in a Turbine Cascade Passage," ASME Journal of Engineering for Power, 102, 864-874 (Oct. 1980).

7. Gaugler, R.E., and Russel, L.M., "Comparison of Visualized Turbine Endwall Secondary Flows and Measured Heat Transfer Patterns," ASME Journal of Engineering for Gas Turbines and Power, 106, 168-172 (Jan. 1984).

8. Sieverding, C.H., and Van Den Bosche, P., "The Use of Coloured Smoke to Visualize Secondary Flows in a Turbine-Blade Cascade," Journal of Fluid Mechanics, 134, 85-89 (1983).

9. Sieverding, C.H., "Recent Progress in the Understanding of Basic Aspects of Secondary Flows in Turbine Blade Passages," ASME Journal of Engineering for Gas Turbines and Power, 107, 248-257 (Apr. 1985).

NOMENCLATURE

a1 - a1	attachment line - Figure 2
C_{iw}	concentration of foreign gas at impermeable wall
C2	concentration of foreign gas
C_∞	concentration of foreign gas in the mainstream
D	diameter of injection hole
h	heat transfer coefficient
H	distance along blade surface from the endwall
M	blowing rate $\rho 2U2/\rho_\infty U_\infty$
q_w	wall heat flow per unit time and area
R	density ratio
$R_{e\infty}$	Reynolds number $\frac{U_\infty D}{\nu}$
S_s1	saddle point - Figure 2
s1 - s2	separation line - Figure 2
T	temperature
T_{aw}	adiabatic wall temperature
T_r	recovery temperature
T_w	wall temperature
U	upstream velocity
U2	mean velocity in injection hole
U_∞	mainstream velocity at the first injection hole location
X	distance downstream for the downstream edge of second injection row
Z	transverse distance from center of injection hole of the second row to sampling hole
$\rho 2$	density of foreign gas
ρ_∞	density of the mainstream
ν	kinematic viscosity of the mainstream

Acknowledgment

This study was conducted with support from the U.S. Air Force Office of Scientific Research.

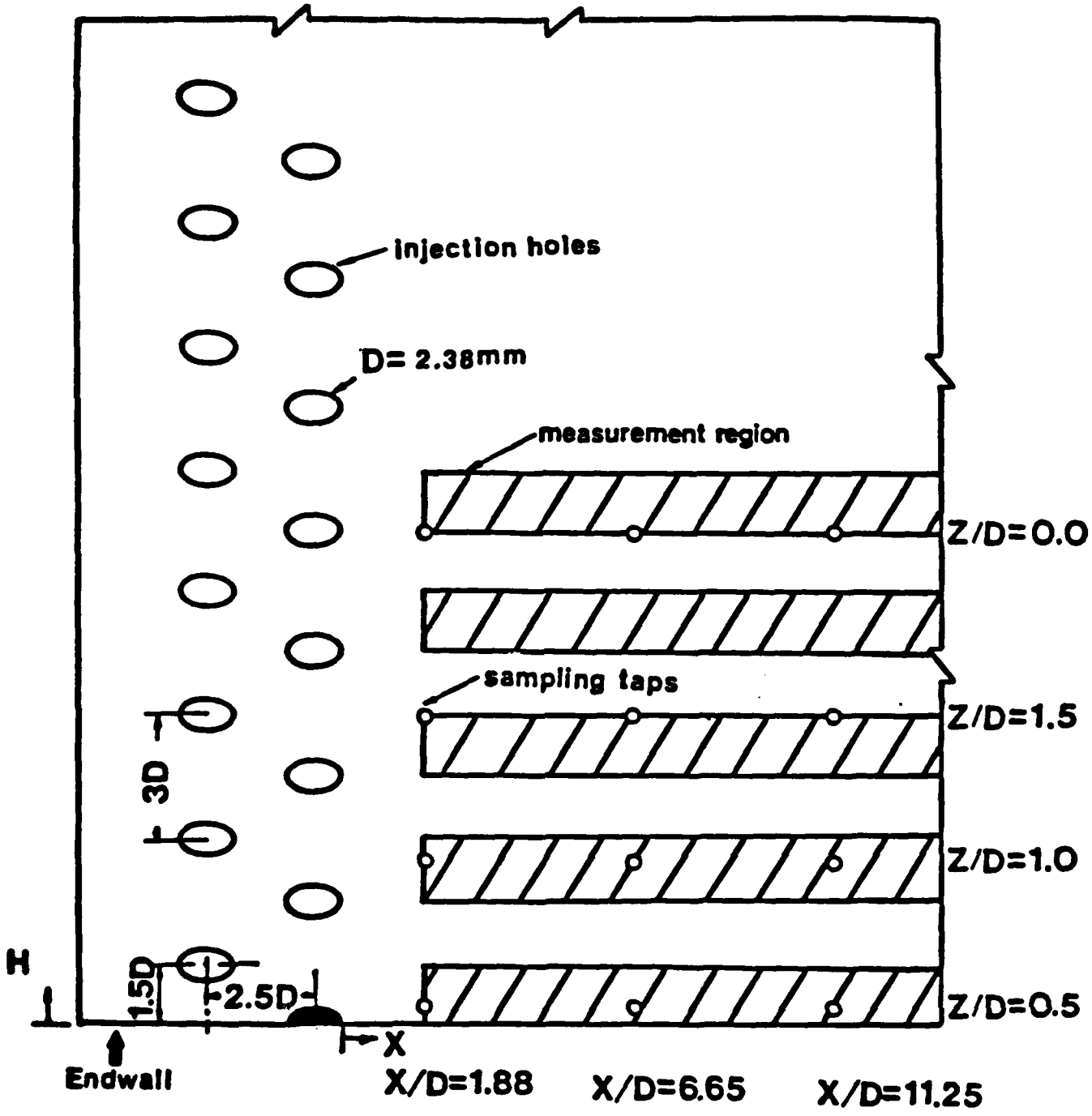

Fig. 1(a) Detail of test blade

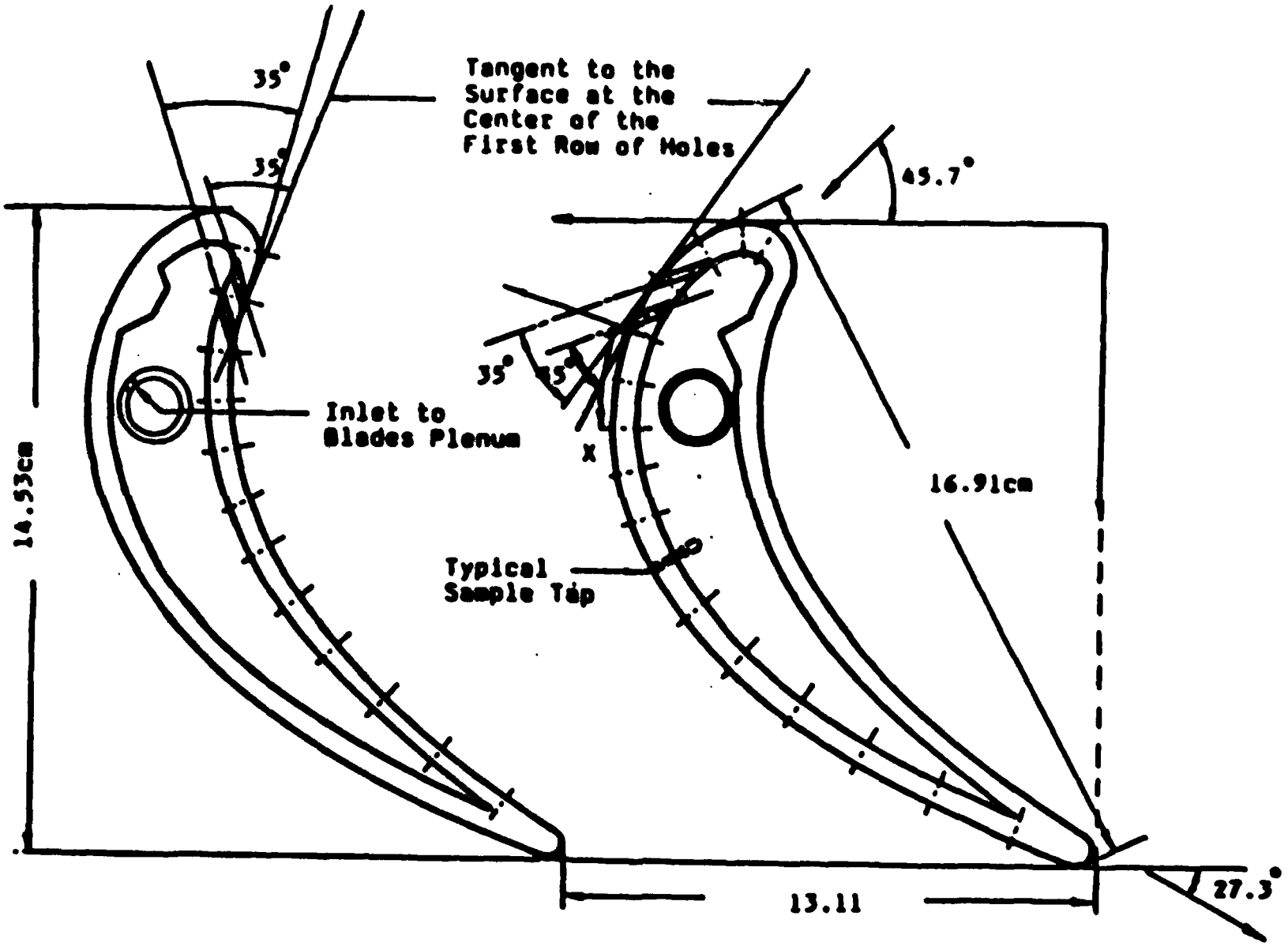

Fig. 1 Test blades

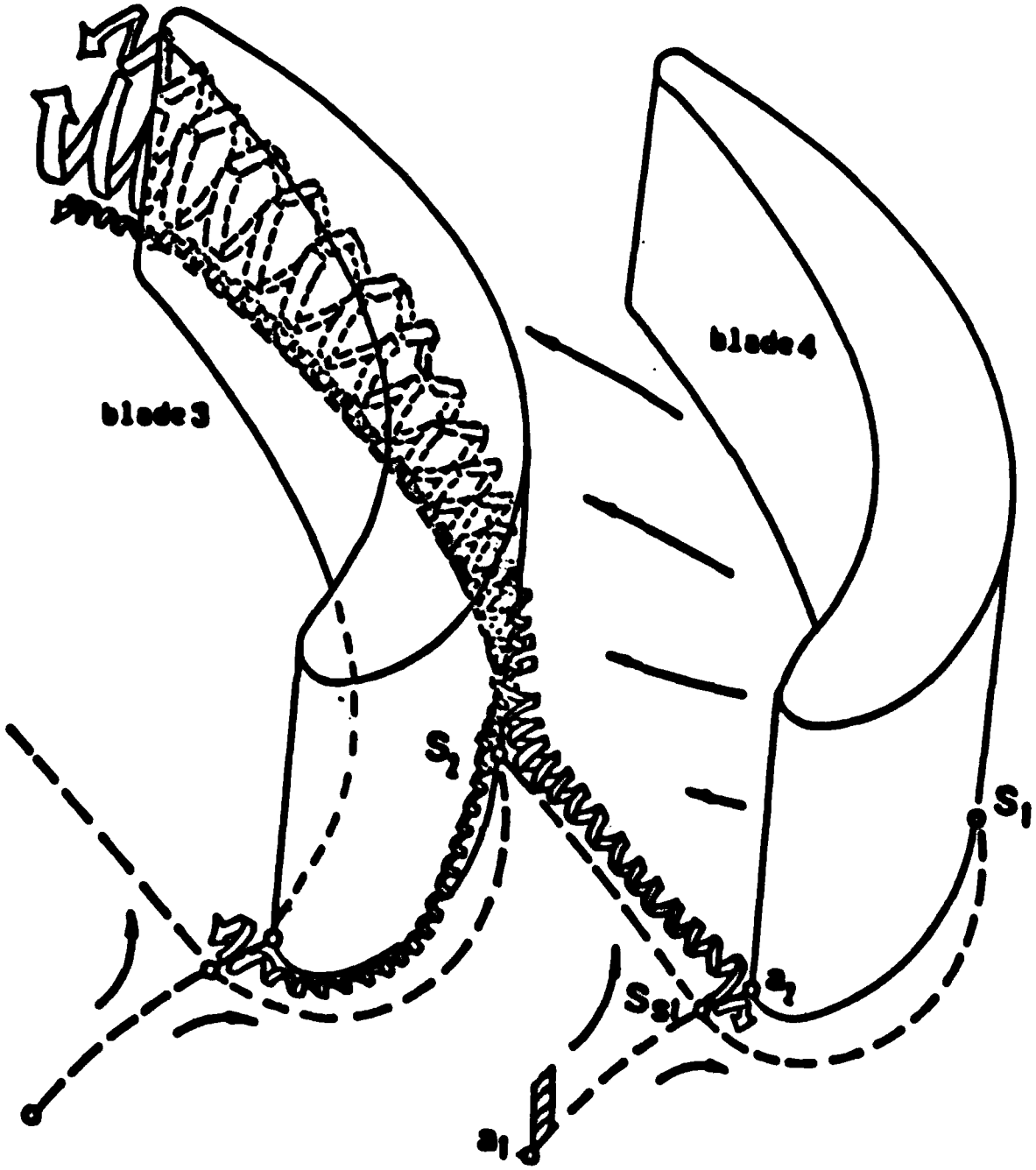

Fig. 2 Sketch of the secondary flow near endwall between blade passage

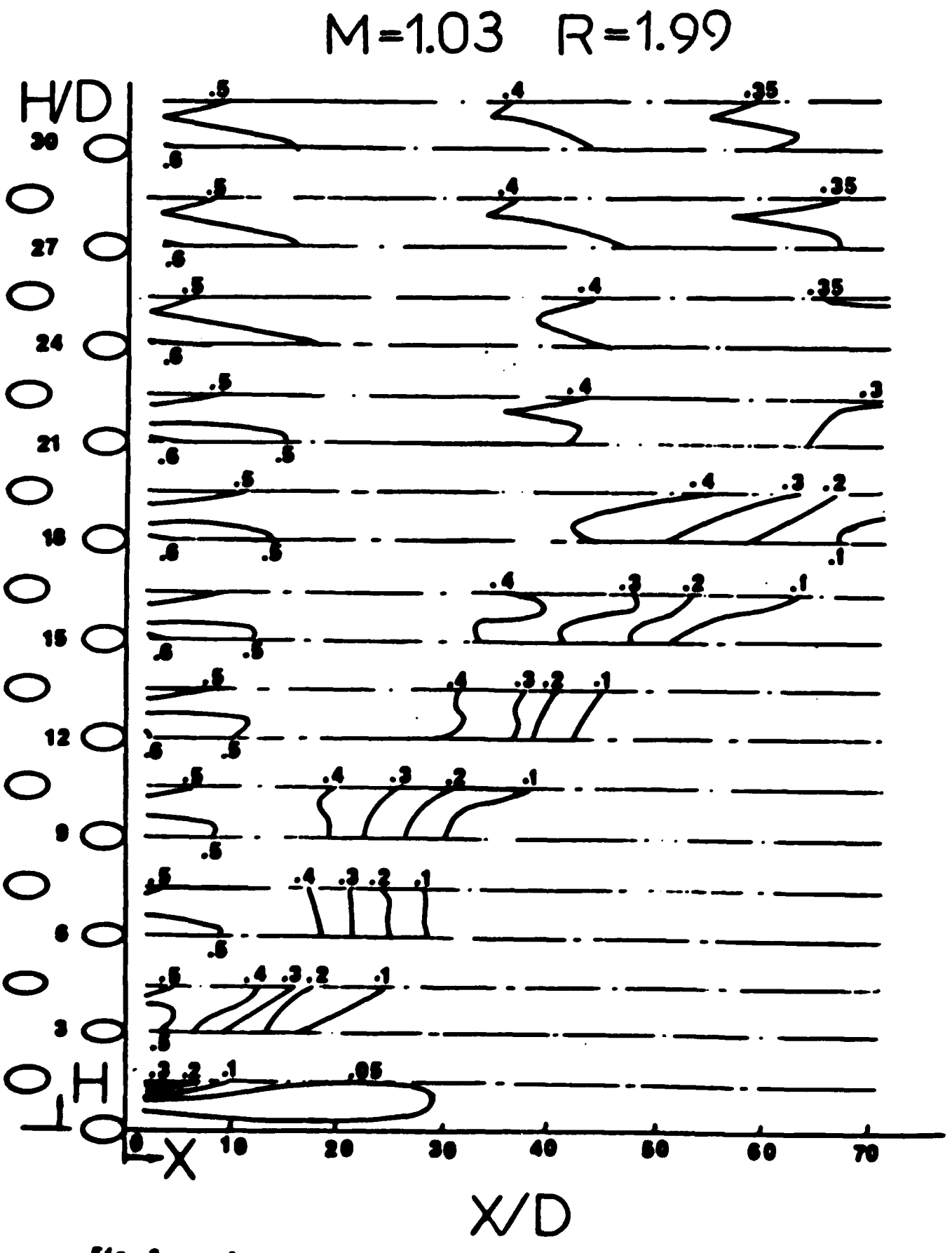

Fig. 3 Iso-effectiveness lines on convex surface at M = 1.03 and R = 1.99

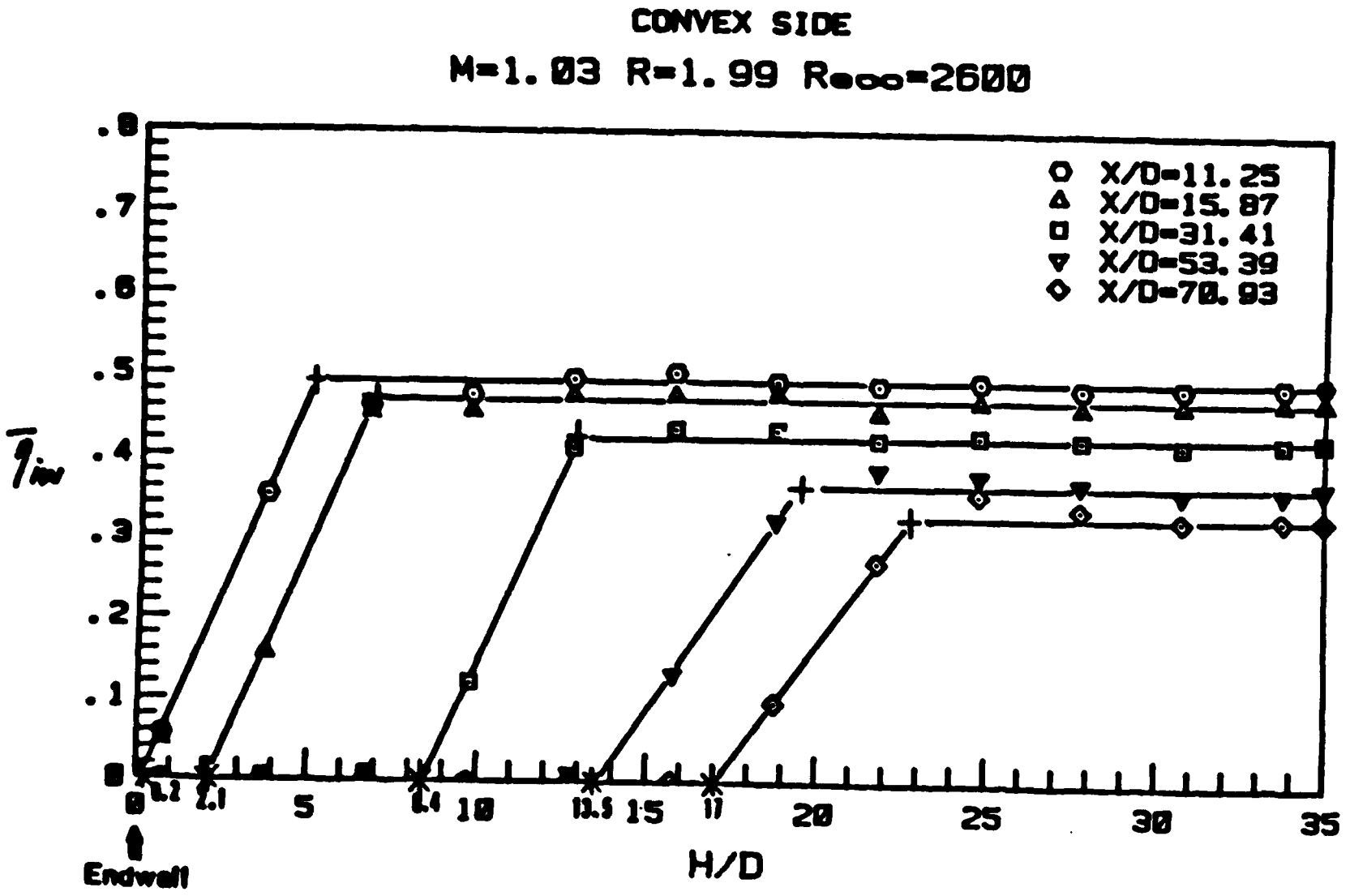

Fig. 4 Average effectiveness on convex surface at M = 1.03 and R = 1.99

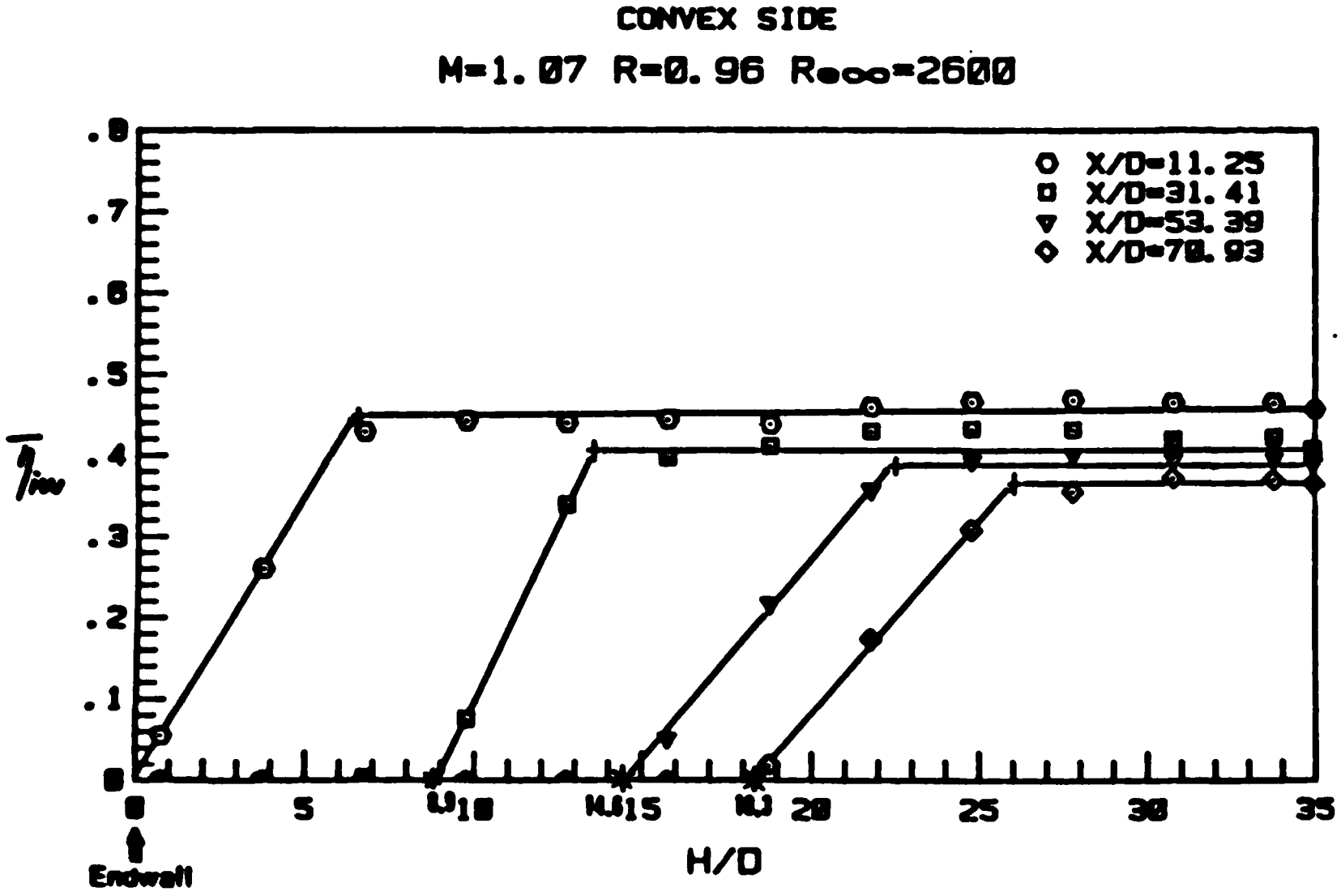

Fig. 5 Average effectiveness on convex surface at M = 1.07 and R = 0.96

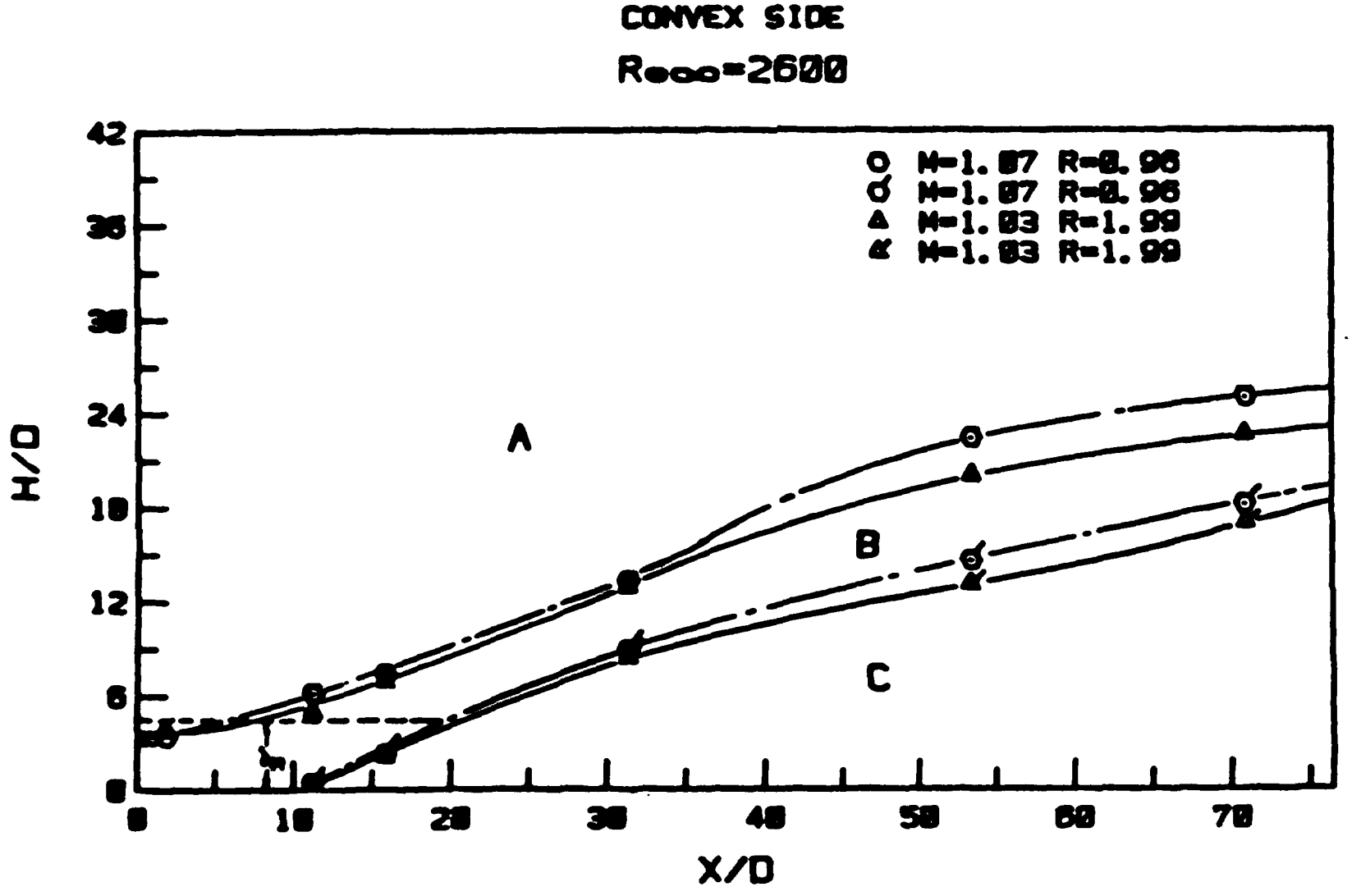

Fig. 6 Distribution range of average effectiveness on the convex surface for two different density ratios, R = 0.96 and R = 1.99

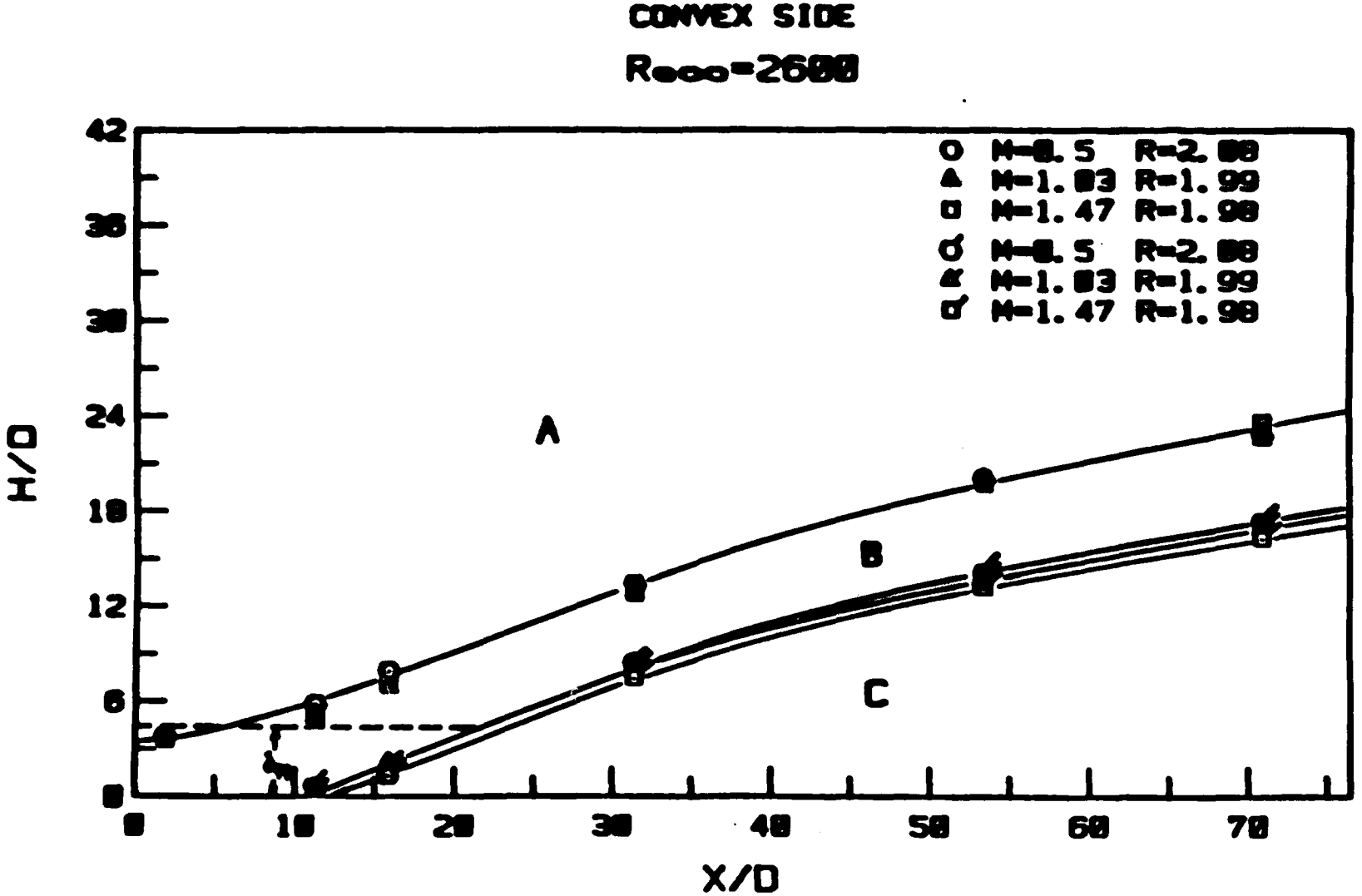

Fig. 7 Distribution range of average effectiveness on the convex surface for three different blowing rates, M = 0.5, 1.03 and 1.47.

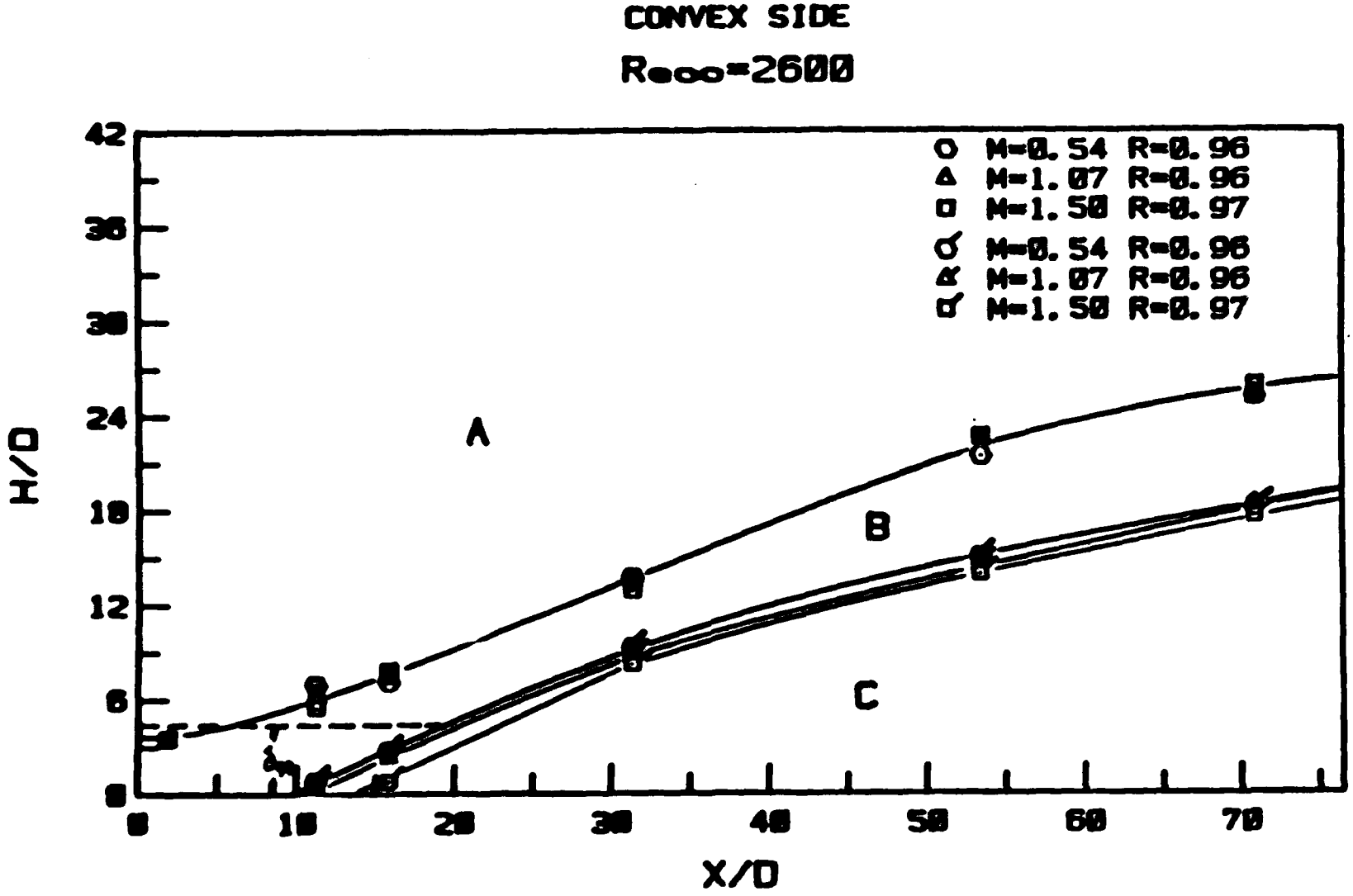

Fig. 8 Distribution range of average effectiveness on the convex surface for three different blowing rates, M = 0.54, 1.07 and 1.50

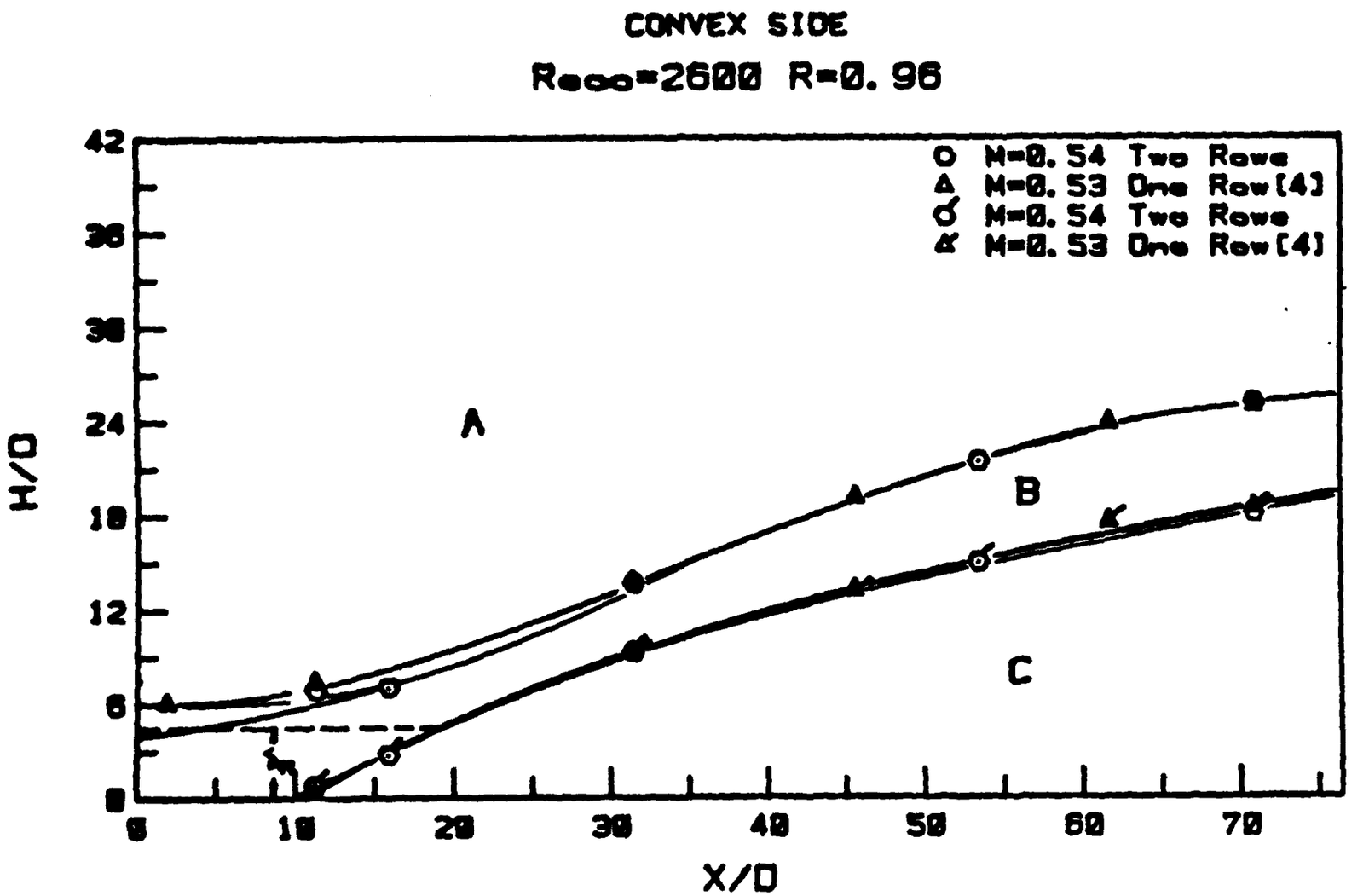

Fig. 9 Comparison of distribution range of average effectiveness between one-row injection and two-row injection

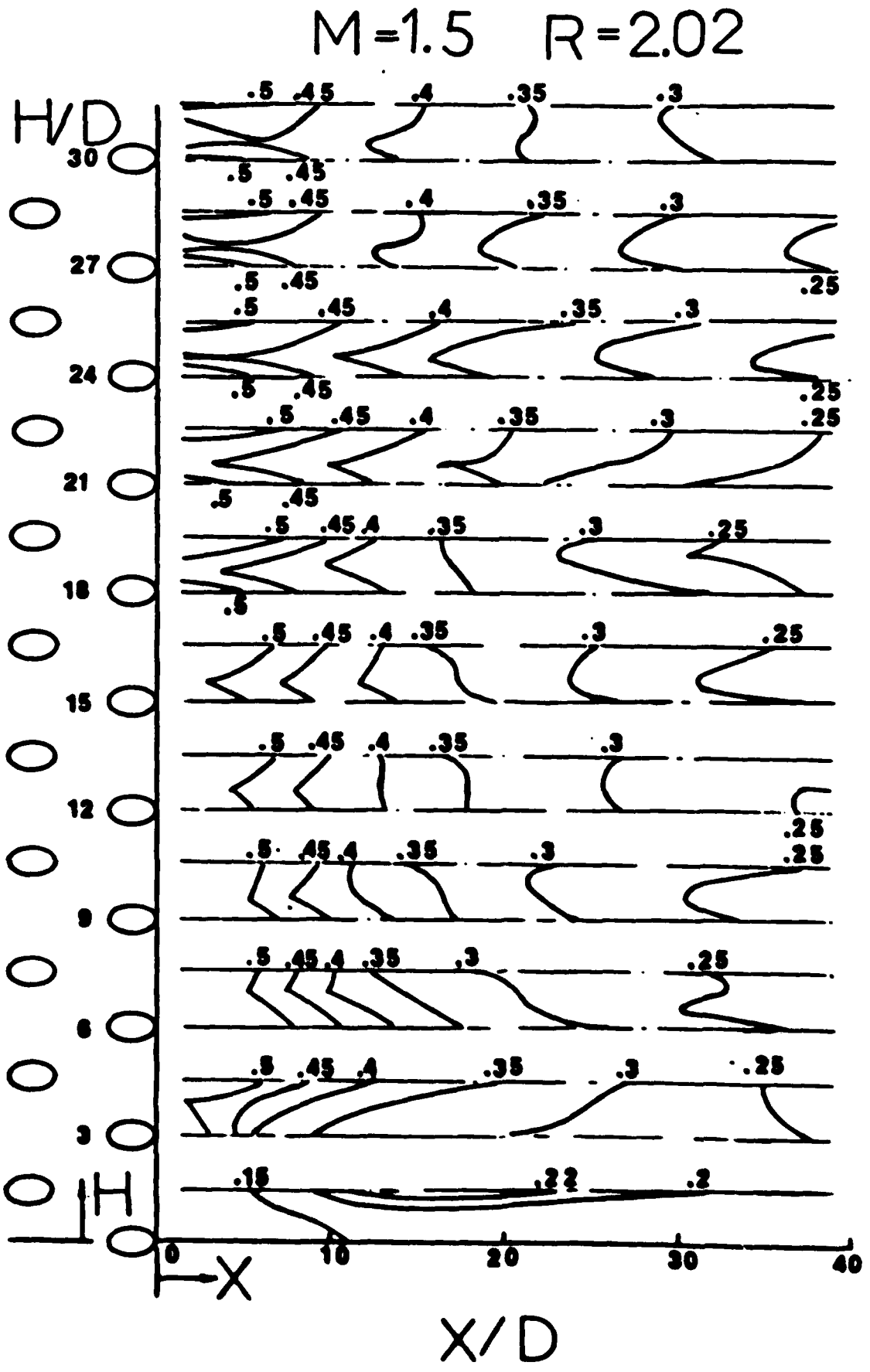

Fig. 10 Iso-effectiveness lines on concave surface at M = 1.5 and R = 2.0

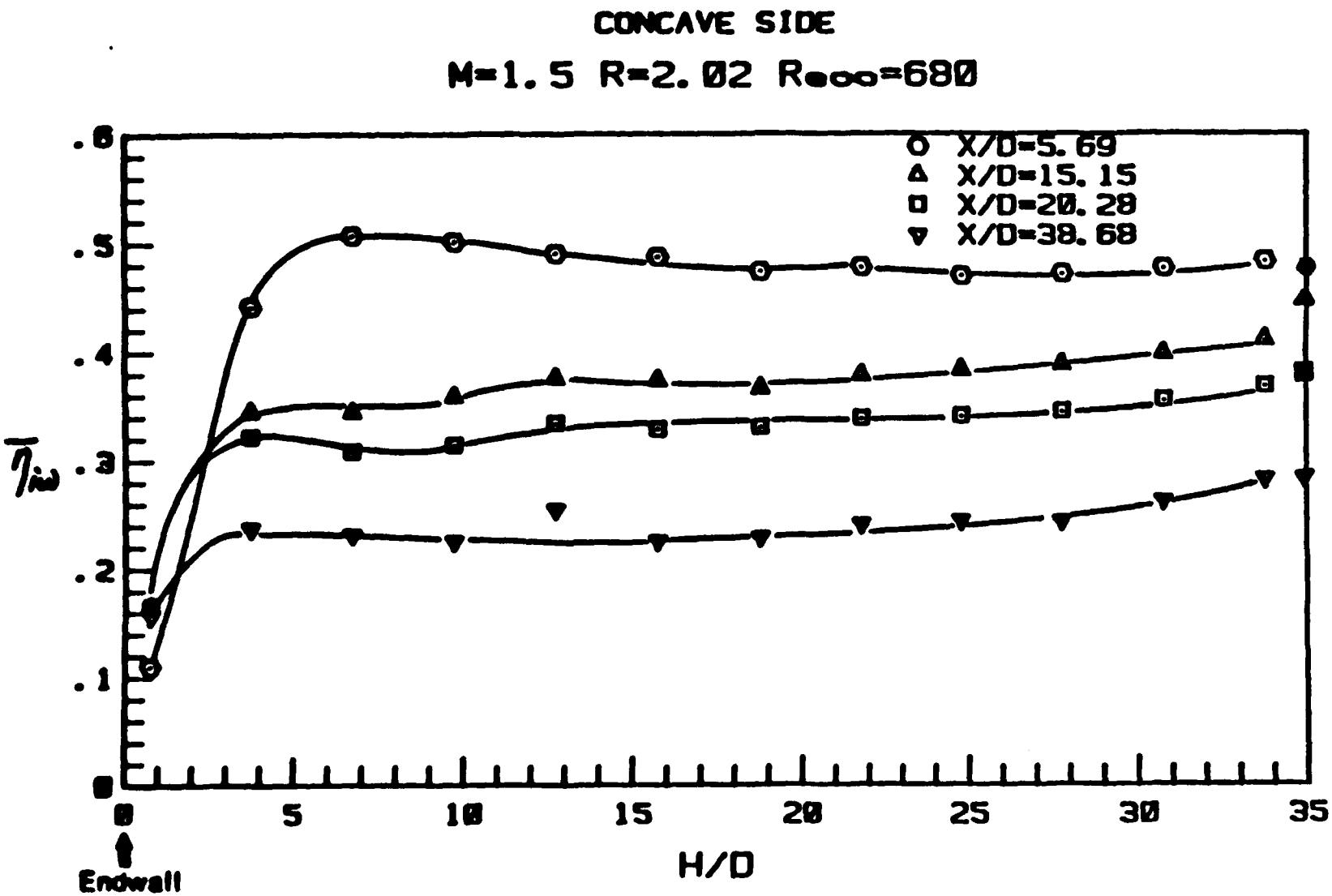

Fig. 11 Average effectiveness on concave surface at M = 1.5 and R = 2.0

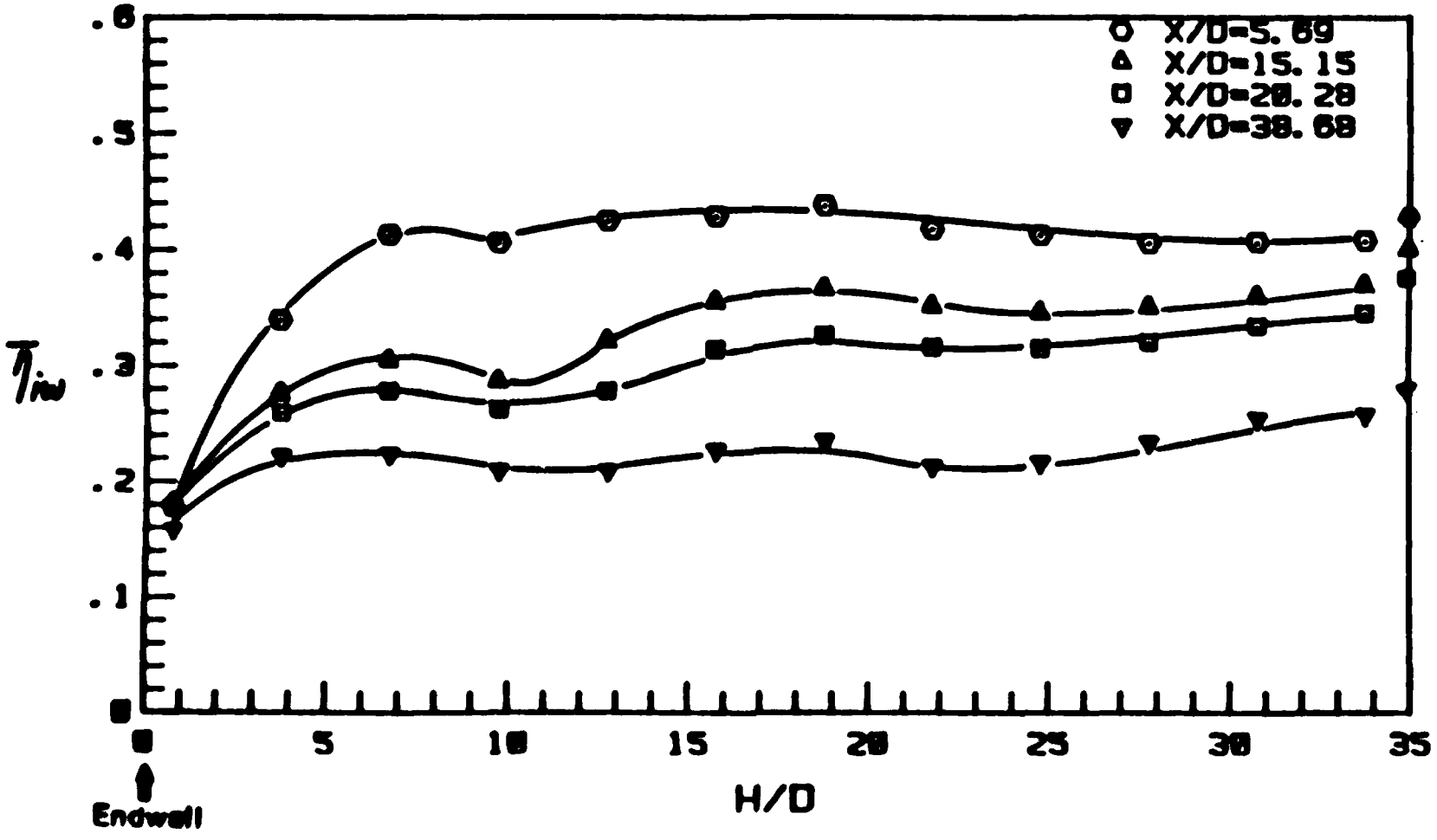

Fig. 12 Average effectiveness on concave surface at M = 1.38 and R = 0.96

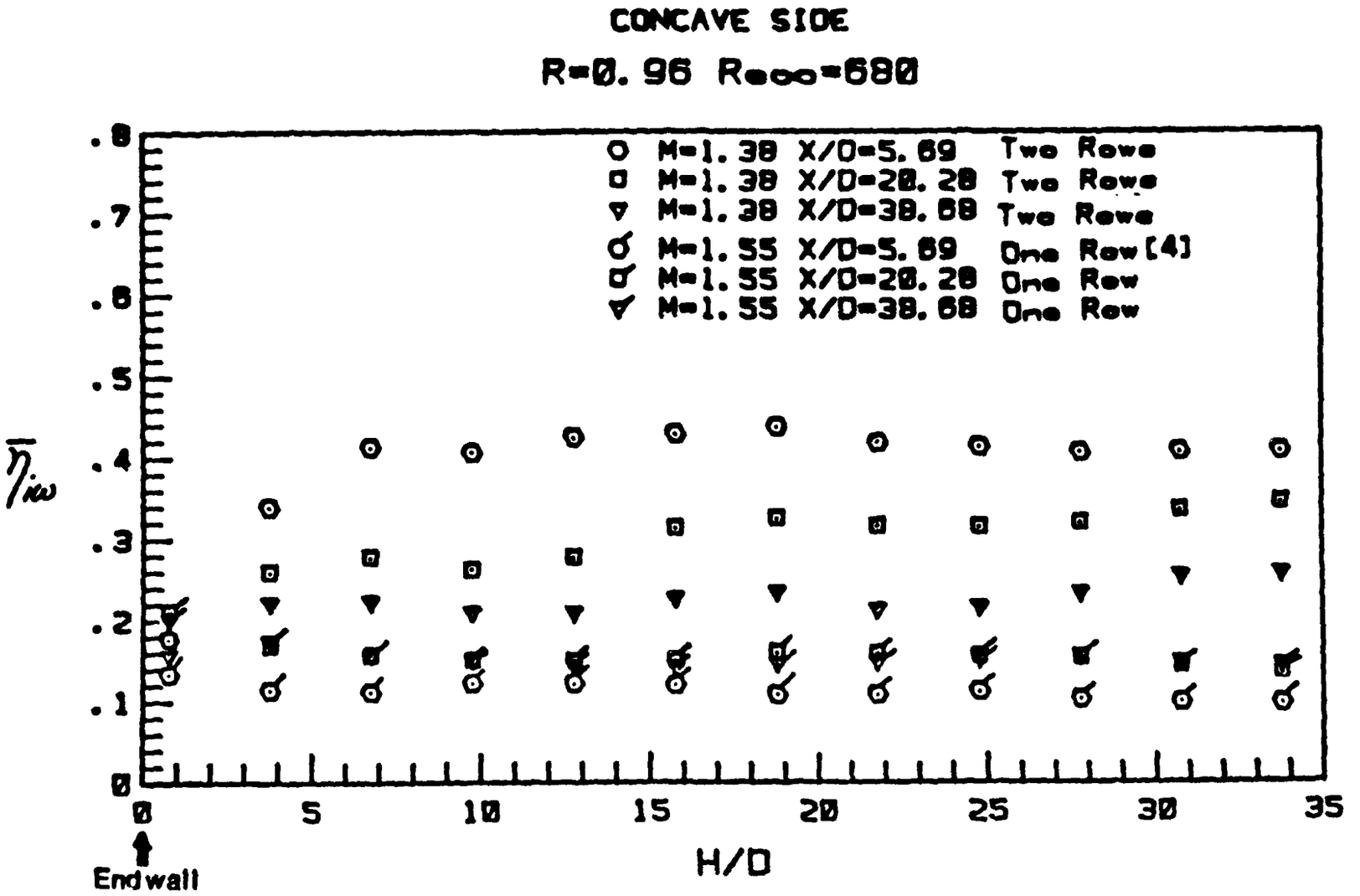

Fig. 13 Comparison of average effectiveness at R = 0.96 between one-row injection and two-row injection

END

7-87

DTIC